INVESTIGATION INTO PRYING FORCE AND BOLT MOMENT IN BOLTED STEEL T-STUBS

PhD Dissertation

Tchabremane Jean de la Croix KOMBATE

Eskişehir 2024

INVESTIGATION INTO PRYING FORCE AND BOLT MOMENT IN BOLTED STEEL T-STUBS

Tchabremane Jean de la Croix KOMBATE

PhD Dissertation
Department of Civil engineering

Supervisors: Assoc. Prof. Dr. Kıvanç TAŞKIN

Dr. Kerem PEKER

Eskişehir

Eskişehir Technical University

Institute of Graduate Programs

May 2024

FINAL APPROVAL FOR THESIS

This thesis titled **Investigation into Prying Force and Bolt Moment in Bolted Steel T-Stubs** has been prepared and submitted by Tchabremane Jean de la Croix KOMBATE in partial fulfillment of the requirements in “Eskişehir Technical University Directive on Graduate Education and Examination” for the Degree of PhD in Civil engineering Department has been examined and approved on 02/05/2024.

Committee Members		**Title, Name and Surname**	**Signature**
Member	:	Assoc. Prof. Dr. Kıvanç TAŞKIN	
Member	:	Assoc. Prof. Dr. Erhan AYAS	
Member	:	Asst. Prof. Dr. Onur TUNABOYU	
Member	:	Asst. Prof. Dr. Özlem ÇALIŞKAN	
Member	:	Asst. Prof. Dr. Uğur ALBAYRAK	

Prof. Dr. Semra KURAMA
Director of the Institute of Graduate Programs

02/05/2024

SUPERVISOR APPROVAL

PhD student Tchabremane Jean de la Coix KOMBATE, whom I supervise, has completed this thesis titled **Investigation into Prying Force and Bolt Moment in Bolted Steel T-Stubs**. According to my inspections, the work is scientifically and ethically appropriate for the student to the thesis defense exam.

Supervisors:

Assoc. Prof. Dr. Kıvanç TAŞKIN | Dr. Kerem PEKER

ABSTRACT

INVESTIGATION INTO PRYING ACTION IN BOLTED STEEL CONNECTIONS

Tchabremane Jean de la Croix KOMBATE
Department of Civil engineering
Eskişehir Technical University, Institute of Graduate Programs, May 2024
Supervisors: Assoc. Prof. Dr. Kıvanç TAŞKIN
Dr. Kerem PEKER

A common characteristic of the behaviour of steel T-stubs subjected to tensile loading is the prying effects which can develop as a result of the deformation of the flanges of the T-stub. Prying effects can induce a substantial increase in bolt forces as well as the flexural engagement of the bolts. Although the T-stub model has been extensively investigated over the years and led to design predictions in terms of strength and stiffness, the flexural engagement of bolts has been disregarded in most studies that investigated prying in bolted T-stubs. Consequently, the actual codes do not account for the bending moment in the bolts. However, the combined action of tension and bending may induce substantial stresses in the bolts and cause premature failure. In this work, an extensive parametrical study was carried out on welded plate T-stubs to investigate prying action. Experimental data from the literature was used to calibrate and validate advanced FE models that were constructed in ABAQUS. Good agreement was obtained, and a large number of FE models were generated to study the influence of different material and geometrical parameters such as flange thickness, edge distance, gauge distance, bolt diameter, steel grade, and bolt class. Various values related to prying effects such as the total bolt force, prying force, bolt moment, and the position of the resultant of contact forces were investigated. The novelty of this study was the focus on the bending moment that may develop in the bolts. Through a curve fitting process using the results from the parametrical study, a formula was proposed for the evaluation of the prying force and the bolt bending moment.

Keywords: FE modelling; Bolted connections; T-stub; Prying action; Bolt bending

ÖZET

CIVATALI ÇELİK BİRLEŞİMLERDEKİ KANIRTMA ETKISININ ARAŞTIRILMASI

Tchabremane Jean de la Croix KOMBATE
Inşaat mühendisliği Anabilim Dalı
Yapı Bilim Dalı
Eskişehir Teknik Üniversitesi, Lisansüstü Eğitim Enstitüsü, Mayıs 2024
Danışman: Dr. Öğr. Üyesi Kıvanç TAŞKIN
Dr. Kerem PEKER

Çekme yüküne maruz kalan çelik T-parçaların davranışının ortak bir özelliği, T-parçanın başlıklarının deformasyonunun bir sonucu olarak oluşabilecek kanırtma etkileridir. Kanırtma etkiler, cıvatalarda oluşan kuvvetlerin önemli bir artışının yanında cıvataların eğilmesine neden olabilirler. Her ne kadar T-parça modeli yıllar boyunca kapsamlı bir şekilde araştırılmış ve dayanım ve rijitlik açısından tasarım tahminlerine yol açmış olsa da, cıvatalı T-parçalardaki kanırtma etkilerini araştıran çoğu çalışmada cıvataların eğilmesi göz ardı edilmiştir. Sonuç olarak, mevcut yönetmeliklerde cıvatalardaki bükülme momenti hesaba alınmamaktadır. Bununla birlikte, çekme ve bükülmenin birleşik etkisi cıvatalarda önemli gerilimlere neden olabilir ve erken kopmaya neden olabilir. Bu çalışmada, kanırtma etkilerini araştırmak için kaynaklı plaka T-parçalar üzerinde kapsamlı bir parametrik çalışma gerçekleştirilmiştir. ABAQUS'ta oluşturulan gelişmiş sonlu eleman modellerini kalibre etmek ve doğrulamak için literatürdeki deneysel veriler kullanılmıştır. İyi bir uyumluluk sağlanmış ve flanş kalınlığı, kenar mesafesi, bulonların arasındaki mesafe, cıvata çapı, çelik sınıfı ve cıvata sınıfı gibi farklı malzeme ve geometrik parametrelerin etkisini incelemek için çok sayıda sonlu eleman modeli oluşturulmuştur. Toplam cıvata kuvveti, kanırtma kuvveti, cıvata momenti ve temas kuvvetlerinin bileşkesinin konumu gibi kanırtma etkilerine ilişkin çeşitli değerler araştırılmıştır. Bu çalışmanın yeniliği cıvatalarda oluşabilecek eğilme momentine odaklanılmasıdır. Parametrik çalışmanın sonuçlarını kullanan bir eğri uydurma işlemi yoluyla, kanırtma kuvvetinin ve cıvata eğilme momentinin değerlendirilmesi için bir formül önerilmiştir.

Anahtar Sözcükler: Sonlu elemanlar modelleme, Cıvatalı bağlantılar, T-parça, Kanırtma etkisi, Cıvata bükülme

ACKNOWLEDGEMENTS

First, I want to express my sincere gratitude to my supervisors Assoc. Prof. Dr. Kıvanç TAŞKIN and Dr. Kerem PEKER for their guidance, support, and contributions throughout my PhD program.

I would also like to thank Prof. Dr. Özgür AVŞAR for providing insightful comments and suggestions. He gave me the first advice when I started my PhD. He told me to brace myself because it would be the most challenging part of my university studies. At that time, I thought I understood what he meant but through my journey I have learnt to understand the depth of his advice.

I gratefully acknowledge the postgraduate scholarship and financial support received from Turkish Government that allowed me to pursue and complete my PhD.

My special gratitude also goes to my family as a whole for their constant encouragement, unwavering support, prayers and motivation. They have always been with me through each step, believing in me and keeping me grounded and focused I would like to offer my special thanks to Beyzanur ORUÇ for her encouragements and for always being the voice that said the right words and offered me comfort in the times I needed to hear them.

Tchabremane Jean de la Croix KOMBATE

02/05/2024

STATEMENT OF COMPLIANCE WITH ETHICAL PRINCIPLES AND RULES

I hereby truthfully declare that this thesis is an original work prepared by me; that I have behaved in accordance with the scientific ethical principles and rules throughout the stages of preparation, data collection, analysis and presentation of my work; that I have cited the sources of all the data and information that could be obtained within the scope of this study, and included these sources in the references section; and that this study has been scanned for plagiarism with “scientific plagiarism detection program” used by Eskişehir Technical University, and that “it does not have any plagiarism” whatsoever. I also declare that, if a case contrary to my declaration is detected in my work at any time, I hereby express my consent to all the ethical and legal consequences that are involved.

Tchabremane Jean de la Croix KOMBATE

CONTENTS

Page

TITLE PAGE .... **I**

FINAL APPROVAL FOR THESIS .... **II**

SUPERVISOR APPROVAL .... **III**

ABSTRACT .... **IV**

ÖZET .... **V**

ACKNOWLEDGEMENTS .... **VI**

STATEMENT OF COMPLIANCE WITH ETHICAL PRINCIPLES AND RULES .... **VII**

CONTENTS .... **VIII**

LIST OF FIGURES .... **XI**

LIST OF TABLES .... **XVI**

SYMBOLS AND ABBREVIATIONS .... **XVII**

1. INTRODUCTION **1**

- **1.1. Background** **1**
- **1.2. Failure Mechanisms of T-Stubs** **3**
- **1.3. Problem Statement** **6**
- **1.4. Research Objective** **6**
- **1.5. Methodology** **6**
- **1.6. Dissertation Outline** **7**

2. LITERATURE REVIEW **8**

- **2.1. Introduction** **8**
- **2.2. Previous Studies and Analytical Models** **9**
- **2.3. Conclusion** **18**

3. NUMERİCAL MODELLİNG OF STEEL BOLTED T-STUBS **20**

- **3.1. Introduction** **20**
- **3.2. Numerical Modelling and Validation** **20**

Page

3.2.1. Geometrical properties 21
3.2.2. Material properties 22
3.2.3. Meshing 23
3.2.4. Modeling of contact elements 25
3.2.5. Boundary and loading conditions 25
3.2.6. Model Validation 29
3.3. Parametrical Study 31
3.4. Results of the Numerical Parametric Investigation 33
3.4.1. Failure modes 33
3.4.2. Plastic resistance 38
3.4.3. Prying effect in the bolt 41
4. EXTENSIVE PARAMETRICAL STUDY USING NOMINAL MATERIAL PROPERTIES 59
4.1. Introduction 59
4.2. Nominal Material Properties 59
4.3. Influence of the Design Parameters 60
4.3.1. Influence of the gauge distance and the edge distance 60
4.3.2. Influence of flange thickness 71
4.3.3. Influence of flange width 77
4.3.4. Influence of steel class 79
4.3.5. Influence of weld throat thickness 83
4.3.6. Influence of bolt diameter 84
4.3.7. Conclusion 86
5. DEVELOPMENT OF AN ASSESSMENT PROCEDURE FOR THE PRYING FORCE AND THE BENDING MOMENT IN THE BOLT 88
5.1. Considerations for the Prying Effects 88
5.2. Mechanical Models Considering Prying Effects 88
5.3. Location of the Prying Force 91
5.4. Estimation of prying force 92
5.5. Estimation of the Bending Moment in the Bolts 93
5.6. Conclusion 93

Page

6. CONCLUDING REMARKS **95**

6.1. Summary of Research **95**

6.2. Recommendations for Future Work **96**

REFERENCES **97**

CURRICULUM VITAE

LIST OF FIGURES

Page

Figure 1.1. Tension-loaded connections (a) Moment T-connection (b) extended endplate moment connection 1

Figure 1.2. T-stub model in the case of beam-to-column endplate moment connection (J. Fernandez-Ceniceros) 2

Figure 1.3. Different types of T-stubs: (a) HR-T-stub and (b) WP-T-stubs 2

Figure 1.4. Prying action in T-stub subjected to tensile loading 3

Figure 1.5. Possible failure modes of bolted T-stubs 4

Figure 1.6. T-stub failure mechanism ranges 5

Figure 2.1. T-stub model with prying force at the edge of the flange 8

Figure 2.2. Prying model by Douty and McGuire (a) before loading (b) after loading 10

Figure 2.3. Prying model proposed by Agerskov 11

Figure 2.4. (a) Prying model by Struik and Back (b) Influence of flange deformations on the location of resultant bolt force 11

Figure 2.5. Equivalent frame model 12

Figure 2.6. (a) Equivalent plastic strain in the flanges and (b) measured distance between the plastic hinges 13

Figure 2.7. T-stub model: (a) at the end of pretension (b) at the end of monotonic T-stem load 15

Figure 2.8. Mechanical model with surface contact 15

Figure 2.9. (a) Typical T-stub element, (b) half part in the deformed state, and (c) sign convention 17

Figure 2.10. T-stub models: (a) disregarding bolt bending (b) considering bolt bending 17

Figure 3.1. Geometrical characteristics and cross section of WT1 specimen (a) and T1 specimen (b) 21

Figure 3.2. Bolt head and nut dimensions 22

Figure 3.3. True stress-logarithmic strain material laws: (a) specimen WT1 (Coelho, 2004) (b) specimen T1 (from Bursi and Jaspart, 1997) 23

Page

Figure 3.4. Meshing techniques for (a) specimen T1 and (b) specimen WT1 24

Figure 3.5. Symmetry applied in X-direction (a) and in Z-direction (b) 28

Figure 3.6. Original T-stub and its reduced model 28

Figure 3.7. Comparison of the experimental and numerical F-D curves of (a) WT1 and (b) T1 specimens 30

Figure 3.8. Deformation and yielding status at ultimate stage of (a) specimen WT1 and (b) specimen T1 31

Figure 3.9. Front view (a) and top view (b) of specimens WT1 after failure 31

Figure 3.10. Geometrical characteristics of the specimens involved in the parametrical study 32

Figure 3.11. Ultimate stage of specimens of t = 8 mm 34

Figure 3.12. Ultimate stage of specimens of t = 10 mm 35

Figure 3.13. Ultimate stage of specimens of t = 15 mm 36

Figure 3.14. Ultimate stage of specimens of t = 20 mm 37

Figure 3.15. T-stub with different failure mechanisms at plastic resistance stage and ultimate stage 38

Figure 3.16. (a) Conventional plastic resistance and (b) F-d curves for different values of w for t = 10 mm - n = 20 mm 39

Figure 3.17. Variation of the T-stub resistance in the function of the n and w for t = 15 mm 39

Figure 3.18. Variation of the resistance in the function of the flange thickness for different n-w combinations 40

Figure 3.19. Variation of Fr and Fec3 in function of the gauge distance for t = 10 mm 40

Figure 3.20. Variation of Fr and Fec3 in function of the gauge distance for t = 15 mm 40

Figure 3.21. Prying forces and force-resultant of the contact stresses 41

Figure 3.22. Variation of the Qmax in function of the flange thickness for different n-w combinations 44

Figure 3.23. Distance between the bolt axis and the plastic hinge arising near the web 44

Page

Figure 3.24. Variation of prying force in function of the edge distance and gauge distance for t = 8 mm ... 42

Figure 3.25. Variation of prying force in function of the edge distance and gauge distance for t = 10 mm ... 43

Figure 3.26. Variation of prying force in function of the edge distance and gauge distance for t = 15 mm ... 43

Figure 3.27. Variation of prying force in function of the edge distance and gauge distance for t = 20 mm ... 43

Figure 3.28. Location of the origin point ... 45

Figure 3.29. Variation of the prying force and XN1 throughout the loading for different cases ... 46

Figure 3.30. Variations of XN3 throughout the loading ... 47

Figure 3.31. XN1 at the attainment of the plastic resistance and at ultimate stage ... 47

Figure 3.32. Position of the resultant of the contact stresses in X-direction ... 48

Figure 3.33. Position of the resultant of prying forces showing the shift from Mode 3 to Mode 2 ... 49

Figure 3.34. Variation of the position of the prying forces resultant for (a) t = 8mm and (b) t = 15 mm ... 49

Figure 3.35. Variation of the total bolt force in the function of n and w for t = 8 mm and t = 10 mm ... 51

Figure 3.36. Variation of the total bolt force in the function of n and w for t = 15 mm and t = 20 mm ... 52

Figure 3.37. Variation of Bmax in function of the flange thickness for different n-w combinations ... 52

Figure 3.38. Variations of the bolt moment throughout the loading ... 53

Figure 3.39. Variations of Mmax in function of n and w for t = 10 mm, 15 mm and 20 mm ... 54

Figure 3.40. Variation of the Mmax in the function of the flange thickness for different n-w combinations ... 55

Figure 3.41. Ratio of Q, M and B to their respective maximum ... 56

Figure 3.42. Interaction curves for t = 8 mm and t = 10 mm ... 57

Page

Figure 3.43. Interaction curves for t = 15 mm and t = 20 mm 57

Figure 4.1. Ultimate stage of S2B1 – M12 – t = 20 mm 61

Figure 4.2. Variations of the Mmax and Mr for S2B1 – M12 – t = 20 mm 61

Figure 4.3. Ultimate stage of S1B1 – M12 – t = 10 mm 62

Figure 4.4. Variations of the Mmax and Mr for S1B1 – M12 – t 10 62

Figure 4.5. Ultimate stage of S2B2 – M24 – t = 10 mm 63

Figure 4.6. Variations of the Mmax and Mr for S2B2–M24 – t = 10 mm 63

Figure 4.7. Variations of Mmax in function of w for T-stubs with large bolts and thin flanges 64

Figure 4.8. Variations of the prying forces in function of w for T-stubs involved in failure Mode 1 65

Figure 4.9. Variations of the prying forces in function of w for T-stubs involved in (a) Mode 3 and (b) Mode 2 64

Figure 4.10. Variations of the bolt moment in function of the edge distance 66

Figure 4.11. Variations of the pring forces in function of the edge distance 67

Figure 4.12. Specimens with the maximum bolt moment ratio at the beginning of the loading 68

Figure 4.13. Variations of M and M/F in function of the gauge distance for S1B1-M12 69

Figure 4.14. Variations of M and M/F in function of the edge distance for S2B2-M16 69

Figure 4.15. Variations of Q and Q/F in function of the edge distance for S1B2 - M12 70

Figure 4.16. Variations of Q and Q/F in function of the gauge distance for S2B1-M24-t 10 (Mode 1) 70

Figure 4.17. Variations of XN1 in function of the applied force for T-stubs with flexible flanges 71

Figure 4.18. Influence of the flange thickness on Q, Q/F, M and M/F 72

Figure 4.19. Influence of the flange thickness on Q, Q/F, M and M/F 73

Figure 4.20. Influence of the flange thickness on Q, Q/F, M and M/F 74

Page

Figure 4.21. Influence of the flange thickness on Q, Q/F, M and M/F 75

Figure 4.22. Influence of the flange thickness on XN1 for S1B1 - M16 76

Figure 4.23. Influence of the flange thickness on XN1 for S3B2 - M12 76

Figure 4.24. Influence of the flange width on M and M/F 77

Figure 4.25. Influence of the flange width on Q and Q/F 78

Figure 4.26. Influence of the flange width on XN1 79

Figure 4.27. Influence of the steel class on M and on M/F for M27 – t 10 – n = 50 mm (Mode 1) 80

Figure 4.28. Influence of the steel class on Q and on Q/F for M27 – t 10 – n = 50 mm (Mode 1) 81

Figure 4.29. Influence of the steel class on the M, M/F, Q and Q/F for M12 – t 20 – n = 40 mm (Mode 3) 82

Figure 4.30. Influence of the steel class on XN1 considering different failure mechanisms 82

Figure 4.31. Influence of the weld throat thickness on the location of the prying force 83

Figure 4.32. Influence of the weld throat thickness for on M/F and Q/F 84

Figure 4.33. Influence of the bolt diameter on M, M/F, Q and Q/F for S1B2 – t = 10 mm 85

Figure 4.34. Influence of the bolt diameter on M, M/F, Q and Q/F for S3B1 – t = 20 mm 86

Figure 5.1. Ratio Br/Brd for different (a) flange thicknesses and (b) bolt diameters 89

Figure 5.2. Mechanical model of T-stub (a) disregarding the bolt bending (b) considering the bolt bending 89

Figure 5.3. Ratio x/n for for different (a) flange thicknesses and (b) bolt diameters 91

Figure 5.4. Prediction of the prying force 92

LIST OF TABLES

Page

Table 1.1. Design resistance of a T-stub flange 5

Table 3.1. Bolt head and nut dimensions for M12 bolts (DIN EN 14399-4) 22

Table 3.2. Geometrical properties of the specimens 22

Table 3.3. Minimum and maximum of edge distance and gauge distance allowed by Eurocode 3 32

Table 3.4. Geometrical properties of the specimens 33

Table 3.5. Maximum bolt moment and their ratios to ultimate bolt flexural resistance 55

Table 4.1. Nominal mechanical properties for plates and bolts 60

Table 4.2. Weld throat thickness 83

Table 5.1. The equations of equilibrium for the different models 90

Table 5.2. Modified prying formulas for the prying force 90

SYMBOLS AND ABBREVIATIONS

a_w	:	Weld throat thickness
Q	:	Prying force
Q_r	:	Prying force at the plastic resistance stage
Q_{max}	:	Maximum prying force
Q_u	:	Prying force at ultimate stage
$M_{f,Rd}$	:	Design flexural resistance of the T-stub flange
B_{Rd}	:	Design axial resistance of a single bolt
L_b	:	bolt elongation length
M_r	:	Bolt moment at the plastic resistance stage
M_{max}	:	Maximum bolt moment
M_u	:	Bolt moment at ultimate stage
M_{ub}	:	Ultimate bolt flexural resistance
M_{pl}		Plastic moment of the flange
n	:	Edge distance
w	:	Gauge distance
m	:	Distance between the bolt axis and the flange-to-web connection section where the formation of a plastic hinge is expected
B	:	Total bolt force
B_{rd}	:	Axial bolt resistance
$CF2$	:	Total force due to contact pressure in direction 2
t_f or t	:	Thickness of the flange
t_w	:	Thickness of the web
E	:	Young Modulus
I_f	:	Moment of inertia of the flange
I_b	:	Moment of inertia of the bolt
PEEQ	:	Equivalent plastic strain
f_y	:	Yield strength of the flange
f_u	:	Ultimate strength of the flange
f_{yb}	:	Yield strength of the bolt
f_{ub}	:	Ultimate strength of the bolt

1. INTRODUCTION

1.1. Background

Connections play a crucial role in the safety and stability of any structure. Therefore, they are of great importance to the engineer. Bolted connections are now more widely used in steel structures than welded connections. Besides their easy fabrication and installation, bolted connections present the advantage over welded connections of exhibiting a ductile behavior. After Northridge earthquake (1994) and Hanshin earthquake (1995), researchers found that many steel frames were damaged due to brittle fracture in the beam-to-column welded connections; whereas the destruction of structures with bolted endplate connections was relatively low. However, due to the various parameters involved as well as nonlinearities (material nonlinearities, nonlinearities associated with contact between the connected elements…), steel bolted connections exhibit nonlinear behavior. The determination of this behavior is very complex and requires approximations. However, the behavior obtained with approximations should be as representative of the real behavior as possible; and should be able to account for the entire phenomenon occurring in the connection. One of these approximations is the utilization of the equivalent T-stub model to represent the behavior of tension-loaded part of connections. Some typical examples of connections where the connection or part of it is subjected to tensile-type loading are shown in **Fig. 1.1**.

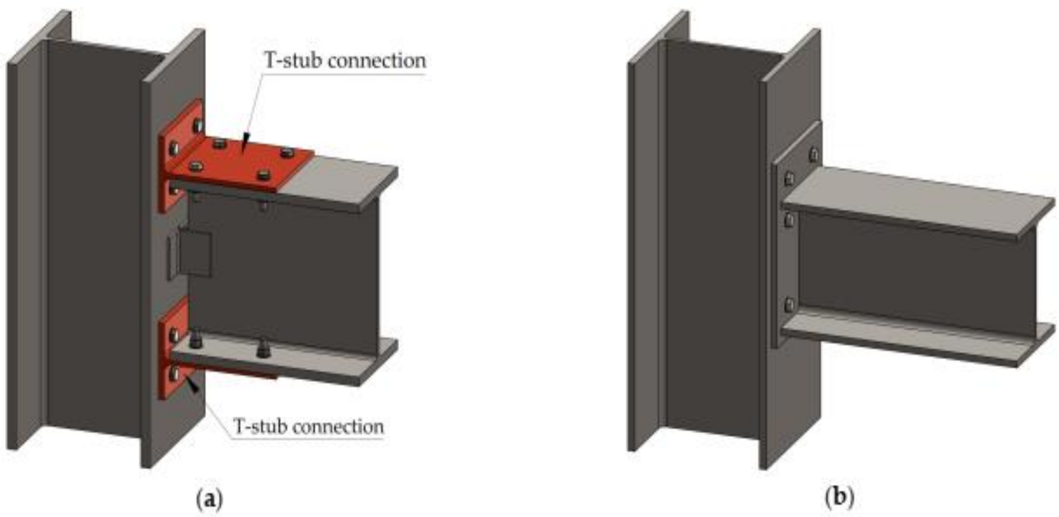

Figure 1.1. *Tension-loaded connections: **(a)** Moment T-connection **(b)** Extended endplate moment connection (Berrospi Aquino et al., 2021)*

The equivalent T-stub model has been widely used to describe the behavior of some elements of the connection under tension. An equivalent T-stub corresponds to two T-shaped elements connected through the flanges by means of one or more bolt rows (See Fig. 1.2).

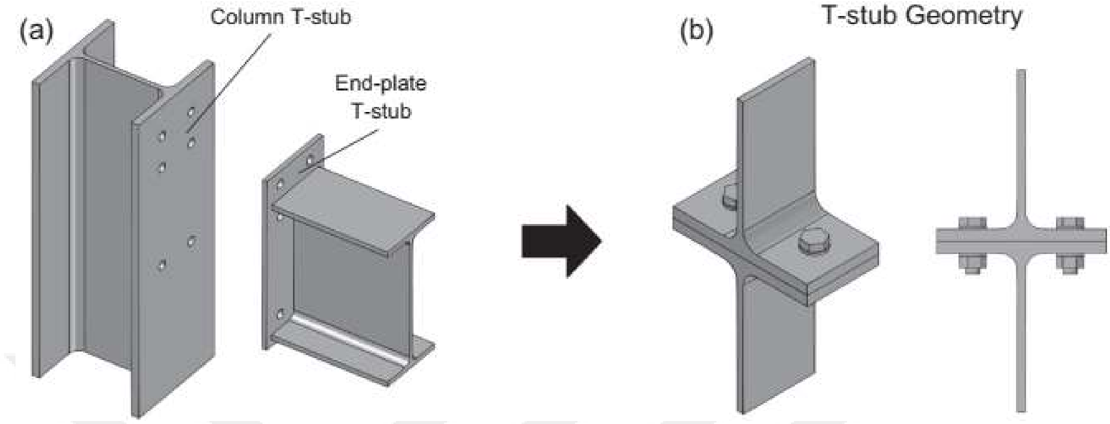

Figure 1.2. *T-stub model in the case of beam-to-column endplate moment connection (J. Fernandez-Ceniceros)*

Depending on how the flanges are connected to the web, two types of T-stubs can be distinguished (See Fig. 1.3): hot-rolled T-stubs (HR-T-stub) and welded plate T-stubs (WP-T-stubs). For the HR-T-stub model, the flanges and the web are connected by means of a fillet radius *r* that ensures the continuity between both plates. In the case of WP-T-stubs, a continuous 45°-fillet weld throat thickness *aw* links the flanges and the web, though the two plates are not necessarily in contact (Girão Coelho et al., 2006)

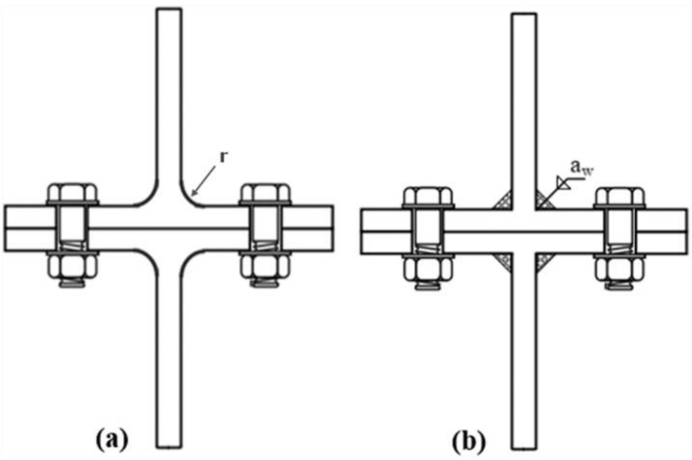

Figure 1.3. *Different types of T-stubs: (a) HR-T-stub and (b) WP-T-stubs (Girão Coelho, 2004)*

T-stubs made of hot-rolled profiles have been extensively studied over the past years. The behavior of T-stubs made up of welded plates (WP-T-stub) is obtained by extrapolating the existing rules for the HR models. However, this way of proceeding can be erroneous and can yield unsafe estimations of the characteristic properties.

One common and significant behavioral characteristic of nearly all types of tensile bolted connections is prying action. In fact, in bolted tension-member connections or on the tension side of bolted moment connections, the bolts are expected to carry a load equal to the tension load applied. However, tests have shown that the flexural deformation of the flanges of the connected members can subject bolts to additional forces and moments. This phenomenon, which is mostly encountered in connections with flexible flanges, is referred to as prying action (See Fig. 1.4). Prying action can cause bolts to fail before the applied tension has reached the design tension load. Hence, the ultimate load of the connection is reduced. In connections with thick flanges, very little prying will develop and the induced forces will be negligible. In connections with more flexible flanges, prying action and the induced forces can be substantial.

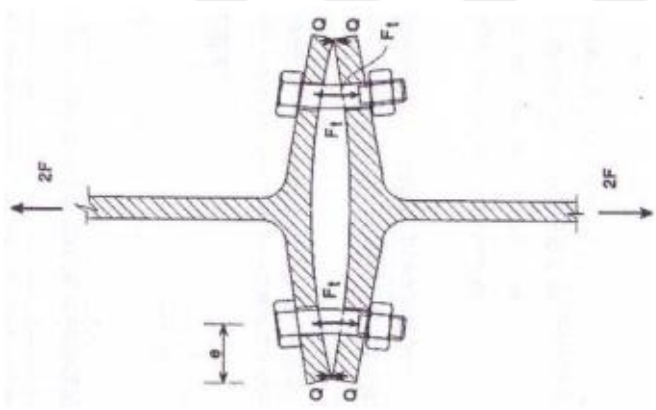

Figure 1.4. *Prying action in T-stub subjected to tensile loading*

One can avoid coping with prying action by using thick flanges. However, these connections exhibits a lower ductility than those with flexible flanges. In addition, the design of connections without taking into consideration prying effect could lead to unsafe design. Several codes and standards consider prying action differently. In EN 1993-1-8, it is implicitly taken into consideration in the evaluation of tension resistance of bolt rows. Nevertheless, there is no formula provided for the computation of prying force. AISC Manual provides formulae for the computation of the prying force and the minimum required thickness to eliminate prying action.

1.2. Failure Mechanisms of T-Stubs

The equivalent T-stub model is used in EN 1993-1-8 for the determination of the behavior (resistance and stiffness) of connections. In the scope of the component method, equivalent T-stub model is employed to simulate the tensile response of variety of connection components such as column flange in bending, end-plate in bending, flange cleat in bending and base plate in bending under tension (EN-1993-1-8). On account of its versatility, the T-stub model is one of the main ingredients of the component method. Therefore, an proper identification of the failure mechanisms of the T-stub is of prime importance.

Starting with the work of Zoetemeijer (1974), extensive studies have been carried out over the years and have permitted the identification of three failure mechanisms. The failure mechanisms, namely Mode 1, Mode 2 and Mode 3 are illustrated in Fig. 1.5. The design resistance corresponding to each failure mechanism is given as follow (See Table 1.1)

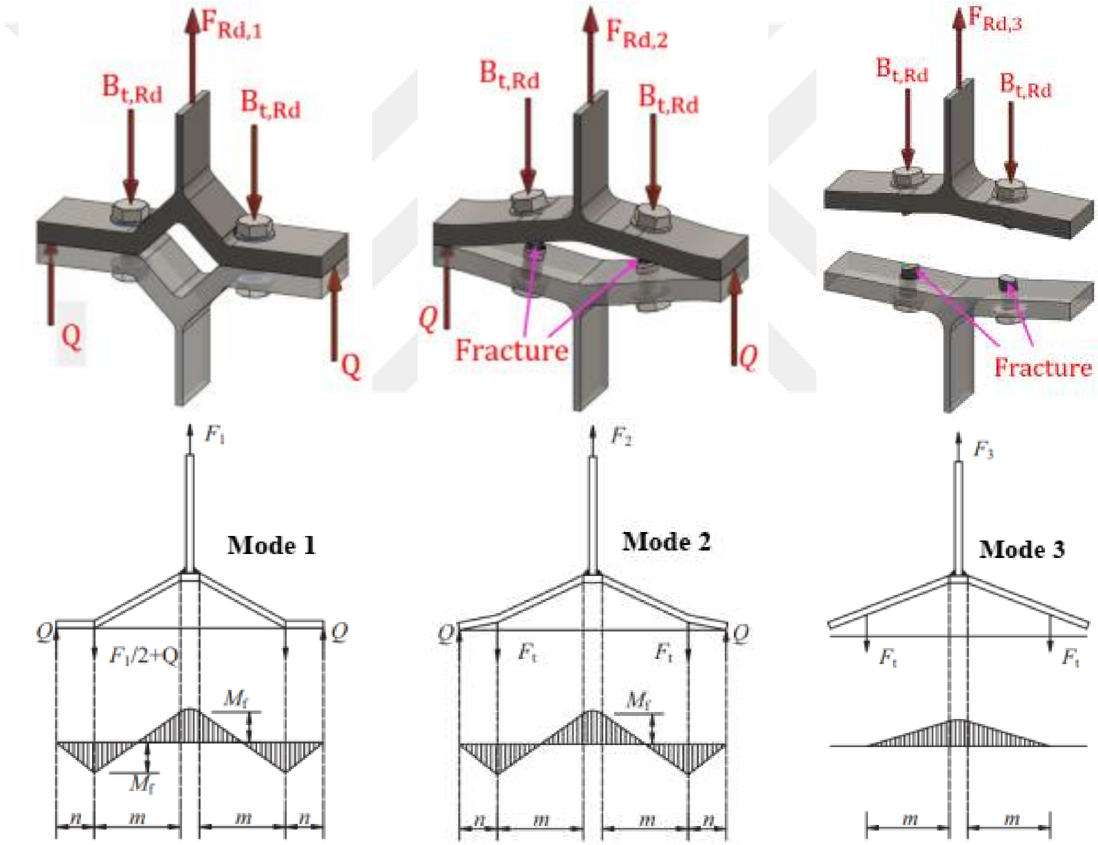

Figure 1.5. *Possible failure modes of bolted T-stubs*

Mode 1 corresponds to the complete yielding of the flange and the formation of four plastic hinges. Two hinges are located at the bolt axes, due to the bending moment caused by the prying forces. The remaining hinges are located at the flange-to-web connection.

Mode 2 corresponds to bolt failure with yielding of the flange. In this case, two plastic hinges develop at the sections corresponding to the flange-to-web connection.

Mode 3 corresponds to bolt failure only.

Table 1.1. *Design resistance of a T-stub flange (EN-1993-1-8)*

	With prying forces	Without prying forces
Mode 1	$F_{1,Rd} = \frac{4M_{f,Rd}}{m}$	$F_{Rd} = \frac{2M_{f,Rd}}{m}$
Mode 2	$F_{2,Rd} = \frac{2M_{f,Rd}+\sum B_{Rd}}{m+n}$	
Mode 3	$F_{3,Rd} = \sum B_{Rd}$	

Prying may develop if $L_b \leq L_b^*$

The expression of L_b *and* L_b^* *is specified in EN 1993-1-8.*

The design tension resistance of a T-stub should be taken as the smallest value for the three possible failure modes 1, 2, and 3 (EN-1993-1-8)

The relation between the failure mode typology and the mechanical and geometrical characteristics of the T-stub can be expressed by the means of a parameter β, which can be defined as the ratio between the resistance of failure mode 1 and that of failure mode 3 (Eq. 1.1). The dependency of the failure modes and the parameter β can represented in a nondimensional graph (See Fig. 1.6)

$$\beta = \frac{4M_{f,Rd}}{m \sum B_{Rd}} \tag{1.1}$$

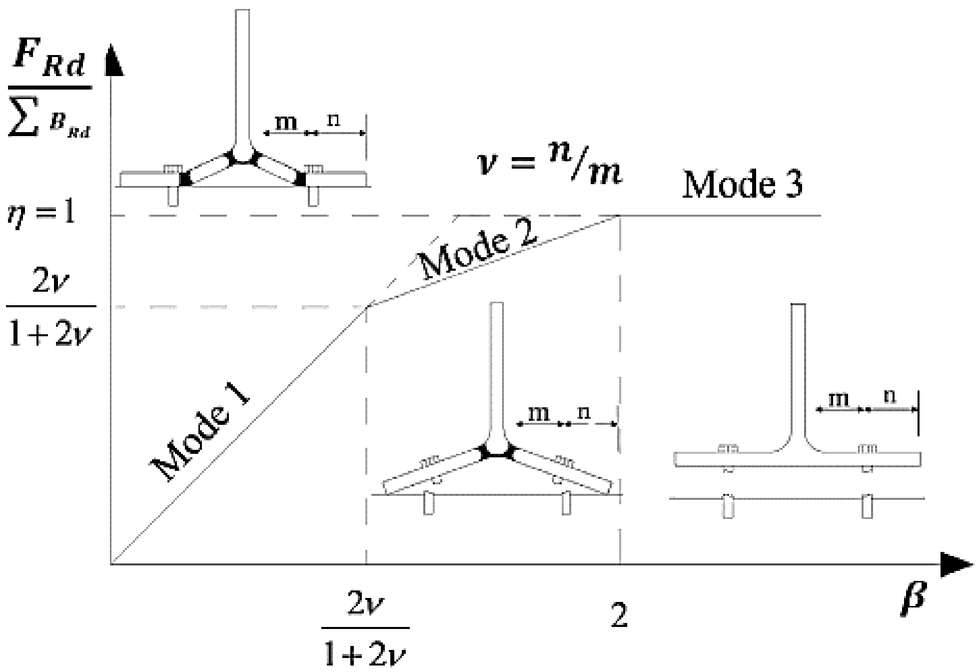

Figure 1.6. *T-stub failure mechanism ranges (Tartagalia et al., 2020)*

1.3. Problem Statement

Prying effects, which depend on many design parameters, can be considerable. Design parameters such as flange thickness, bolt diameter, pretension in bolts, distance from bolt line to the edge of flange, and distance from bolt line to the T-stem, bolt grade, and steel class have been investigated. However, in most of the studies dedicated to prying action and in the analytical formulations for the estimation of prying forces, enough attention has not been given to the moment induced in bolts. This can lead to an underestimation of the prying effects.

1.4. Research Objective

This work aims to provide more insight in prying effects in bolted steel T-stubs subjected to tensile loading. Disregarding the prying action in bolts can lead to an overestimation of the resistance capacity of some connection components. Experimental data in the literature were used to calibrate an advanced finite element model developed. Following the validation of the model, an extensive parametric study was conducted in order to investigate the influence of different material and geometrical properties on the prying effects in bolted steel T-stubs. The prying force, the position of the resultant of contact forces (location of the prying force), the total bolt force and the bending moment in the bolt were evaluated. Using the obtained results, an improved formulation taking into account the flexural engagement was proposed.

1.5. Methodology

Three dimensional finite element analysis was employed in this study. Taking into consideration the element types, mesh, material and contact, the models were constructed using ABAQUS (2004) software and they were calibrated and validated by using relevant test data obtained from literature. Various values related to prying effects were extracted and the influence of many design parameters on these values was investigated in an extensive parametric study. Considering that a large number of data was obtained, a curve fitting process was undertaken with PYTHON (Van Rossum, G. & Drake, F. L., 2009) and an improved formula which incorporates the bending of the bolts was proposed for the estimation of prying force and the bolt moment.

1.6. Dissertation Outline

The dissertation is organized as follows:

Chapter one, which is the introduction, presented the background of this study, the research objectives and the methodology.

Chapter two presents and discusses an overview of previous studies pertinent to this work. Relevant models are also summarized. This chapter is part of an article that was published in the Journal of Constructional Steel Research.

Chapter three reports the modelling, calibration and validation of an advanced FE model using data available in the literature. Following the validation of the model, over 200 models are generated and a parametrical study is conducted to investigate the influence of geometrical parameters such as edge distance, gauge distance and flange thickness on the prying forces and bolt moment. Experimental material properties from the work of Coelho (2004) are used.

Chapter four presents an extensive investigation of both geometrical and material properties on the prying effects in bolted T-stubs. Nominal material properties were adopted, and the investigated parameters included the edge distance, gauge distance, flange thickness, bolt diameter, effective width, weld throat, bolt class and steel grade.

Chapter five is conclusion and recommendations.

2. LITERATURE REVIEW

2.1. Introduction

Prying action is an important feature of bolted T-stubs which has sparked the interest of many researchers. The occurrence of prying effects and their influence on the behavior of bolted connections have been highlighted in many studies. Subsequently, analytical models have been developed and prying action has been incorporated in many strength and stiffness models. Analytical models use the basic concepts of structural analysis: equilibrium, compatibility and material constitutive relations, to evaluate the behavior of T-stubs. In most models, the T-stub element is modelled as a beam with simple supports at the edges. Additionally, prying is accounted for by considering concentrated forces *Q* located at the edges of the flange (See Fig. 2.1). This assumption is reasonable only for specific configurations because in reality, prying forces are the resultant of contact stresses distributed over a certain portion of the flange and its location depends not only on the flexibility of the flange, but also on the flexibility of the bolts.

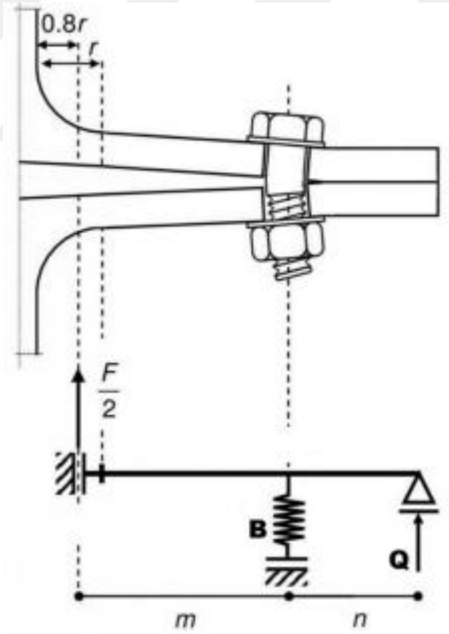

Figure 2.1. *T-stub model with prying force at the edge of the flange*

Some codes such as Steel Construction Manual of AISC (American Institute of Steel Construction [AISC], 2023) provide formulations for the evaluation of prying forces, whereas other codes such as EN 1993-1-8 only consider prying action implicitly.

2.2. Previous Studies and Analytical Models

The earliest studies on T-stubs and prying action include that of **Leahey** & **Munse** (1954). The authors performed both static and fatigue tests on tee connections loaded in direct tension. Authors studied the effect of bolt pretension and concluded that it had little effect on the ultimate load of the connection. Further investigation was carried out by **Munse et al.** (1959), who conducted static tests on symmetrical tee-connections fastened with two and four lines of A325 bolts. The thickness of the flanges and the grip length of the bolts were varied. Changes in the flange thickness were found to have a substantial influence on the bolt efficiency (in a range of 30%); whereas changes in grip length had negligible effect. The authors also observed that, in connections with four-bolt lines, the applied load was carried almost only by the inner bolts. In the early stages of loading, the inner bolts carried the entire load.

Douty & **McGuire** (1965) performed experiments on a variety of T-stubs with two lines of A325 bolts. Flange thickness, edge distance, and the bolt diameter were varied to study their effect on prying forces. Assuming that the flange behaved as a simply supported elastic beam spanning across the edges, the authors developed an analytical model. Before the external load is applied, only pretension load B_0 exerts on the T-stub flange. After the application of the external load, the force on the bolt becomes (F + Q + C) where C stands for the compressive contact force between flange and base plate and where Q stands for prying force acting at the tip line of the flange (see **Fig. 2.2**). Douty and McGuire formulated semi-empirical equations (based on both the analytical model and the test results) to estimate the prying force, respectively, in elastic range (under working load), Q_W, and in plastic range (under ultimate load), Q_U (**Eqs. 2.1 and 2.2**). They emphasized that prying load could not be assessed directly by analytical models without empirical modifications.

With the aim of determining the behaviour and formulating design methods of ASTM A325 and A490 high strength bolts in tee connections**, Nair et al.** (1969) performed series of static and fatigue tests on tee-connections with ASTM A325 and A490 bolts under prying. Authors used experimental results to back an analytical study consisting of parametric numerical analyses. The investigated parameters were: the number, diameter and grip length of the bolts; the bolt type; the bolt pretension and the yield stress of the steel in the tee-connections. The study was based on bolt failure as the critical failure mode of the connection. The experimental and numerical results were used to evaluate prying ratios. Semiempirical equations were formulated for the evaluation of prying force and prying force ratio.

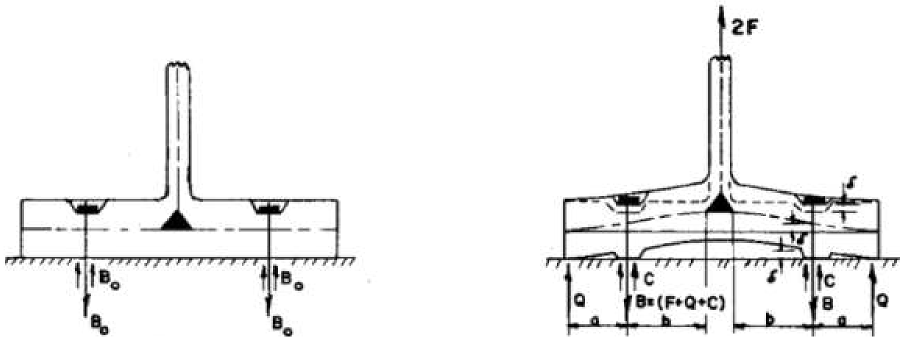

Figure 2.2. *Prying model by Douty and McGuire (1965)* ***(a)*** *before loading* ***(b)*** *after loading*

$$Q_W = \left[\frac{\frac{1}{2} - \frac{wt^4}{30ab^2A}}{\frac{3a}{4b}\left(\frac{a}{4b}+1\right) + \frac{wt^4}{30ab^2A}} \right] F \tag{2.1}$$

$$Q_U = \left[\frac{\frac{1}{2} - \frac{wt^4}{30ab^2A}}{\frac{a}{b}\left(\frac{a}{3b}+1\right) + \frac{wt^4}{6ab^2A}} \right] F \tag{2.2}$$

Aggerskov (1977) conducted a series of tests to measure prying force for different geometries. The author used a similar approach as **Douty & McGuire** (1965) and presented a development for the prediction of prying action that is similar in some major respects to that of **Douty & McGuire** (1965). However, unlike the previous studies, the author took into consideration the effect of shear stresses. He also considers two cases in the study: one where flange separation at bolt location occurs before yield moment is reached and another case where flange separation at bolt location occurs after the yielding of the flange. In the latter, contact force C between the plates at bolt location will be still available when yield moment stress is reached in the flange.

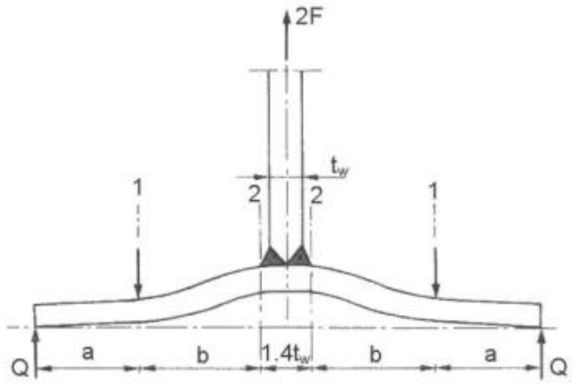

Figure 2.3. *Prying model proposed by Agerskov (1977)*

In the study of the tension side of beam-to-column connections, **Zoetemeijer** (1974) emphasized the role played by prying force in the failure mode of the T-stub and expressed the maximum prying force, *Qmax*, as a function of the moment of the flange and the edge distance.

Kulak et al. (2001) presented analysis and design considerations for tension-type connections, covering prying action. The authors summarized the existing prying models such as that of **Douty & McGuire** (1965), **Agerskov** (1977), **Nair et al.** (1969), and Struik and de Back. In their model, Struik and Back also focused on forces and moments equilibrium. In **Fig. 2.4.a**, α is the ratio of moment at the bolt location (section 1) to the flange moment at the web face (section 2). δ is the ratio of the sectional area at the bolt location to the sectional area of the flange at the inner end. Taking into consideration the bolt deformation and the distribution of contact pressure between the flange and the bolt head, the model of Struik and Back was further improved by substituting a' and b' for a and b. (**Fig. 2.4.b**). Considering that those models were formulated for specific bolt and plate combinations, **Kulak et al.** (2001) suggested a more general methodology for prying forces and design recommendations for T-stubs.

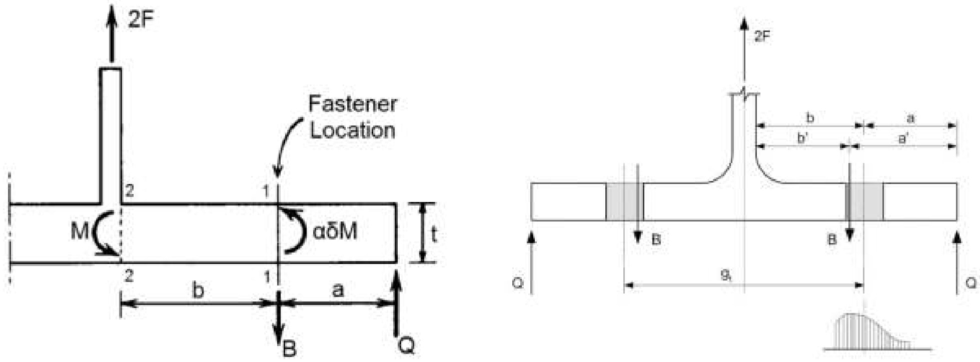

Figure 2.4. ***(a)*** *Prying model by Struik and Back* ***(b)*** *Influence of flange deformations on the location of resultant bolt force (Atasoy, 2012)*

The previous analytical models being restricted to specific bolt-plate combinations, **Thornton** (1985) presented a more general model that includes all significant parameters influencing the prying action. It is one of the main works that allowed the development of the current prying provisions of AISC.

In addition to the traditional simply supported beam model, some researchers suggested different models. An equivalent frame model (**Fig. 2.5**), designed for hand calculation, has been developed by **Loureiro et al.** (2010) to predict the axial stiffness of non-preload T-stubs. The flanges and the bolts are modelled using the beam analogy. The results of an implemented FE model showed reasonable agreement between the numerical value of m, the distance between the plastic hinges, and the value suggested by Eurocode 3 provisions, m_{EC3}. The numerical value of m is obtained by evaluating the center of gravity of the plastic strain area (**Fig. 2.6**) whereas m_{EC3} is computed by using **Eq. 2.3**. A parametric study was carried out to obtain an expression of the flange effective width to be used in the model. The authors also provided an expression for the prying forces and estimations of the total bolt force ratio B/F, where B is the total force in the bolt and F is the load applied on the T-stub. The work later was extended to preload bolts by **Reinosa et al.** (2013).

$$m_{EC3} = d - 0.8r \tag{2.3}$$

d is the distance between the bolt axis and the interior face of the T-stub web, and r is the root radius.

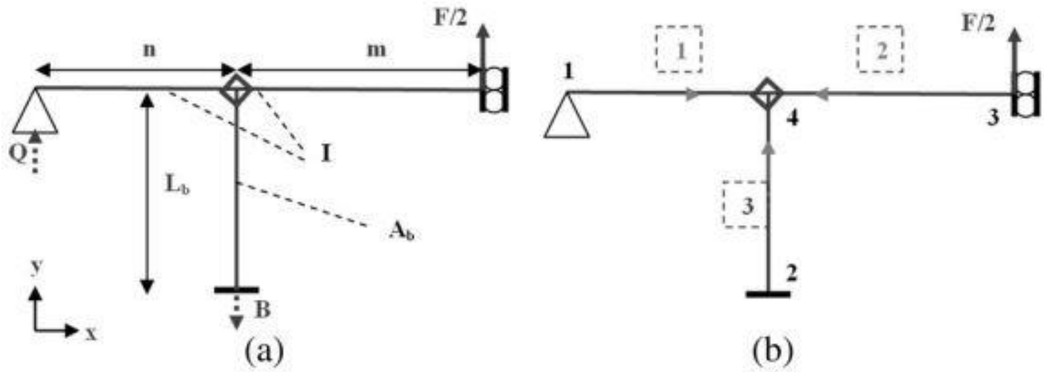

Figure 2.5. *Equivalent frame model (Loureiro et al., 2010)*

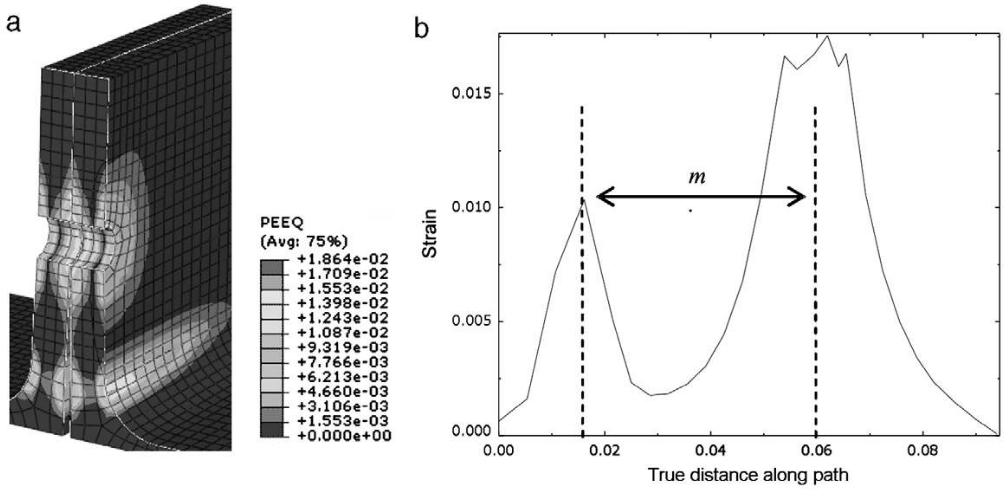

Figure 2.6. ***(a)*** *Equivalent plastic strain in the flanges and* ***(b)*** *measured distance between the plastic hinges (Loureiro et al., 2010)*

Simon and Hengehold (1978) implemented a FE model that could accurately simulate prying action in bolted joints. Being one of the first numerical studies on prying action, the authors aimed at providing guidelines in the analysis of bolted joints by a detailed procedure. Several factors were investigated: bolt-flange interaction, application of preload, and nonlinear effects of plate separation.

Atasoy (2012) performed approximately 1800 FE analyses on L and T bolted connections with various design combinations. Using the FEA results, the author suggested some corrections for the expressions formulated by Douty and McGuire and Struik and de Back, depending on the ratio of the flange thickness to the bolt diameter, *t/D*.

Similarly, **Bezerra et al.** (2020; 2022) conducted a numerical investigation into the influence of the flange thickness on the magnitude and location of the prying force. The authors concluded that the existing analytical models, which assumes a fixed location of the prying force, could not adequately represent the prying action.

Yang et al. (2013; 2013) proposed an improved analytical model to predict the initial axial stiffness and the ultimate strength of a T-stub, taking into account prying action. The foundation of the model was set through an experimental program supplemented with a finite element analysis. The authors suggested correcting the bolt action line based on bolt stress distribution obtained from the numerical analysis. The following equations were proposed:

$$a' = a + 0.3d_b \tag{2.4}$$

$$b' = b - 0.3d_b \tag{2.5}$$

The effects of bolt spacing on prying force in tee-connection were the aim of the experimental study carried out by **Raebel et al.** (2013). The results were compared to the AISC prying model. A decrease in prying force could occur as spacing exceeds 2.0*b*. The authors suggested that AISC provisions could be improved to take advantage of the reduction in prying force at lengths exceeding 2.0*b*.

In double tee moment connections, prying may develop due to tee-flange bending deformation (primary prying) or column flange bending deformation (secondary prying). An experimental investigation into secondary prying was performed by **El Kalash & Hantouche** (2018). Seven specimens, designed to cover all possible failure modes, were tested under cyclic and monotonic loadings. Using the beam model, the authors suggested a mechanical approach to predict the behaviour of the connection in terms of force-deformation curve, bolt force variation, and energy dissipation.

Hantouche et al. (2012; 2015) investigated prying action in T-stub connections. The authors focused on thick-flange built-up T-stub connections where the deformation of the column flange can be significant. Considering the effect of secondary prying, the total amount of prying that develops in the connection is evaluated to allow for a more suitable design of the bolts. Further efforts were made to create a stiffness model to predict the behaviour of thick-flange in built-up T-stub connections. Using finite element results, **Hantouche et al.** (2013) proposed a modified stiffness model to predict the behaviour of thick-flange in built-up T-stub connections with Complete Joint Penetration (CJP) and fillet welds. Deformations from tension bolt elongation, T-stub flange, and prying force were modelled using linear and nonlinear springs (Fig. 9). A model including primary and secondary prying effects was also suggested by **Hantouche and Abboud** (2014) for the prediction of the behaviour of bolted thick built-up T-stub connections. Furthermore, **Hantouche et al.** (2012) conducted a series of tests and FE analyses, and the results were used to establish prying ratios for thick-flange built-up T-stub connections with CJP and fillet welds. Afterwards, the authors proposed a subsequent design procedure taking into account the magnitude of prying forces.

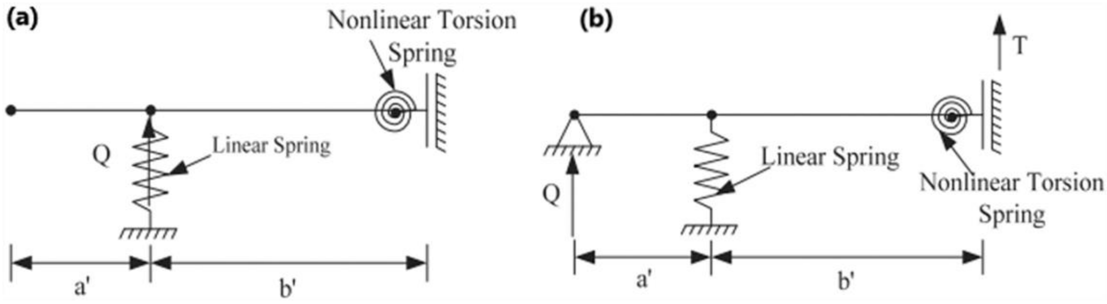

Figure 2.7. *T-stub model: **(a)** at the end of pretension **(b)** at the end of monotonic T-stem load (Hantouche et al., 2013)*

Prying force is commonly represented by a couple of forces acting at the edges of the T-stub flange. This assumption, which can be valid for thick flanges, is a simplification of the reality. Prying force is a distributed action over a certain region of the flange. The location of the resultant force is dependent on the location of the bolts and the stiffness of both the bolts and the T-stub flange. **Chasten et al.** (1992) carried out a study to investigate contact force distribution between the end-plate and column flange and determine the magnitude and location of the prying forces. It was found that the prying force resultant is not located at the plate edge. For design purposes, the authors recommended using the more conservative $x = 0.6lv$. **Couchaux et al.** (2017) proposed a mechanical model (**Fig. 2.8**) to predict the elastic behaviour of L-stubs and T-stubs. The model was based on an improved beam model. 3D finite element models were used for the validation of the model. According to the different contact cases, expressions of the total bolt force, separation length, and prying force location were given. The authors concluded that the magnitude of the external load did not affect the contact zone length in a non-preloaded connection.

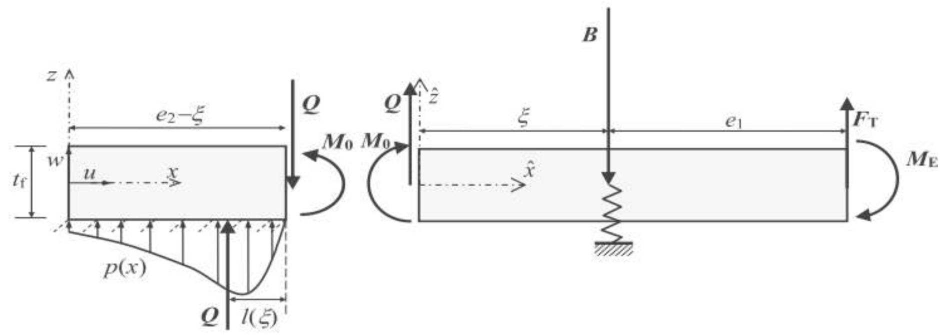

Figure 2.8. *Mechanical model with surface contact (Couchaux et al., 2017)*

Furthermore, stressing that traditional approaches, which assume a fixed location of the prying force, could underestimate the prying force in an elastic analysis, **Hu et al.** (2020) carried out analyses for evaluating the bolt force and the prying force using three different approaches: the Euler-Bernoulli beam model where the shearing deformations are not considered, the Timoshenko model where beam shear deformation effect are considered, and a three-dimensional finite element analysis using SolidWorks. More recently, **Khani et al.** (2023) used the energy method to derive analytical formulas for the assessment of the ratio of prying to the applied load and the location of the prying force. The authors considered two cases. In the first case, the shear deformation effect was disregarded whereas in the second case, it was taken into consideration. The performance of the method was tested against experimental and numerical models. The formulas yielded reasonable accuracy. The authors concluded that the previous models that assumed the location of the prying force at the edge of the flange resulted in an underestimation of the real value of the prying force.

These rules are, yet, insufficient. In fact, prying effect doesn't only cause an increase in bolt force; it also results in a flexural engagement of the bolts, mostly in thinner flanges. The phenomenon was already reported in early studies such as that of **Nair et al.** (1969), **Piluso et al.** (2001), **Coelho** (2004) and **Coelho et al.** (2004). In their work, **Sherbourne & Bahari** (1996) investigated some critical features of T-stub behaviour, such as prying action (magnitude and location) and the influence of the thickness of the T-flange. The authors also emphasize the bending of the bolts. The work, which was part of a comprehensive research program, is usually cited as one of the pioneering works on the numerical study of bolted connections. Several authors such as **Piluso & Rizzano** (2008) and **Hu et al.** (2011; 2012) recommended that bolt bending should be considered in the design model.

On the one hand, several authors investigated the effect of bolt bending on the resistance and stiffness of T-stubs, and suggested ways of taking it into account. **Stamatopoulos & Ermopoulos** (2010) carried out a finite element investigation into the influence of the flange flexibility on the ultimate resistance of T-stubs. The authors developed an analytical model considering the bolt bending due to flange deformation (**Fig. 2.9**).

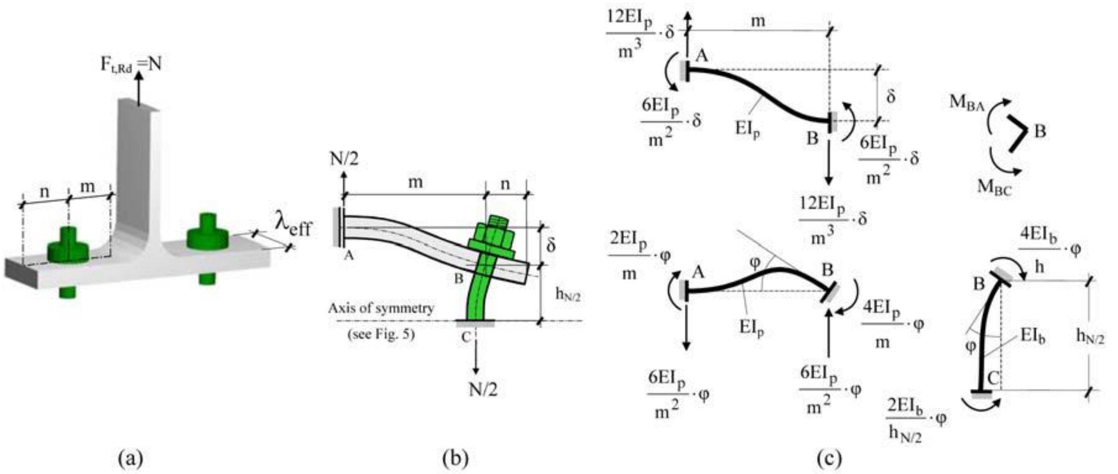

Figure 2.9. *(**a**) Typical T-stub element, (**b**) half part in the deformed state, and (**c**) sign convention (Stamatopoulos & Ermopoulos, 2010)*

The combined tension and bending that develop in the bolts due to the deformation of the T-stub flanges were also the focus of the numerical study carried out by **Abidelah et al.** (2014). The ultimate plastic resistances of the bolts were analysed by using interaction curves. A modified model was suggested to consider the effect of the bolt bending by adding rotational springs. More recently, using the principle of the stationary value of strain energy, and taking into account the effect of prying action on the initial stiffness, **Qiang et al.** (2020) developed models to predict the prying force position. The authors considered both the case where bolt bending is disregarded (Non-thin-walled T-stubs) and the case where it is considered (thin-walled T-stubs) (see **Fig. 2.10**).

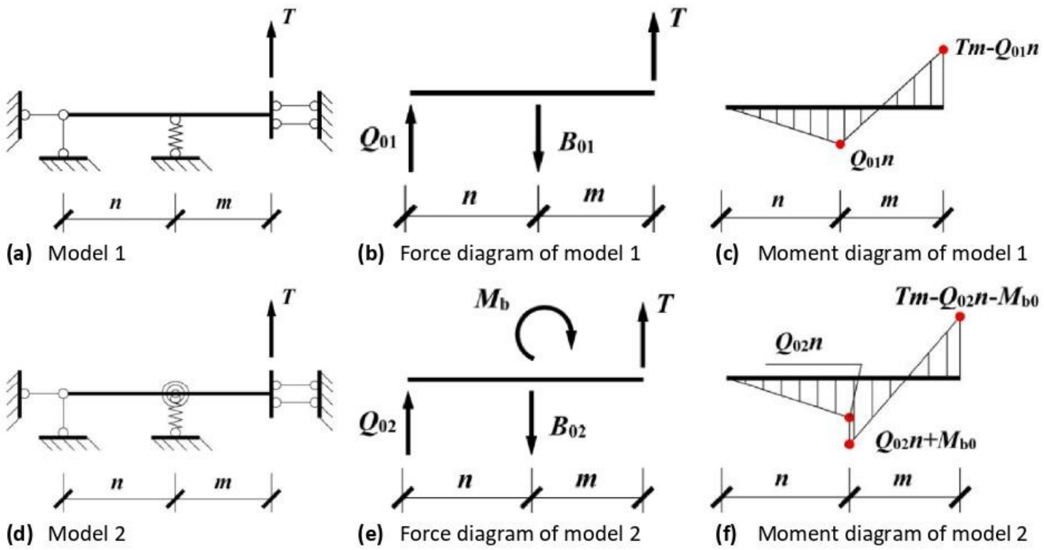

Figure 2.10. *T-stub models (**a**) disregarding bolt bending (**b**) considering bolt bending (Qiang et al., 2020)*

Tartaglia et al. (2020) examined the behaviour of bolted T-stubs under large deformations. Two types of bolt assemblies were investigated: HR bolts, designed to obtain ductility predominantly by plastic elongation of the bolt (EN 14399-1:2015) and covered by EN 14399-3:2015; and HV bolts, designed to obtain ductility predominantly by plastic deformation of the engaged threads (EN 14399-1:2015) and covered by EN 14399-4:2015. Other parameters included the flange thickness and the edge distance. Concerning the edge distance, two values were considered: the minimum value and the maximum value (1.25 m) defined by EN 1993-1-8. Bolts were subjected to bending and shear, with considerable shear in specimens with short flanges. The authors suggested a range of values for the resistance reduction factor to account for the bending and shear. Also, a broad experimental, numerical and analytical investigation carried out by **Faralli et al.** (2021) showed that possible bolt failure could occur due to the combined actions of shear, tension, and bending. The authors proposed an analytical model that could take into consideration 2^{nd} order effects.

On the other hand, few attempts have been made in order to provide assessment of bending moment that occurs in bolts. **Bao et al.** (2019) performed six static tests on bolted T-stubs, supplemented with finite element models, to investigate the behaviour of bolts. The effects of the flange thickness, bolt position, and bolt diameter were studied. The authors found a bending moment distribution relationship between the bolt and the outer flange. Using that relationship, the authors developed formulas to assess total bolt force (hence prying force) and bending moment. After discussing and comparing the prying provisions in several codes - namely Chinese code, Eurocode 3 (EN 1993-1-8:2005), Hong Kong code and AISC manual, **Bai et al.** (2015) proposed corrections and formulas for assessing prying forces and bending moment in the bolts.

2.3. Conclusion

The equivalent T-stub model is often used to stimulate the tensile response of some components of steel connections. The T-stub model has been investigated in numerous studies. Various aspects of the behaviour under static and cyclic loading have been examined, including the strength, stiffness, deformation capacity, prying action. Although the provisions in the existing codes can yield reasonable predictions of the strength and stiffness, additional studies are necessary for the prying effects which can result in a combined increased bolt tension and bending moment and cause a premature failure of the bolts. The consideration that prying forces are concentrated forces acting at the edge of the flange is not always correct. As for the flexural engagement of the bolts, it has been the focus of few studies and the attempts to evaluate the bolt bending are still scarce. Improved formulations, taking into account bolt bending, prying force, and the location prying force and their effect on the T-stub behaviour, are essential for a more adequate design of bolted connections

3. NUMERICAL MODELLING OF STEEL BOLTED T-STUBS

3.1. Introduction

In the first part of Chapter 3 (section 3.2), the potential and the advantages that present FE modelling are reported.

In the second part of the Chapter 3 (section 3.3), a numerical model, which is built in ABAQUS upon a previous experimental research on bolted steel T-stubs in tension conducted by **Bursi & Jaspart** (1997) and **Coelho** (2004), is reported in detail. The development and validation of an advanced FE model able to satisfactorily predict the behaviour of bolted Tstubs in tension is reported in detail.

In the third part of Chapter 3 (section 3.4), the calibrated model is used to generate 226 models and carry out a parametrical study in order to examine the influence of the flange thickness, the edge distance and the gauge distance on the prying action in T-stubs; more precisely on the forces and moments that the bolts may be subjected to.

3.2. Numerical Modelling and Validation

Due to the various components involved, as well as nonlinearities (material nonlinearities, contact nonlinearities…), steel bolted connections exhibit a nonlinear behavior. The determination of this behavior is very complex. Several methods are available for determining the behavior of connections. Experimentation, which is the most accurate method, is costly in terms of time and money. It is practically limited to research activities. Besides, the results being limited in number, they do not allow to cover all configurations. Numerical (finite element) modelling can be used as an alternative to experimentation for some reasons:

(i) numerical models can yield results that offer good agreement with experiments.
(ii) finite element models are able to describe some phenomena such as contact stress distribution that cannot be accurately measured experimentally.
(iii) a wide range of configurations can be covered; allowing for parametrical studies and analytical formulations.

The last decades have seen an increasing use of FE modelling due to progress in computer technology and non-linear numerical algorithms. The most commonly used software packages are ABAQUS and ANSYS which are capable of predicting the behavior of simple or complex connections. In this study, a finite element model of bolted steel T-stubs was developed in ABAQUS. The model incorporated geometrical, material and contact nonlinearities.

3.2.1. Geometrical properties

A finite element model was developed in ABAQUS and calibrated with test data obtained from the work of **Bursi & Jaspart** (1997) and **Girão Coelho** (2004). The specimens WT1 from **Coelho** (2004) and T1 from **Bursi & Jaspart** (1997) were selected for the calibration procedure. The geometrical characteristics of the specimens are depicted in **Fig. 3.1** and **Fig. 3.2**, and specified in **Table 3.1** and **Table 3.2.**

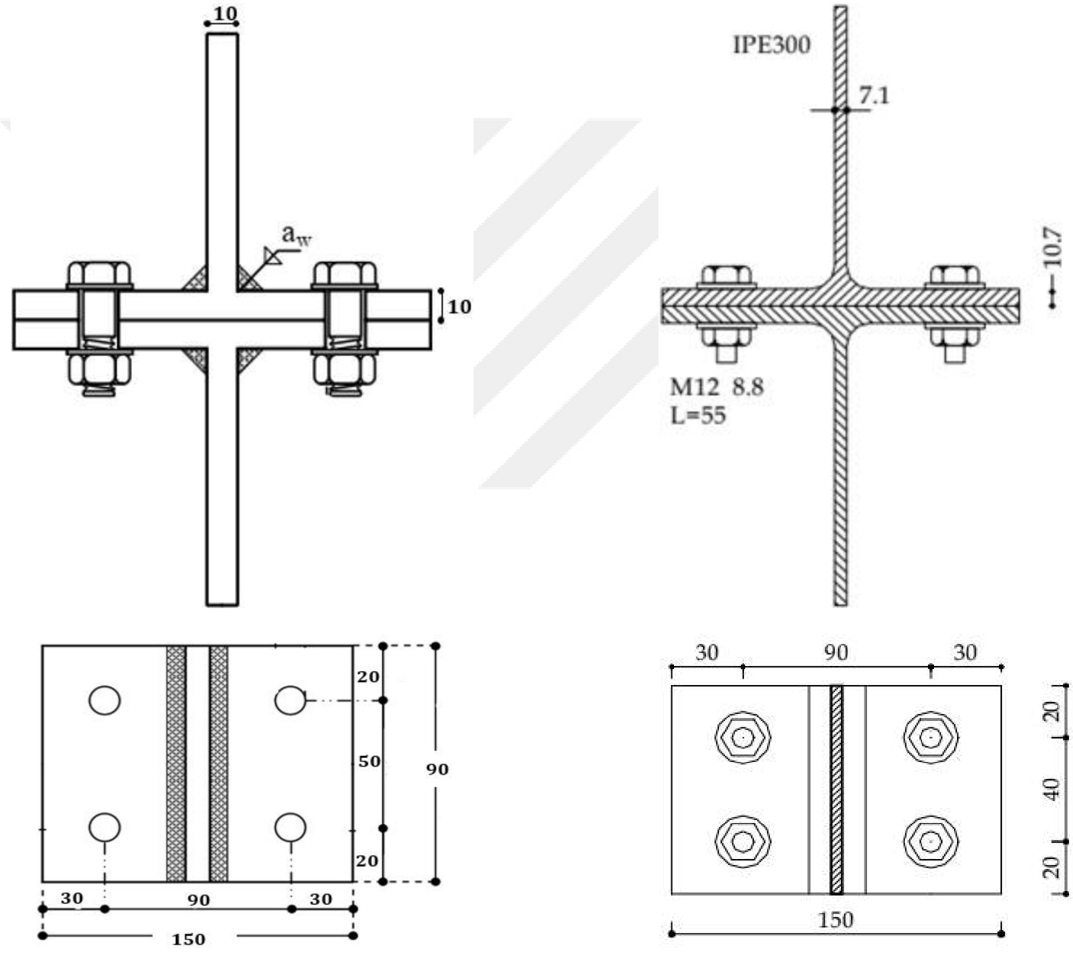

(a) *(b)*

Figure 3.1. *Geometrical characteristics and cross section of **(a)** WT1 specimen (Girão Coelho, 2004) and **(b)** T1 specimen (Bursi & Jaspart, 1997)*

The diameter of the bolt hole and shank were taken equal to the nominal bolt diameter. Considering that the bolt head and nut dimensions were not provided, the nominal values mentioned in DIN EN 14399-4 were used (See **Table 3.1**). Also, in compliance with the experimental conditions, the washers were not modeled.

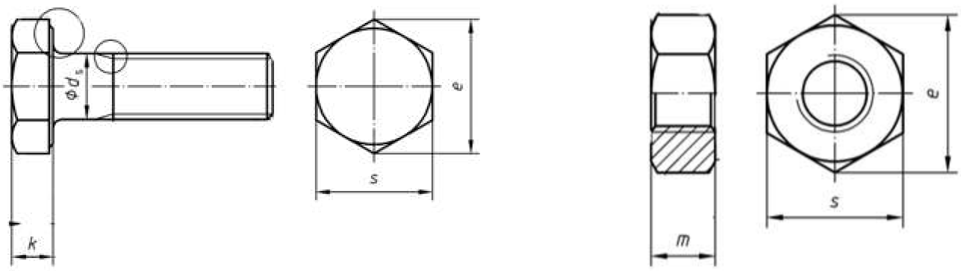

(a) *(b)*

Figure 3.2. *Bolt head and nut dimensions*

Table 3.1. *Bolt head and nut dimensions for M12 bolts (DIN EN 14399-4)*

Bolt head		Nut	
k	***s***	***m***	***s***
8 mm	22 mm	10 mm	22 mm

Table 3.2. *Geometrical properties of the specimens*

	Specimen WT1	**Specimen T1**
$\boldsymbol{n}$	30 mm	30 mm
$\boldsymbol{w}$	90 mm	90 mm
$\boldsymbol{e_1}$	20 mm	20 mm
$\boldsymbol{p}$	50 mm	40 mm
$\boldsymbol{t}$	10 mm	10.7 mm
$\boldsymbol{t_w}$	10 mm	7.1 mm
$\boldsymbol{a_w}$	5 mm	-
$\boldsymbol{\emptyset_b}$*	12 mm	12 mm
t: flange thicknes		t_w: web thicknes
$\emptyset_b$: bolt diameter		

3.2.2. Material properties

An elastoplastic constitutive law with isotropic strain hardening based on the Von Mises yield criterion is adopted for the material nonlinearity. The failure condition was set as the attainment of the ultimate strain ε_u either for the bolt or any component of the T-section. For good correlation with experimental results, the entire stress-strain curves of the materials were adopted in the FE models (see **Fig. 3.3**). As a simplification, the welds in the WP-T-stubs were provided the same material properties as the T-flanges and T-webs.

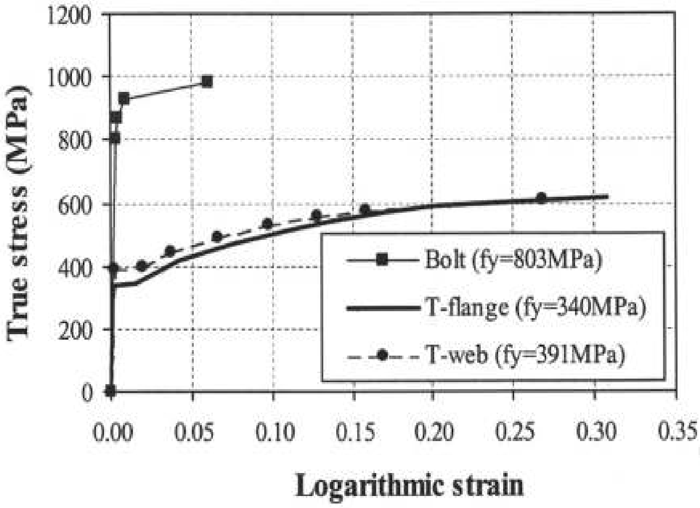

(a)

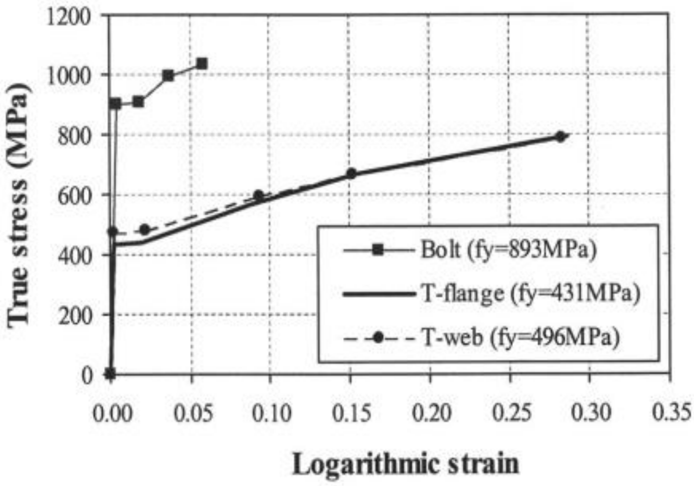

(b)

Figure 3.3. *True stress-logarithmic strain material laws:* ***(a)*** *specimen WT1 (Coelho, 2004)* ***(b)*** *specimenT1 (from Bursi and Jaspart, 1997)*

3.2.3. Meshing

The different components - namely webs, flanges, welds, and bolt – were meshed using solid elements C3D8R (i.e., 8-node linear brick with reduced integration). C3D8R elements, which present advantages such as reduced computation time and hour-glass control, yielded satisfactory results. In order to have an appropriate element shape, the "Structured" meshing technique was utilized for most elements, except from the fillet radius in the case of specimen T1. “Sweep” meshing was used because “Structured” meshing led to poor meshing for fillet radius (See **Fig. 3.4**).

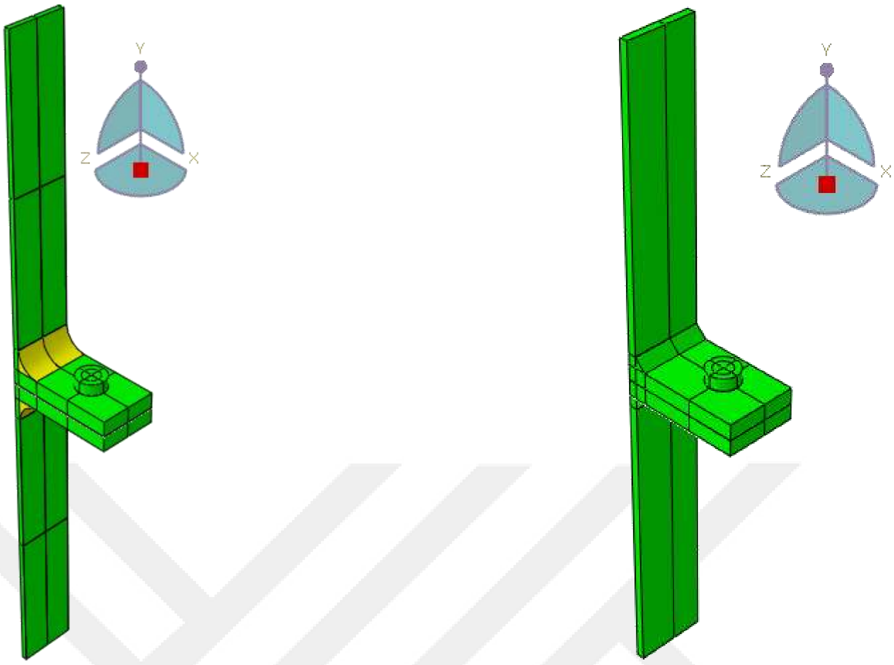

(a) ***(b)***

Figure 3.4. *Meshing techniques for* ***(a)*** *specimen T1 and* ***(b)*** *specimen WT1*

The mesh size and the flange discretization (number of elements through the thickness) were investigated. A mesh sensitivity study was carried out to obtain a model with satisfactory results and acceptable computation time. The bolt and the T-stub mesh sizes were identical and chosen proportionally to the thickness T-stub flange. Three mesh sizes were examined: $t_f/3$, $t_f/5$ and $t_f/10$. An element size of $t_f/3$ was deemed adequate. In the aftermath, T-stub models with different flange discretizations were investigated. Previous studies concluded that, for problems involving bending, a minimum of three elements through the plate thickness is recommended to ensure accurate results (Faella et al., 1998). Consequently, in our study, models with 3, 4, 5, 7, and 10 elements through the flange thickness were compared. The model with seven elements through the flange thickness was chosen because it yielded satisfactory results within a reasonable computation time.

3.2.4. Modeling of contact elements

For contact interactions, standard surface-to-surface formulation with finite sliding was defined. It requires the definition of "master" and "slave" surfaces. The considered pairs were:

- Bolt head and nut – flanges
- Flanges – webs
- Upper flange – Lower flange
- Bolt shank – Bolt hole

The contact properties were defined such that the normal behavior was simulated with hard contact, while the classic isotropic Coulomb friction law was used to model the tangential behavior. A penalty friction coefficient of 0.25 was taken, as suggested by the authors (Coelho, 2004; Bursi & Jaspart, 1997). Considering that, in reality, the bolt holes are larger than the bolt diameters, frictionless contact properties was considered in the hole area. Additionally, the welds were attached to the T-web and the T-flange by using tie constraints.

3.2.5. Boundary and loading conditions

Adequate boundary conditions and loading patterns are among the requirements for an efficient numerical simulation. The boundary conditions should reflect those of the tests. Hence, the end of the lower T-web was fully fixed; only the end of the upper T-web was allowed to move in the direction of the applied load.

Making use of symmetry, if any, it is possible to avoid modelling the whole T-stub. Generally, YZ and YX planes may be geometrical planes of symmetry. However, the XZ plane cannot be strictly considered a symmetry plane because the bolt heads and nuts generally possess different rigidities. For this reason, in our model, only YZ and YX symmetry planes were considered by applying both X- and Z-symmetry boundary conditions (See **Fig. 3.5**). Consequently, a reduced model (see **Fig. 3.6**), requiring less memory and computing time than the full model, was obtained.

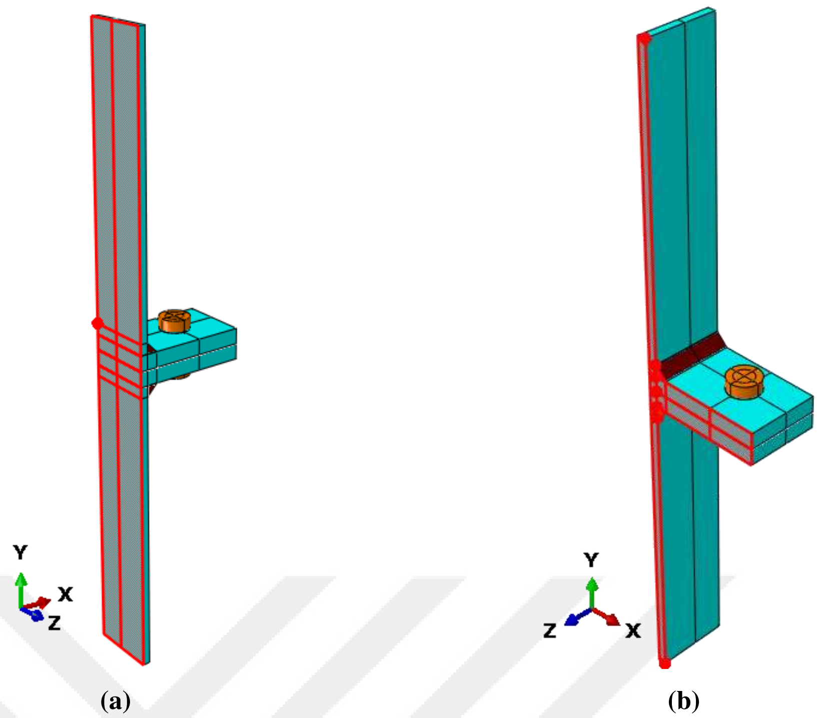

Figure 3.5. *Symmetry applied in X-direction* ***(a)*** *and in Z-direction* ***(b)***

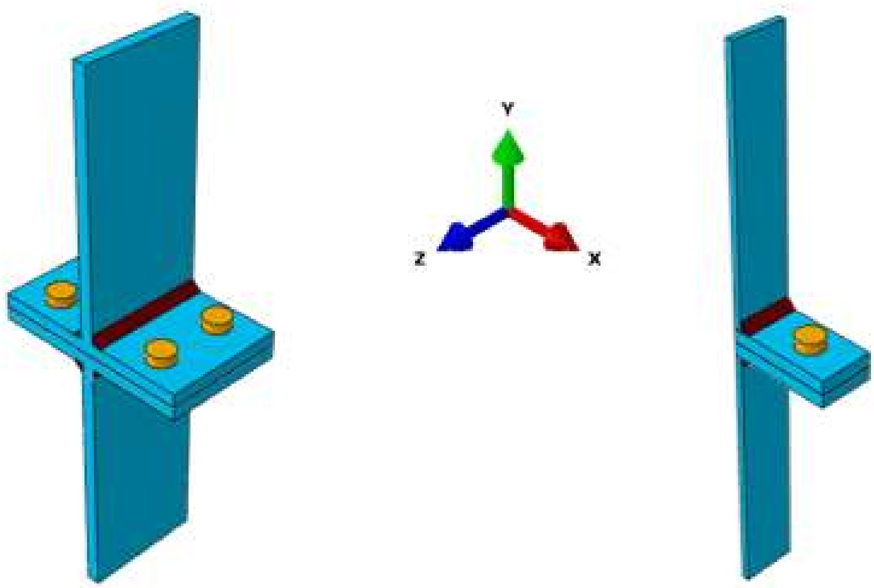

Figure 3.6. *Original T-stub and its reduced model*

The load was applied at the top of the upper T-web in the positive Y-direction by displacement control. The results of both displacement-controlled and load-controlled analyses were compared and were proven to yield similar results. However, displacement control could offer better convergence conditions (Lemonis & Gantes, 2003).

3.2.6. Model Validation

Following the sensitivity analysis, an element size of $t_f/3$ and seven elements through the flange thickness were deemed adequate. Numerically, the failure criterion was set as the attainment of the ultimate strain ε_u without considering ductile damage.

For the model validation, it is important to compare the load-deformation curve, which is the most significant characteristic describing the overall behavior of the model, as well as the failure mode of the model. The load-displacement curves obtained from the FE analyses showed satisfactory agreement with the experimental curves **(Fig. 3.7)**.

For the T-stub specimen WT1, the experimental observations indicated that, at a deformation level around 14 mm, there was a smooth drop of load that continued until bolt fracture at 20.5 mm. As a consequence, the curve obtained from the finite element modelling stopped at a deformation level of 13.5 mm, showing a rather good agreement with the experimental results. As for the T-stub specimen T1, an ultimate deformation of 9.20 mm was reached, which is very close to the experimental value ~9.49 mm. For both specimens, the experimental observations revealed combined failure involving significant flange yielding (with cracking of the flange in the heat affected zone of the welds for WT1) and bolt fracture. Although, the experimental cracking in the welded zone was not observed in the finite element model, a pronounced yielding was observed(**Fig. 3.8.** and **Fig. 3.9**). The difference may derive from the modelling of the fillet weld and the heat affected zone, near the weld toe. In fact, the welding process can render the material more brittle. These effects are complex to quantify and take into consideration. Therefore, they were not included in the simulations and the welds in the WP-T-stubs were provided the same material properties as the T-flanges and T-webs.

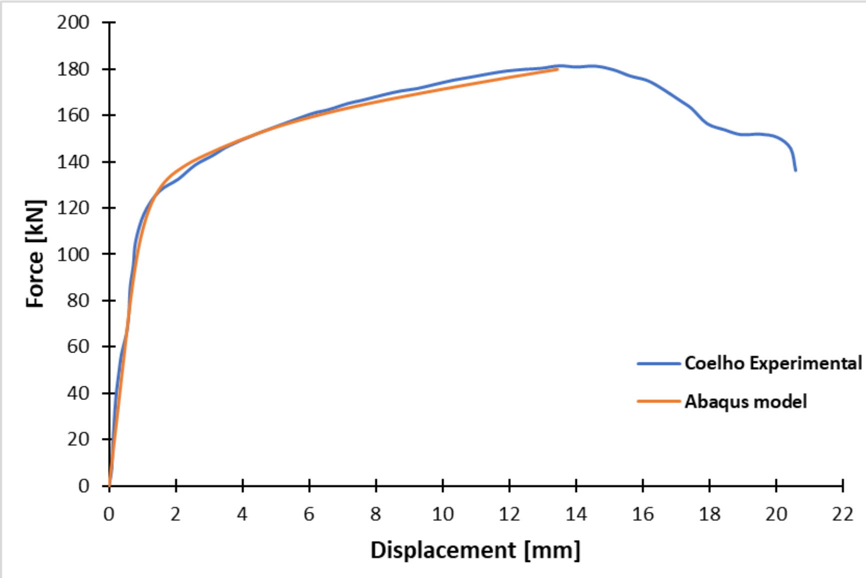

(a)

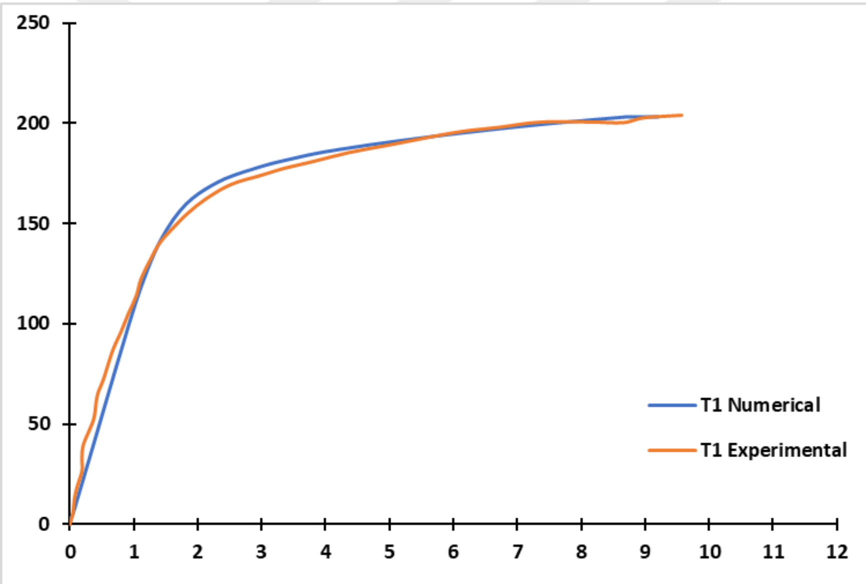

(b)

Figure 3.7. *Comparison of the experimental and numerical F-D curves of* ***(a)*** *WT1 and* ***(b)*** *T1 specimens*

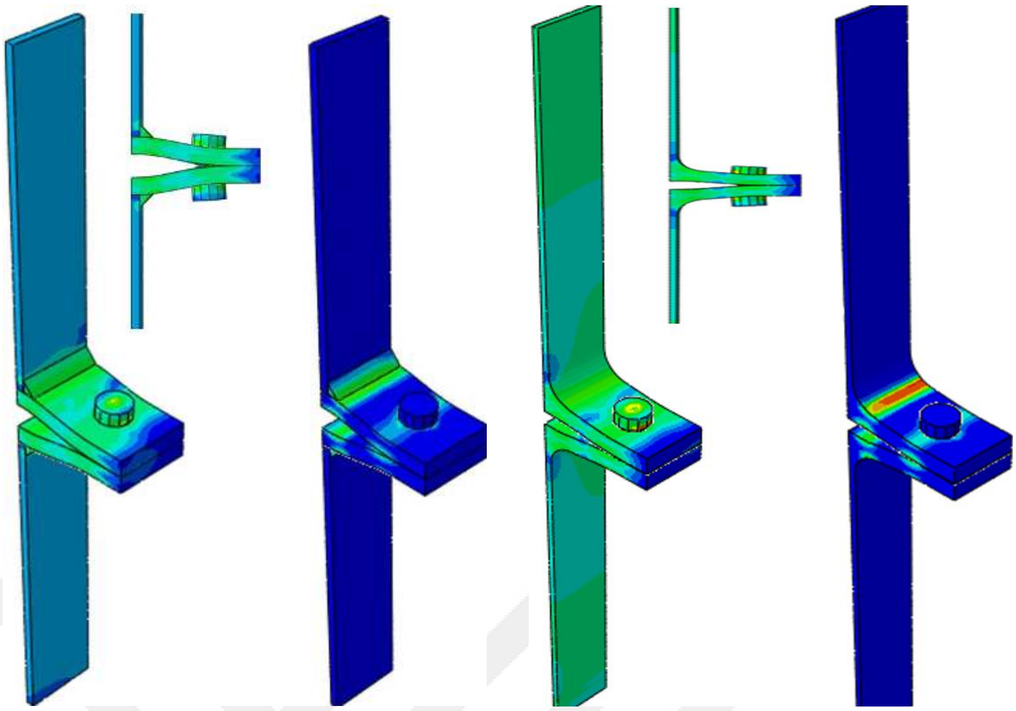

(a) *(b)*

Figure 3.8. *Deformation and yielding status at ultimate stage of* ***(a)*** *specimen WT1 and* ***(b)*** *specimen T1*

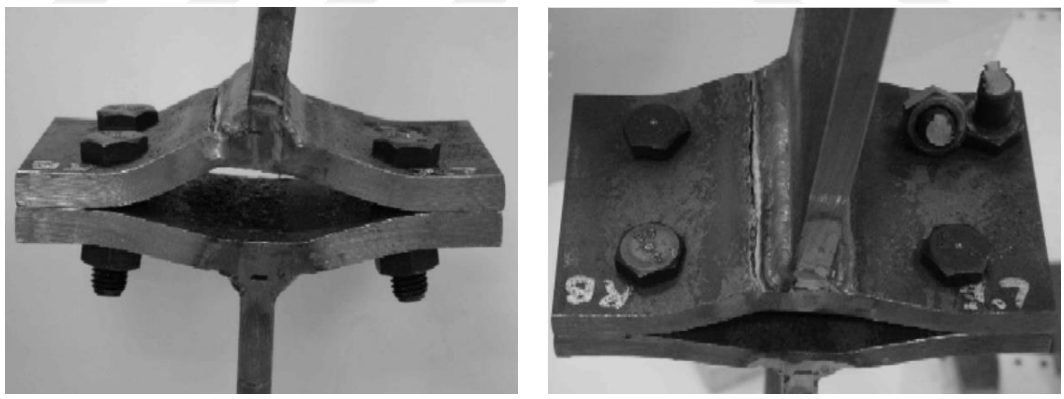

(a) **(b)**

Figure 3.9. *Front view* ***(a)*** *and top view* ***(b)*** *of specimens WT1 after failure (Girão Coelho, 2004)*

3.3. Parametrical Study

The calibrated model was used to generate 226 WP-T-stub models in order to carry out a parametrical study. The investigated parameters were flange thickness t, edge distance n, and gauge distance w. The edge distance and gauge distance value ranges were chosen in agreement with the provisions of EN 1993-1-8 (**Table 3.3**)

For the models included in the parametrical study, only X-symmetry was considered. In fact, unlike the initial T-stubs that had four bolts and a width $b = 2e_1 + p$ (see **Fig. 3.1**), the T-stubs involved in the parametrical study had only two bolts and a width $b = 2e_1$ (see **Fig. 3.10)**

Table 3.3. *Minimum and maximum of edge distance and gauge distance allowed by EN 1993-1-8*

Parameter	Minimum value according to EN 1993-1-8	Maximum value according to EN 1993-1-8
Edge distances	14.4 mm	80 mm for t = 10 mm 100 mm for t = 15 mm 120 mm for t = 20 mm
Gauge distances (spacing)	26.4 mm	140 mm for t = 10 mm 200 mm for t = 15 mm 200 mm for t = 20 mm

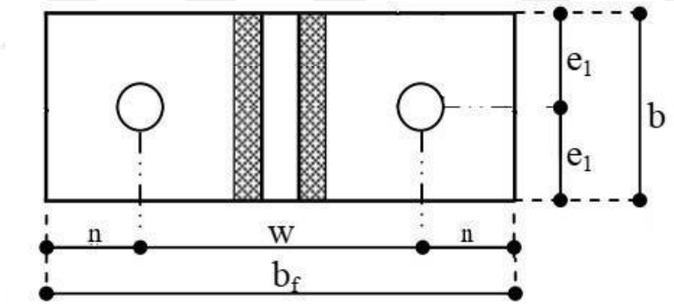

Figure 3.10. *Geometrical characteristics of the specimens involved in the parametrical study*

Table 3.4. *Geometrical properties of the specimens*

	Specimen	Parametrical study			
	WT1	$t = 8\,mm$	$t = 10\,mm$	$t = 15\,mm$	$t = 20\,mm$
n	30 mm	15 – 50 [mm]	15 – 70 [mm]	15 – 100 [mm]	15 – 100 [mm]
w	90 mm	50 – 110 [mm]	50 – 140 [mm]	60 – 200 [mm]	70 – 200 [mm]
e_1	20 mm	50 mm	50 mm	50 mm	50 mm
p	50 mm	-	-	-	-
$t = t_w$	10 mm	8 mm	10 mm	15 mm	20 mm
a_w	5 mm	5 mm	5 mm	8 mm	8 mm
$\emptyset_b$*	12 mm	12 mm	12 mm	12 mm	12 mm

* t: flange thickness t_w: web thickness $\emptyset_b$: bolt diameter

The same material properties were used for all the thicknesses based on the similarities of the true stress-strain curves for flange thicknesses of 10, 15, and 20 mm (Faralli et al., 2021). In order to extend the study of the behavior of T-stubs with thin flanges, 8 mm thickness was also included.

3.4. Results of the Numerical Parametric Investigation

3.4.1. Failure modes

Following the validation of the numerical model, 226 models are generated to study the influence of parameters such as flange thickness t, edge distance n, and gauge distance w. With reference to steel T-stubs, EN 1993-1-8 highlights three possible failure modes: complete yielding of the flange (Mode 1), bolt failure with yielding of the flange (Mode 2), and bolt failure (Mode 3). Failure mode 2 was observed in specimens with a flange thickness of 8 mm and 10 mm for short edge and gauge distances. Minor deformation of the flange occurred, and the bolt was subjected to bending deformation. As n and w increased, the failure mechanism shifted closer to mode 1. Bolt failure associated with yielding at both the web-to-flange toe region and bolt line region was observed. The flange exhibited double curvature deformation, and the bending of the bolt was more pronounced **(Fig. 3.11, Fig. 3.12).**

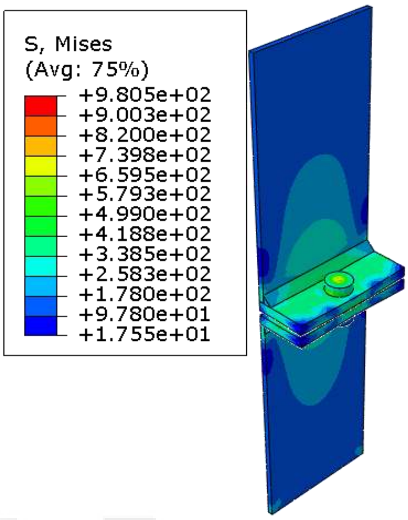

(a) n = 15 mm & w = 50 mm

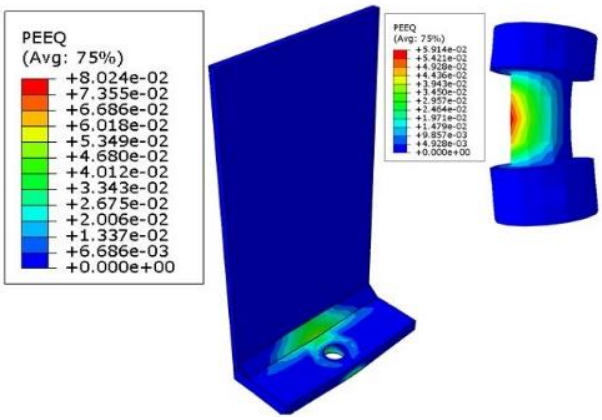

(b) n = 15 mm & w = 50 mm

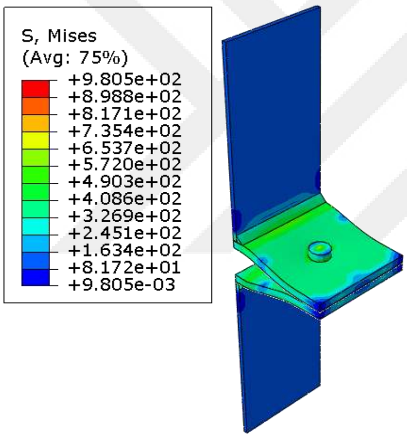

(c) n = 50 mm & w = 110 mm

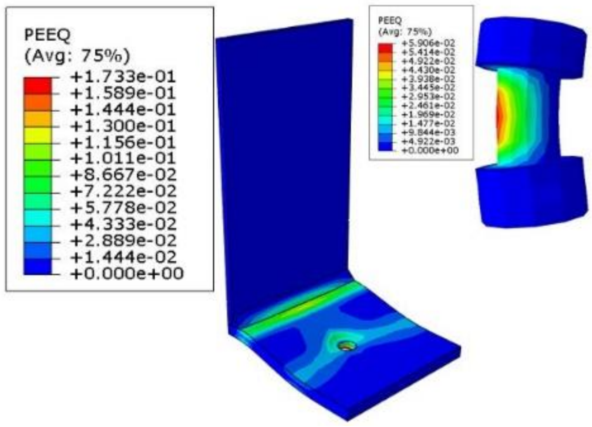

(d) n = 50 mm & w = 110 mm

Figure 3.11. *Ultimate stage of specimens of t = 8 mm*

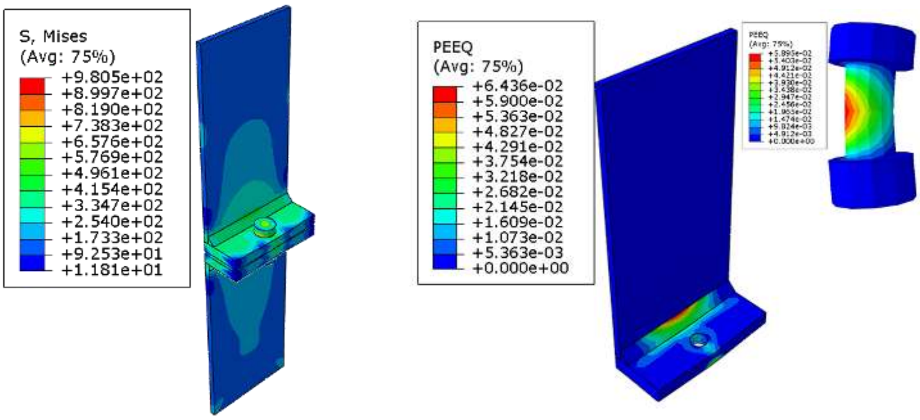

(a) n = 15 mm & w = 50 mm **(b) n = 15 mm & w = 50 mm**

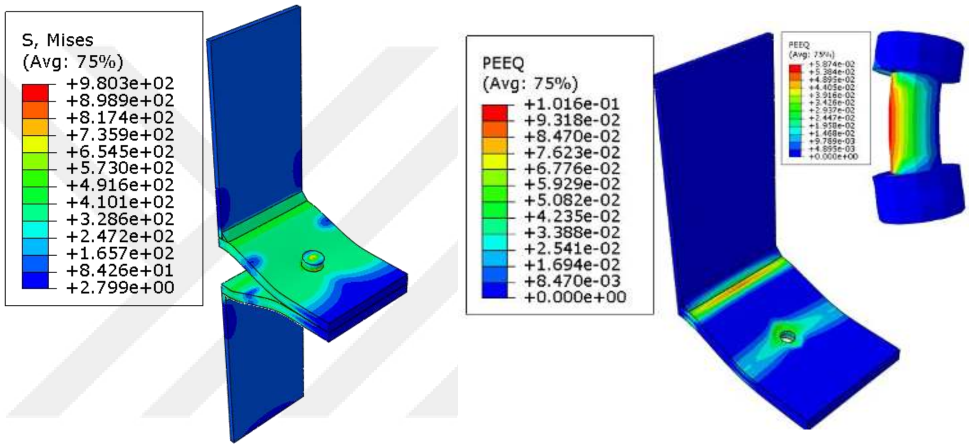

(c) n = 70 mm & w = 140 mm **(d) n = 70 mm & w = 140 mm**

Figure 3.12. *Ultimate stage of specimens of t = 10 mm*

With a flange thickness of 15 mm or 20 mm, when n and w were small, the T-stubs failed by bolt fracture (Mode 3). Little or negligible deformation took place in the flanges. The bolt exhibited a straight shank at the end of the loading, corresponding to only tensile deformation **(Fig. 3.13.b, Fig. 3.14.b).** For larger values of the edge and gauge distances, specimens with a flange thickness of 15 mm exhibited a failure mode 2. A double curvature of the flange and bending of the bolt were observed, despite being less pronounced than for thinner flanges. As depicted **Fig. 3.13.c** and **Fig. 3.13.d**, yielding took place at both the web-to-flange toe region and bolt line region and bolt failure occurred. It can hence be said that the specimens failed in a Mode 2 close to 1.

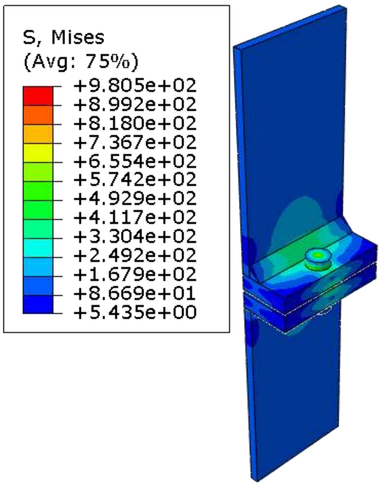

(a) n = 15 mm & w = 60 mm

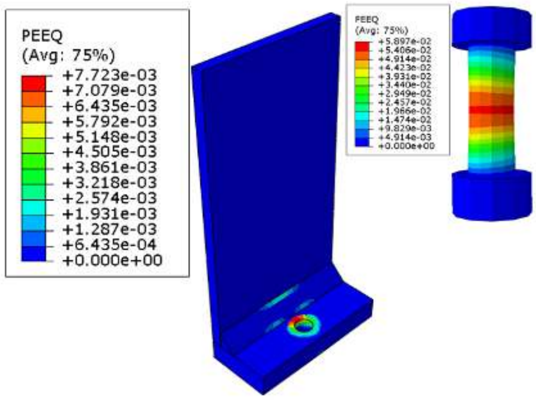

(b) n = 15 mm & w = 60 mm

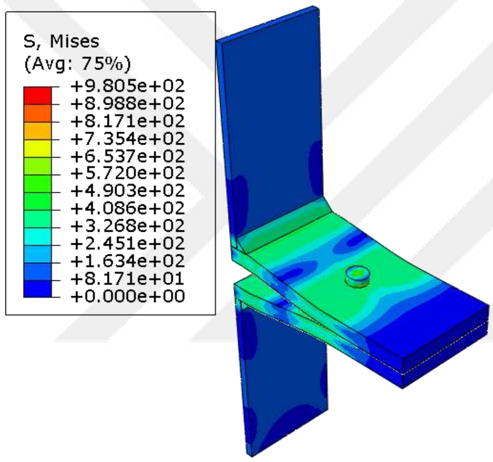

(c) n = 100 mm & w = 200 mm

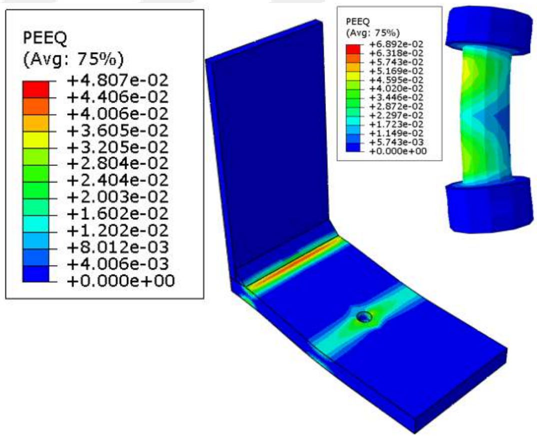

(d) n = 100 mm & w = 200 mm

Figure 3.13. *Ultimate stage of specimens of t = 15 mm*

With a thickness of 20 mm flanges, the yielding of the flange affected only the web-to-flange toe region. Both the flange and the bolt exhibited negligible flexural deformation **(Fig. 3.14.c, Fig. 3.14.d)**.

For the T-stubs that exhibited a failure of the bolt in addition to yielding at web-to-flange toe region and bolt line region, the failure mechanism at the plastic resistance stage was different from the failure mechanism at ultimate stage. When the plastic resistance is attained, yielding at the bolt line and at the flange-to-web connection may be observed (failure mechanism 1). However, a reserve of resistance would allow the T-stub to continue deforming until the failure of the bolt occurs, leading to a failure mechanism 2 (See **Fig. 3.15**).

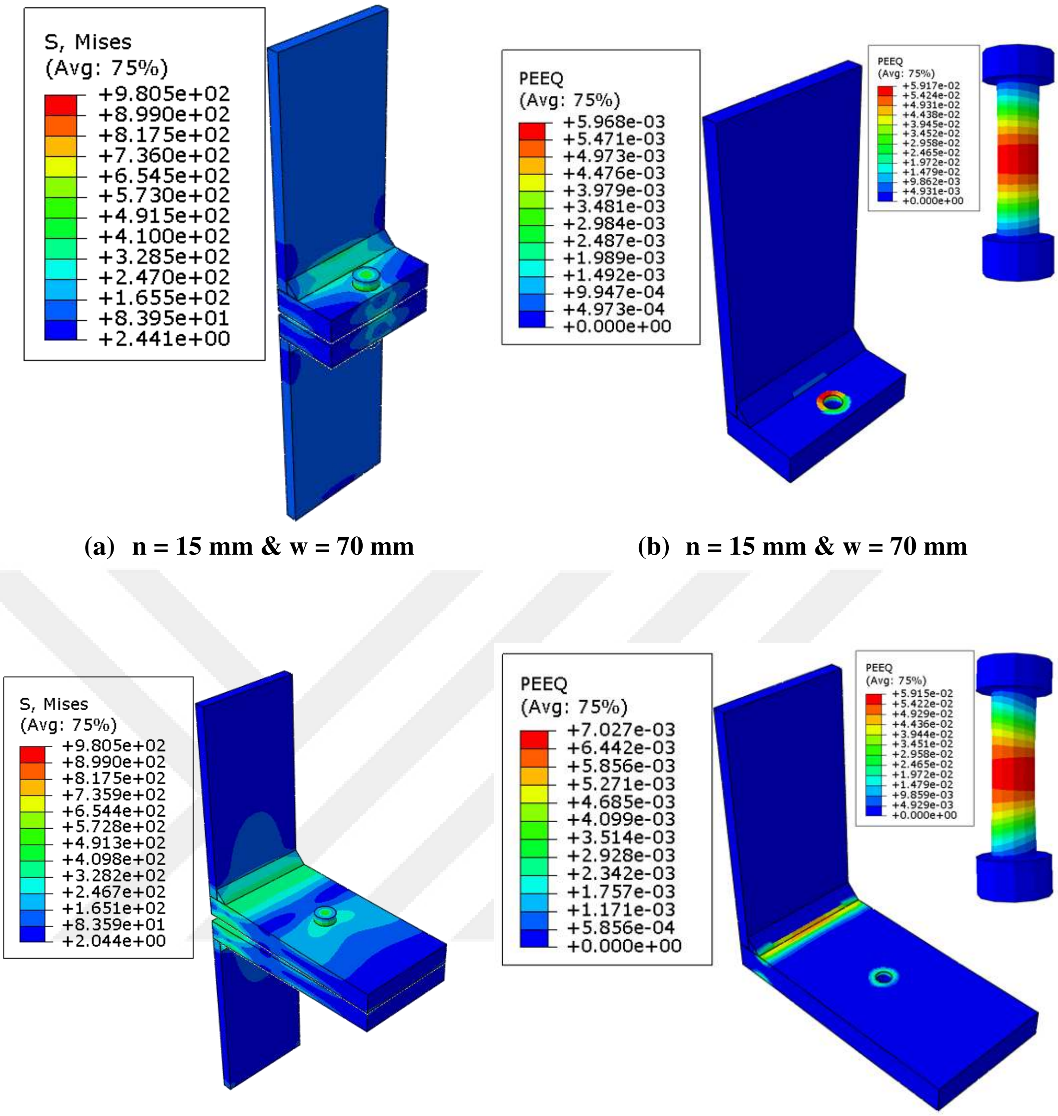

(a) n = 15 mm & w = 70 mm **(b) n = 15 mm & w = 70 mm**

(c) n = 100 mm & w = 200 mm **(d) n = 100 mm & w = 200 mm**

Figure 3.14. *Ultimate stage of specimens of t = 20 mm*

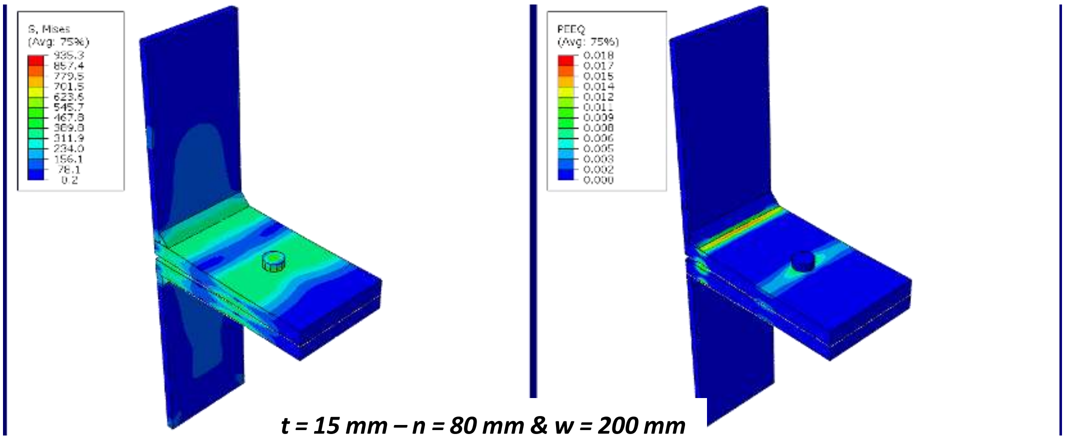

(a) Plastic resistance stage

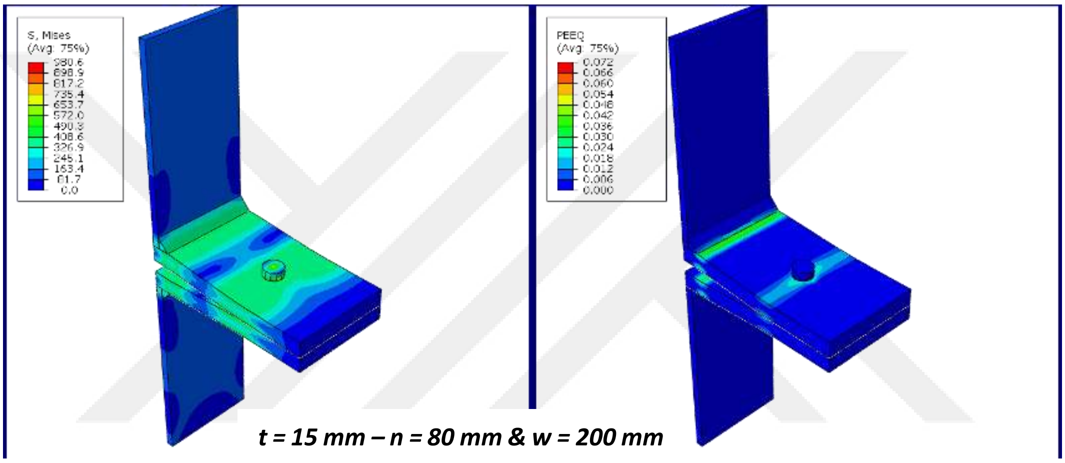

(b) Ultimate stage

Figure 3.15. *T-stub with different failure mechanisms at plastic resistance stage and ultimate stage*

3.4.2. Plastic resistance

Although the plastic resistance was not the focus of this study, it was examined with the aim of obtaining insight into the failure modes and the behavior of the flanges and the bolts when the plastic resistance is reached. The plastic resistance of the T-stub F_r was set as the intersection between the two tangent lines of the load-displacement curve of the T stubs at the initial and the final stages of the monotonic load (see **Fig. 3.16.a**). For a given edge distance, F_r decreased when the gauge distance was increased. Conversely to the gauge distance, as the edge distance was increased, the plastic resistance F_r is increased as well. However, for high values of the gauge distance, there seemed to be a value of the edge distance for which the increase ratio of the plastic resistance in function of the edge distance would be low. The influence of the edge distance and gauge distance on the plastic resistance is illustrated **Fig. 3.17.** As for the flange thickness, it had a significant influence on the plastic resistance: an increase in thickness resulted in a higher resistance (see **Fig. 3.18**). For specimens exhibiting a failure mode 3, the resistance had a value of approximately **198 kN**. This value corresponds to the tensile resistance of the bolts, which can be assessed using **eq. 3.1** and **eq. 3.2.**

$$F_r = \sum F_{tb} \tag{3.1}$$

$$F_{tb} = A_b . f_{ub} \tag{3.1}$$

A_b is the cross-sectional area of the bolt. In general, the tensile stress area A_s is used but in our case the nominal gross area was used. f_{ub} is the ultimate tensile strength of the bolt.

It is worth noting that the rate of change in the plastic resistance was higher in the case of thickness or gauge distance variation.

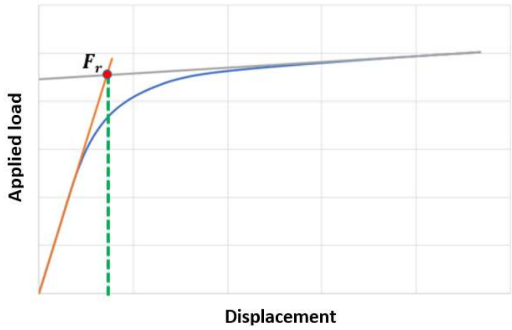

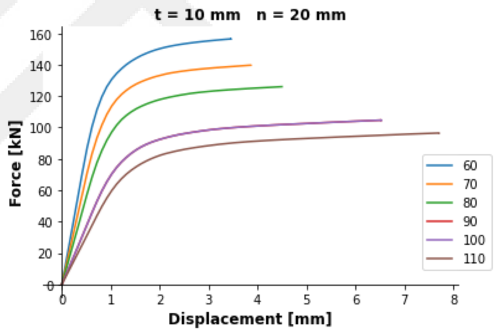

(a) **(b)**

Figure 3.16. *(**a**) Conventional plastic resistance and (**b**) F-d curves for different values of w for t = 10 mm - n = 20 mm*

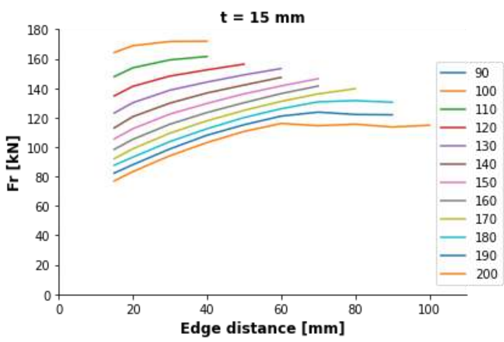

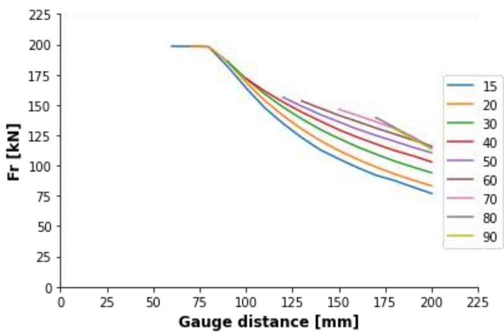

(a) **(b)**

Figure 3.17. *Variation of the T-stub resistance in the function of the n and w for t = 15 mm*

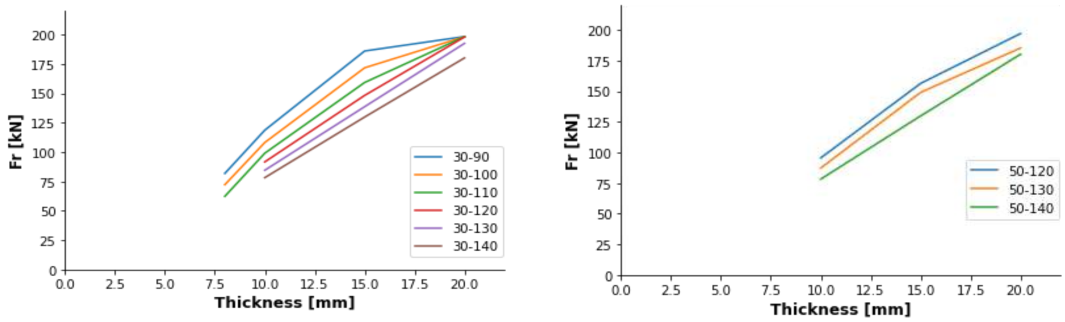

(a) n = 30 mm **(b) n = 50 mm**

Figure 3.18. *Variation of the resistance in the function of the flange thickness for different n-w combinations*

Furthermore, as depicted in **Fig. 3.19** and **Fig. 3.20**, it can be seen that the resistance F_{EC3}, predicted by Eurocode 3 formulation and using the experimental material properties, was lower than the numerical plastic resistance F_r; showing that the Eurocode predictions are conservative. The ratio between the predicted and the numerical plastic resistances ranged from 1.15 to 1.38 for a flange thickness of 8 mm; and from 1.3 to 1.47 for a flange thickness of 10 mm. With t = 15 mm and t = 20 mm, the ratio ranged respectively from 1.3 to 1.63, and from 1.28 to 1.63. A ratio of 1.63 was found common to all the specimens involving a mode 3 failure.

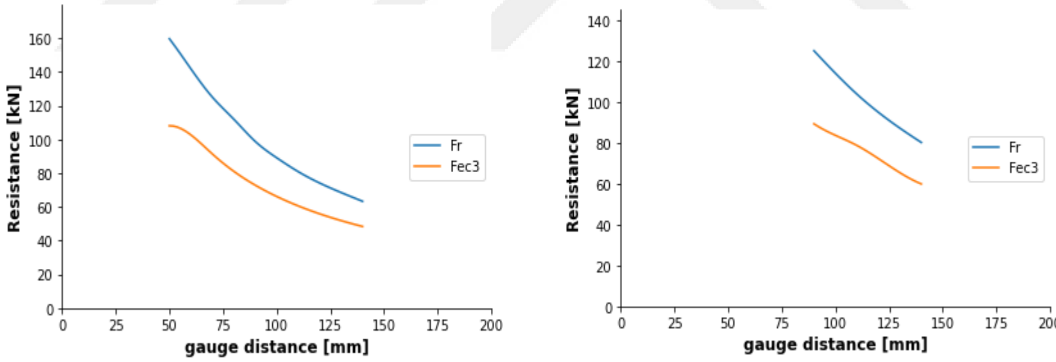

(a) n = 15 mm **(b) n = 40 mm**

Figure 3.19. *Variation of Fr and Fec3 in function of the gauge distance for t = 10 mm*

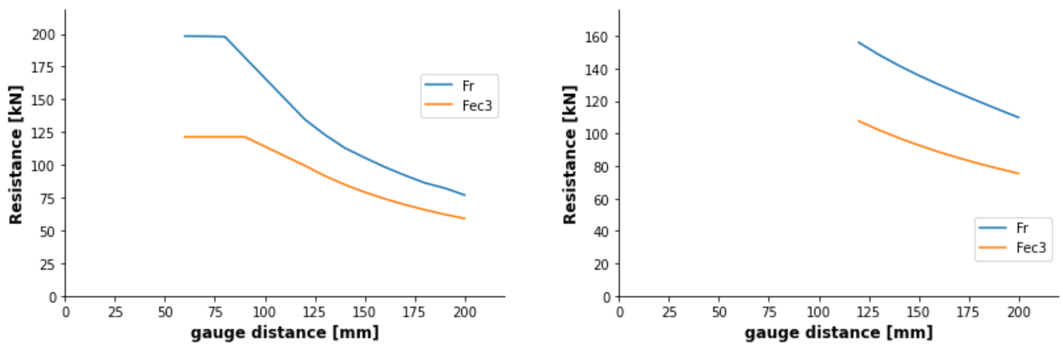

(a) n = 15 mm **(b) n = 50 mm**

Figure 3.20. *Variation of Fr and Fec3 in function of the gauge distance for t = 15 mm*

3.4.3. Prying effect in the bolt

The effects of prying can be evaluated by examining the induced prying force Q, the total bolt force B and the moment in the bolts M. Two situations were considered: the values corresponding to the attainment of the plastic T-stub resistance and the maximum values.

Prying force:

The difference between the total bolt force B and the applied load expresses the prying force Q arising in the bolt.

$$Q = B - F \tag{3.3}$$

Prying action, especially prying force, has long been considered related to contact phenomena. Prying forces are induced by the normal contact stress distribution between the connected parts. In the case of non-preload bolts, prying force can be obtained by the integral of the normal stress distribution over the contact zone (Couchaux et al., 2017). The prying forces assessed by using **Eq. 3.3** were compared to the force-resultant of the contact stresses CF2 throughout the loading. As illustrated in **Fig. 3.21,** the graphs coincide throughout the loading.

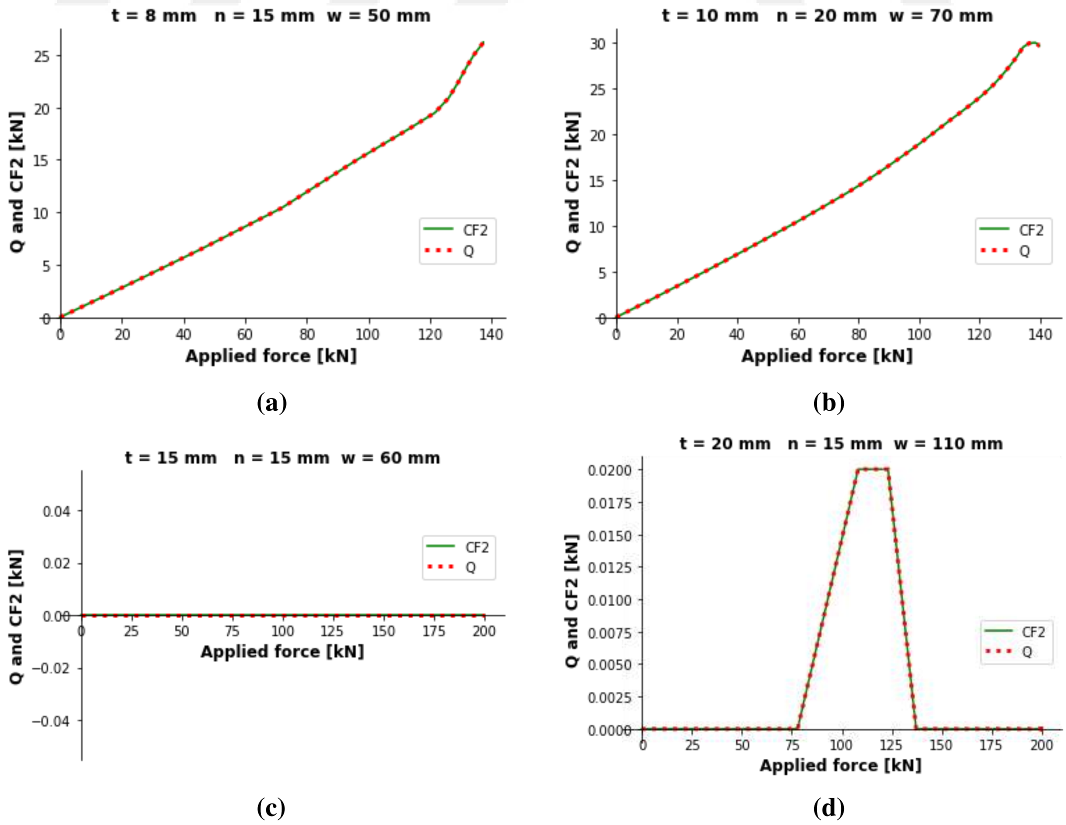

Figure 3.21. *Prying forces and force-resultant of the contact stresses*

The variations of prying force in the function of the edge distance and the gauge distance are illustrated in **Fig. 3.22 – Fig. 3.26**. The prying for at the attainment of the plastic T-stub resistance Q_r and the maximum prying force were considered.

For all the T-stubs, as observed in previous studies (Swanson & Leon, 2000; Coelho, 2004), an increase in the gauge distance resulted in an increase in the prying force (**Fig. 3.22 - Fig. 3.25**). The deformation of the T-stub flange is correlated to the gauge distance. A flange with a longer gauge distance will deform more. The deformation of the flange will induce contact stresses between the connected parts (in our case the flanges), causing prying forces.

As the edge distance increased, prying forces exhibited a decreasing pattern for thinner flanges (**Fig. 3.22 & Fig. 3.23**). However, for T-stubs with thicker flanges, initially an increasing pattern of was observed, followed by the decreasing pattern observed in the specimens with thinner flanges. This observation was compatible with the assumption of Nair et al. (1969) about the existence of an “optimum” value of the edge distance. While this feature is noticeable in all the specimens for a flange thickness of 20 mm, it is noticeable for only lower values of the gauge distance in the case of flange thickness of 15 mm.

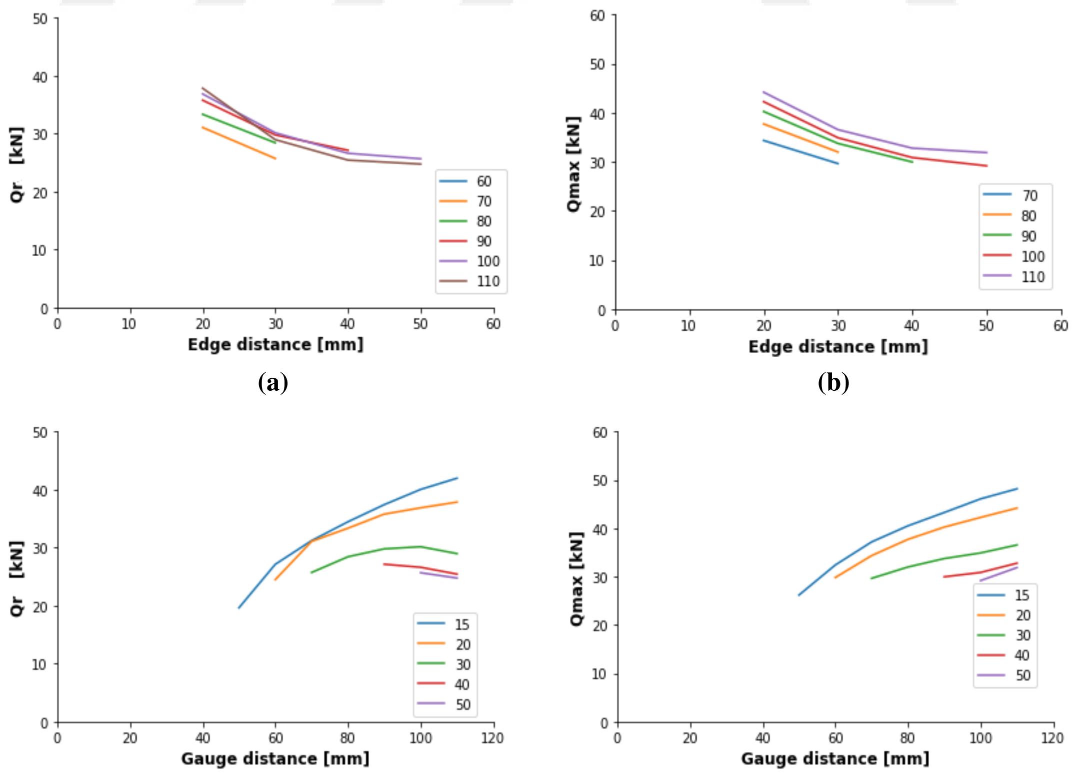

Figure 3.22. *Variation of prying force in function of the edge distance and gauge distance for t = 8 mm*

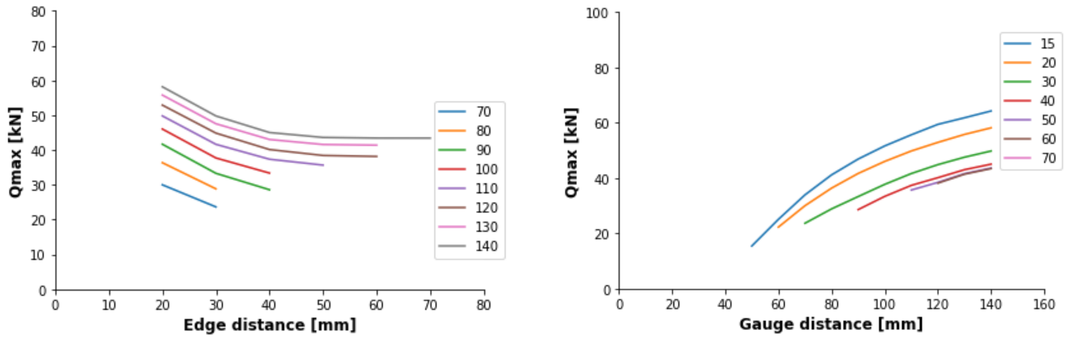

(a) **(b)**

Figure 3.23. *Variation of prying force in function of the edge distance and gauge distance for t = 10 mm*

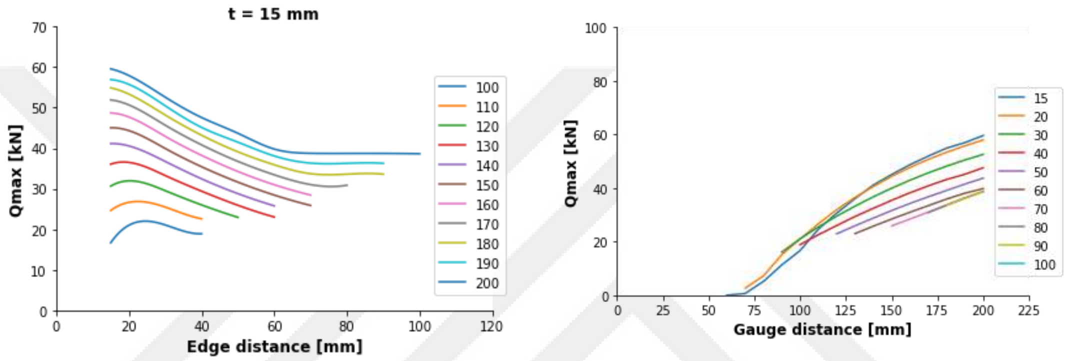

(a) **(b)**

Figure 3.24. *Variation of prying force in function of the edge distance and gauge distance for t = 15 mm*

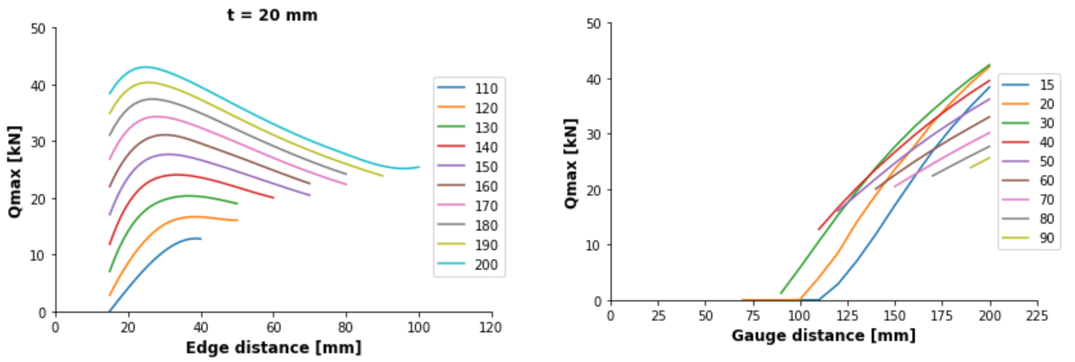

(a) **(b)**

Figure 3.25. *Variation of prying force in function of the edge distance and gauge distance for t = 20 mm*

An increase in the flange thickness expectedly resulted in a substantial decrease in the prying force (See **Fig. 3.22**). As the thickness of the flanges is increased, the rigidity of the flanges increases and they become relatively less deformable as compared to the bolt, leading to lower prying forces.

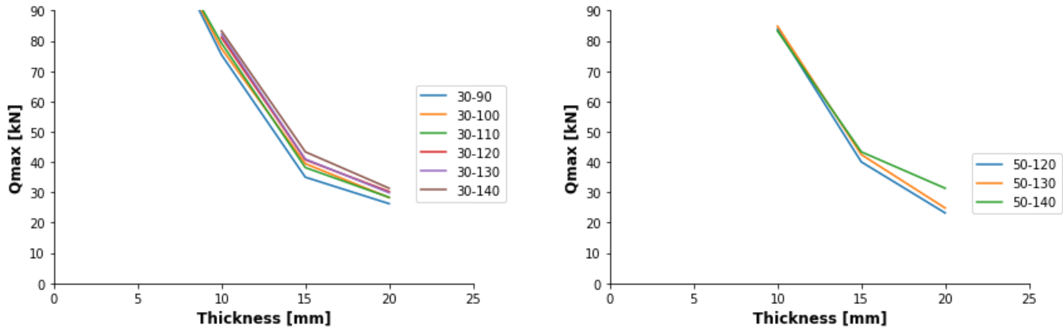

(a) n = 30 mm **(b) n = 50 mm**

Figure 3.26. *Variation of the Q_{max} in function of the flange thickness for different n-w combinations*

For each thickness, the maximum values of prying force were found in specimens with the smallest value of n/m (corresponding to a combination of the highest value of w and the smallest value of n). The dimension m, illustrated in **Fig. 3.27,** is the distance between the bolt axis and the plastic hinge arising near the web.

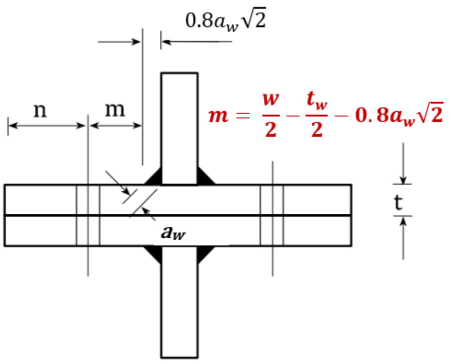

Figure 3.27. *Distance between the bolt axis and the plastic hinge arising near the web*

With thicker flanges (15 mm and 20 mm), zero or negligible prying (less than 10% of ultimate axial resistance of the bolt) was observed in some specimens. The specimens were all involved in a failure mode 3. In the case of zero prying throughout the loading, from the beginning, the deformation of the flanges was negligible compared to the elongation of the bolt. As the gauge distance increases, although small, the deformation of the flanges is enough to induce contact in early stages of the loading. However, as the load increases, the bolt elongation exceeds the flanges deformation, leading to a loss of contact between the connected members.

Considering that prying forces are equivalent to the resultant of the contact stresses, it was deemed important to examine the position of the resultant. Two directions were considered: X-direction and Z-direction. The center of the force due to contact pressure in Z-direction is labelled XN3 and center of the force due to contact pressure in X-direction is labelled XN1.

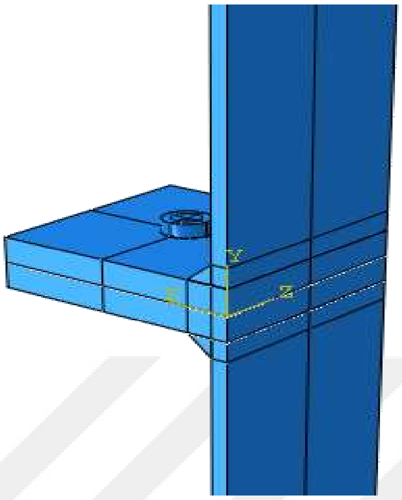

Figure 3.28. *Location of the origin point*

Considering the variations throughout the loading, three cases (See **Fig. 3.29**) were observed:

Case 1: no contact throughout the loading

Case 2: initial contact followed by a loss of contact

Case 3: the connected elements remained in contact throughout the loading. This was the case of most specimens.

For all the specimens, throughout the loading, XN3 is located approximately at 50 mm from the origin (See **Fig. 3.30**), indicating the symmetry of the contact stresses in Z-direction.

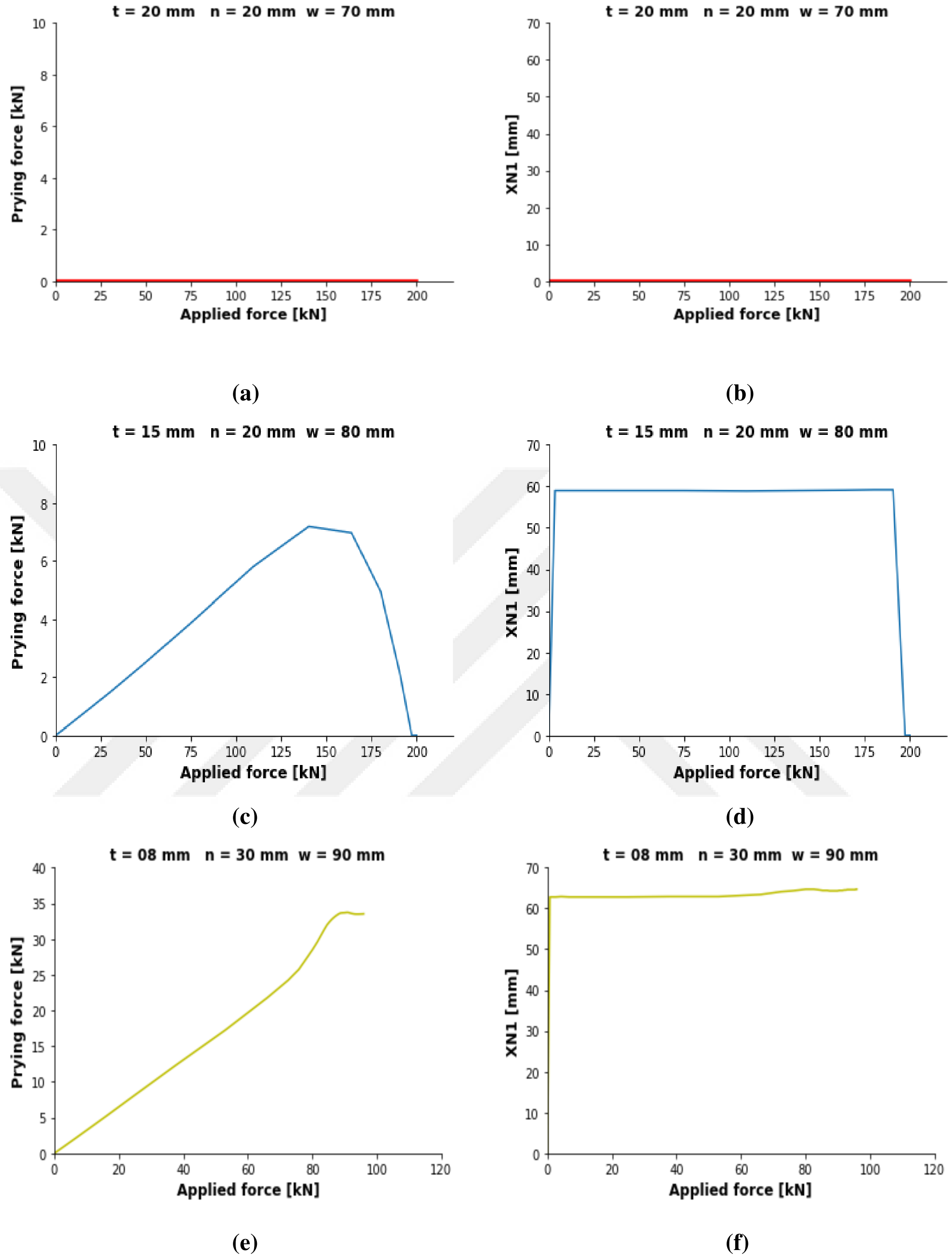

Figure 3.29. *Variation of the prying force and XN1 throughout the loading for different cases*

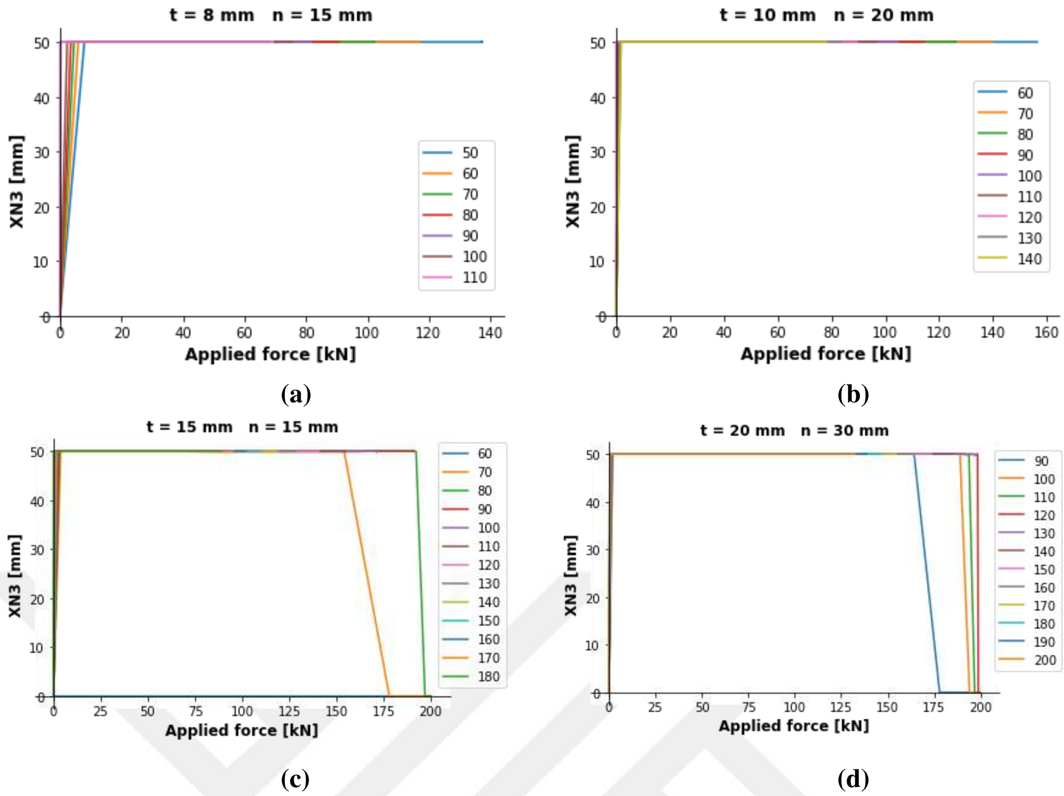

(a) (b)

(c) (d)

Figure 3.30. *Variations of XN3 throughout the loading*

The center of the forces due to contact pressure in X-direction varied throughout the loading; indicating an evolution of the contact pressure. Two stages were considered and compared: the attainment of the T-stubs plastic resistance and the ultimate stage. As depicted in **Fig. 3.31**, the values were similar or had little difference. It could be inferred that the position of the resultant of the contact stresses is not dependent on the loading in the case of non-preload bolts.

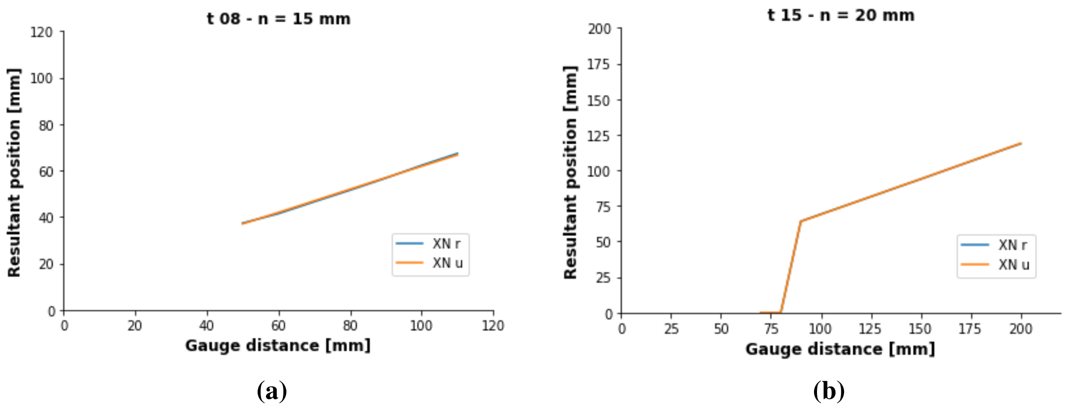

(a) (b)

Figure 3.31. *XN1 at the attainment of the plastic resistance and at ultimate stage*

For the same edge distance, the position of the resultant in X-direction, calculated according to the tip of flange, did not exhibit much variation as the gauge distance increased (**Fig. 3.32**). Nevertheless, in cases where higher gauge distance led to a shift in the failure mode from 3 to 2, the T-stub changed from a complete lift-off (no contact) instance to situation with contact stresses. The resultant of the contact stresses was, however, close to the edge. As illustrated in **Fig. 3.29** and **Fig. 3.33**, the lift-off can concern the whole loading or just a portion. For the same configuration, when the edge distance increased, the resultant moved farther from the tip by the approximately the same amount as the edge distance increase, except for case with no contact. It can be inferred that the position of the resultant of the contact stresses depends on the relative flexibility between the flange and the bolt.

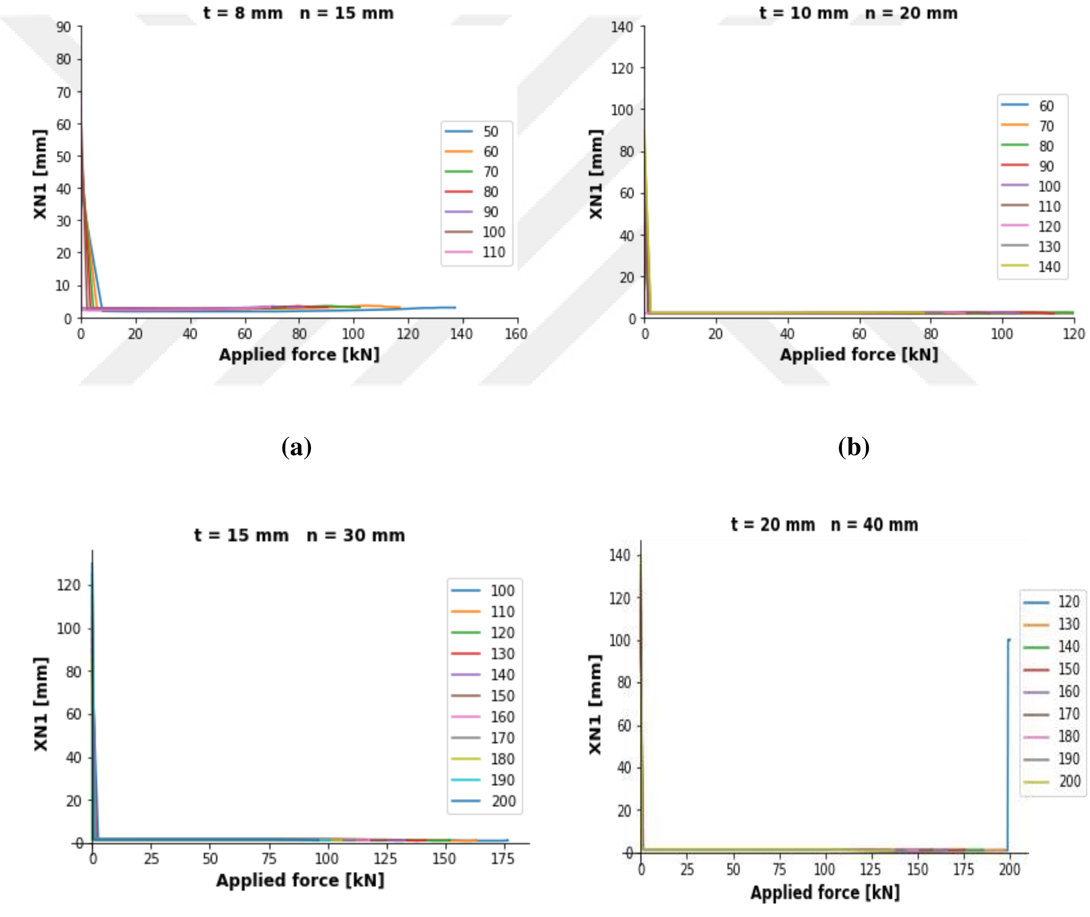

(a) **(b)**

(c) **(d)**

Figure 3.32. *Position of the resultant of the contact stresses in X-direction*

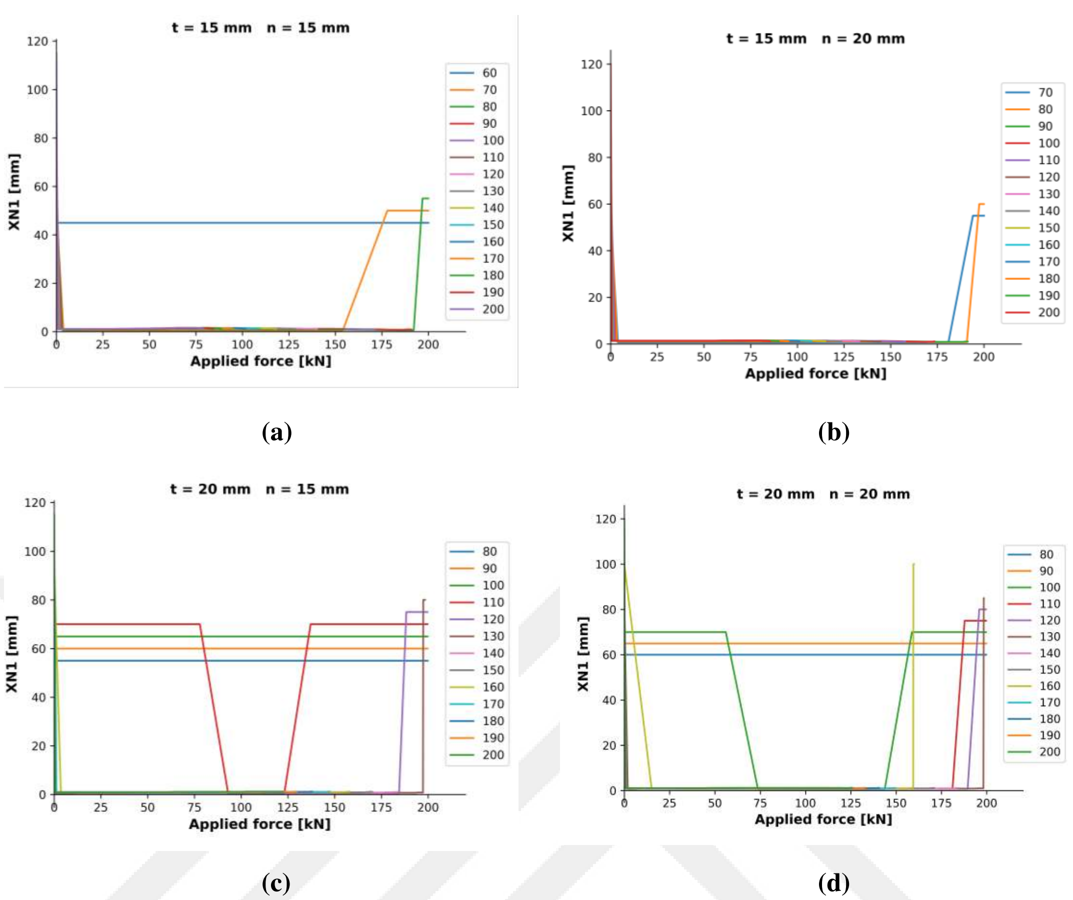

Figure 3.33. *Position of the resultant of prying forces showing the shift from Mode 3 to Mode 2*

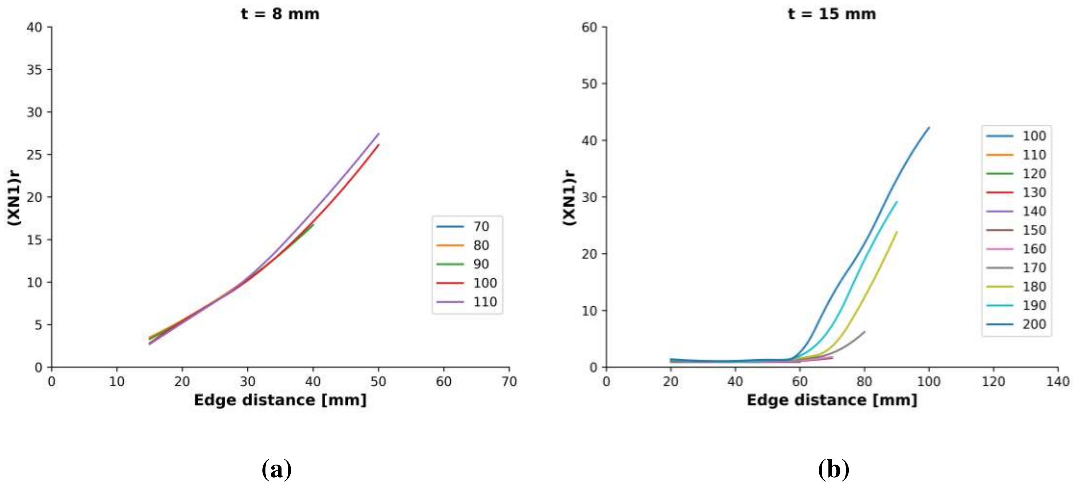

Figure 3.34. *Variation of the position of the prying forces resultant for **(a)** t = 8mm and **(b)** t = 15 mm*

Total bolt force

Conversely to the prying force, the total bolt force B decreased as the gauge distance was increased. As mentioned in the previous sections, an increase in the gauge distance resulted in a decrease in the resistance of the T-stubs, as well as an increase in the prying force. The decrease ratio of the resistance being greater than the increase ratio of Q, in accordance with **eq. 3.3**, it led to a decrease in the total bolt force. Concerning the variations in function of the edge distance, a decreasing pattern was observed for specimens involving thinner flanges ($t = 8\ mm$ and $t = 10\ mm$) while the opposite was observed for $t = 15\ mm$ and $t = 20\ mm$. Furthermore, with thinner flanges, the variations of B_{max} are more distinct from one another than they are with thicker flanges **(Fig. 3.35).** The highest values of the total bolt force corresponded to specimens combining the smallest values of both w and n. With thinner flanges, the total bolt force decreases as the edge distance increases. A similar variation is observed with the gauge distance. However, as illustrated in **Fig. 3.36**, in specimens with thicker flanges (t = 15 mm and t = 20 mm), a linear relationship can be assumed between B_{max} and the gauge distance, as well as the edge distance. Moreover, the variations of B_{max} can be approximated by a single line, showing that the maximum total bolt force is not dependent on the edge and gauge distances when thicker flanges are used. Since the failure of the specimens involved the failure of the bolts, the maximum total bolt force, which is equivalent to the total bolt force at ultimate stage, is more dependent on the bolt characteristics than it is on the flange characteristics. In some specimens, the maximum bolt force was as low as **77 kN**; which is rather small, compared to the ultimate bolt resistance. The variations of the maximum bolt force in function of the flange thickness are illustrated in **Fig. 3.37.**

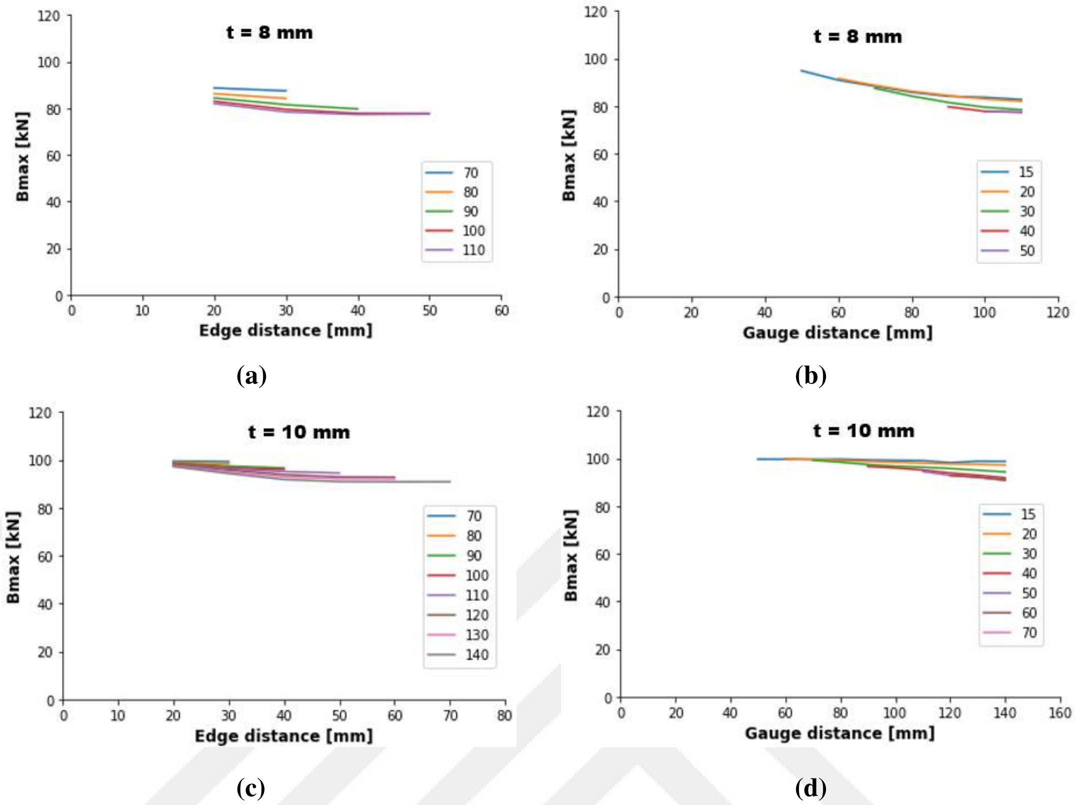

Figure 3.35. *Variation of the total bolt force in the function of n and w for t = 8 mm and t = 10 mm*

Bolt moment

The moment in the bolts is induced by the deformation of the flanges, which subjects the bolts to flexural deformation. Even in specimens that exhibited zero prying force, the moment in the bolts was present throughout the loading. It could be considered that, unlike the prying force that is related to contact stresses, the bolt moment is related to the rigidity of the flanges and that of the bolts. In other words, the moment in the bolts is strongly dependent on both the deformability of the flanges and the deformability of the bolts.

For all the specimens, the moment in the bolt exhibited the same variation throughout the loading: as the applied load increases, the bolt moment increases until a maximum value. Beyond that point, the bolt moment decreases as the applied load increases, until the ultimate load (See **Fig. 3.38**).

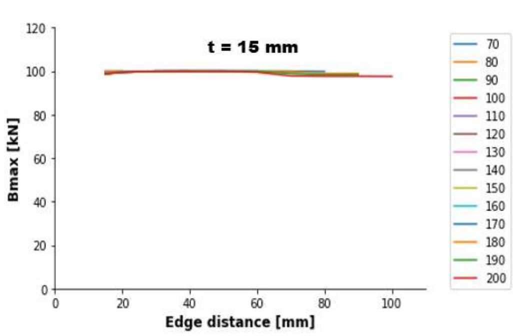

(a)

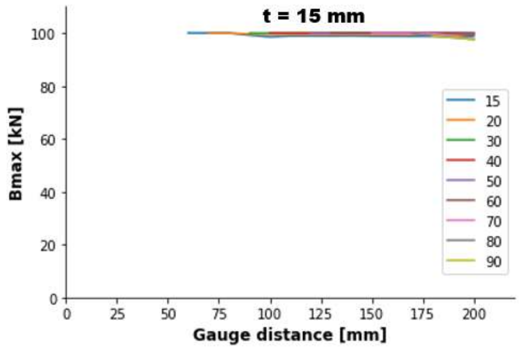

(b)

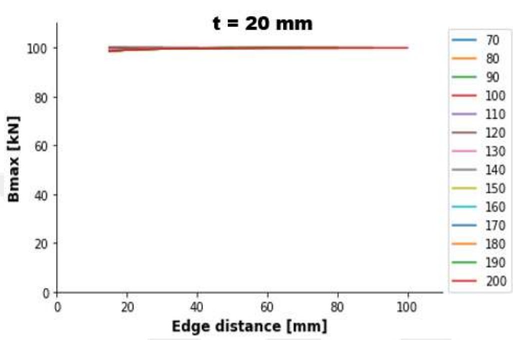

(c)

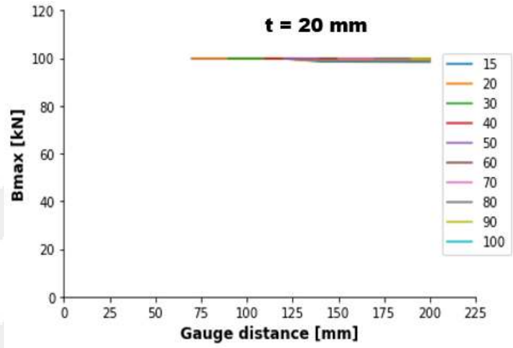

(d)

Figure 3.36. *Variation of the total bolt force in the function of n and w for t = 15 mm and t = 20 mm*

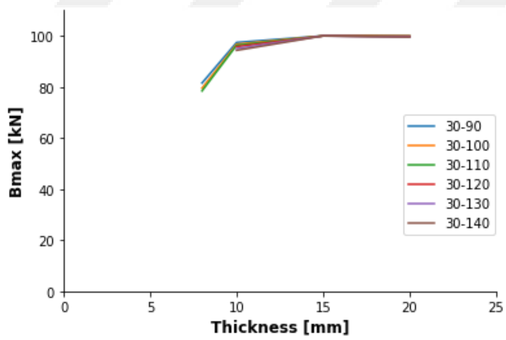

(a) n = 30 mm

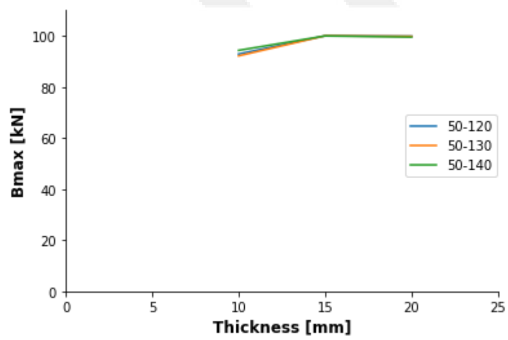

(b) n = 50 mm

Figure 3.37. *Variation of Bmax in function of the flange thickness for different n-w combinations*

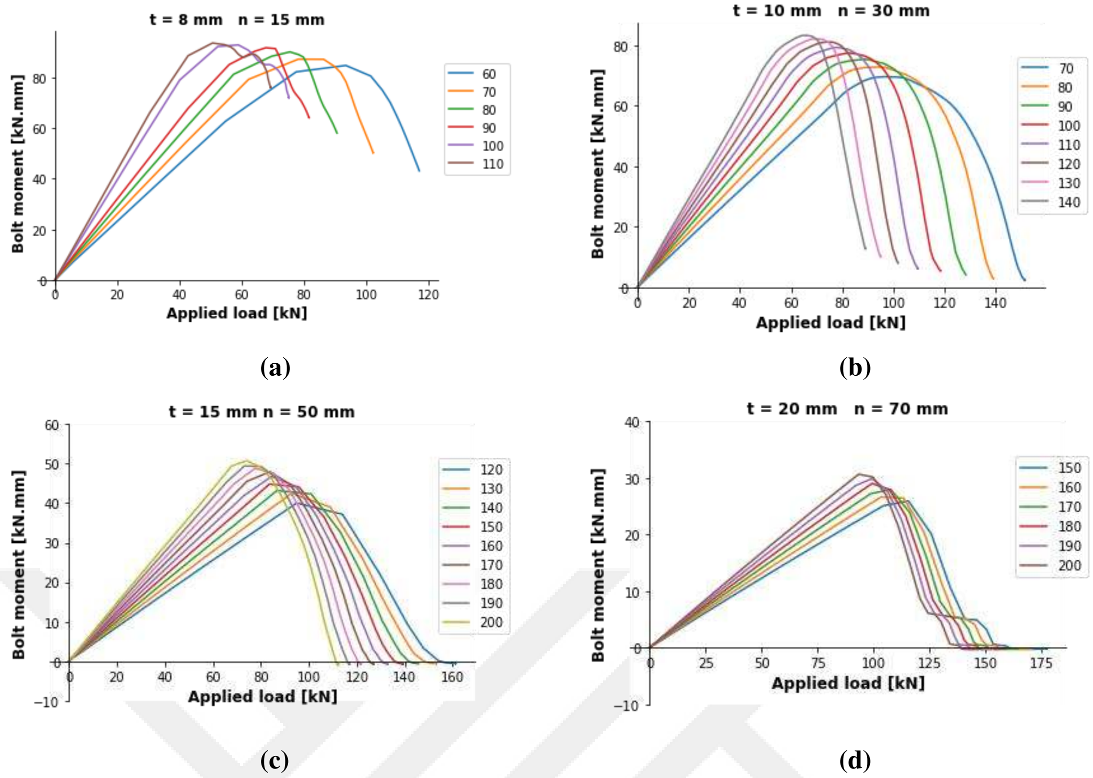

Figure 3.38. *Variations of the bolt moment throughout the loading*

The bolt moment variations were similar to that of the prying force vis-à-vis the gauge distance. For all the specimens, the increase in the gauge distance resulted in an increase in bolt moments. Considering a certain edge distance, the rigidity of the flanges decreases and the deformability increases as the gauge distance increases. The deformation of the flanges, then, subjects the bolts to flexural action.

However, the variations of the bolt moment in function of the edge distance are different in specimens with thinner flanges (t = 8 mm and t = 10 mm) and specimens with thicker flanges (t = 15 mm and t = 20 mm). With thinner flanges, moment in the bolt increases as the edge distance increases. It should also be noted that the influence of the edge distance is lower for high values of n.

In T-stubs with a thinner flange (t = 8 mm and t = 10 mm), despite being much lower than M_{max}, the moment at the ultimate stage was still positive **(Fig. 3.38.a, Fig. 3.38.b)**. The positive sign of moment indicated that the flange continued to deform, subjecting the bolt to a bending (failure mode involving the flange). However, only a few specimens presented ultimate positive moments for t = 15 mm and t = 20 mm. In most specimens, the ultimate moment was negative (See **Fig. 3.38.c, Fig. 3.38.d**). Considering that the flanges possess a relatively higher rigidity than the bolts, after the separation of the flanges, a further increase in the applied load would only result in a tension of the bolts; which would tend to cancel the bending that previously occurred in the bolt due to the flange deformation. It is worth mentioning that, with thicker flanges, the ultimate moment (positive or negative) was negligible enough to be considered equal to zero.

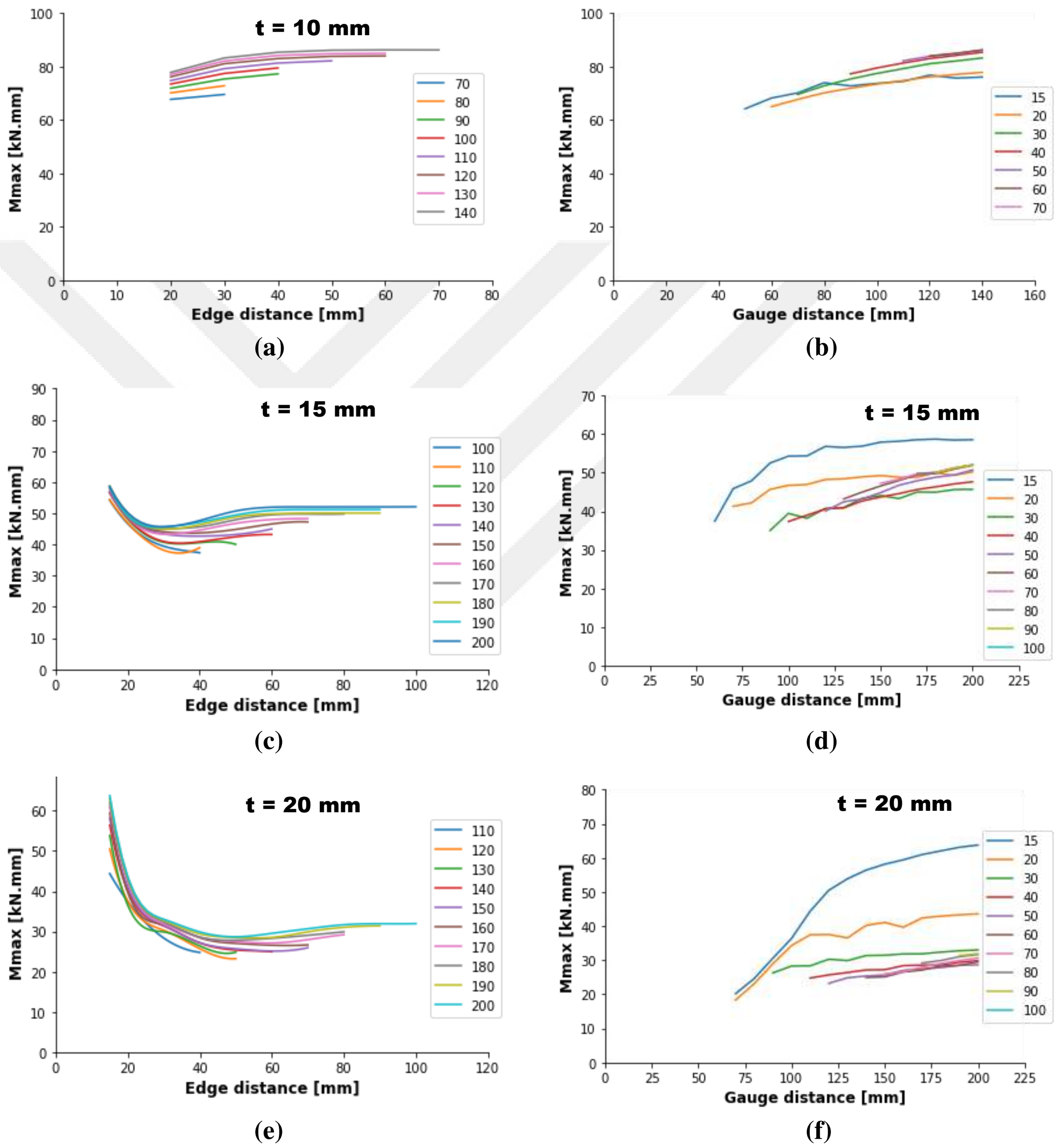

Figure 3.39. *Variations of Mmax in function of n and w for t = 10 mm, 15 mm and 20 mm*

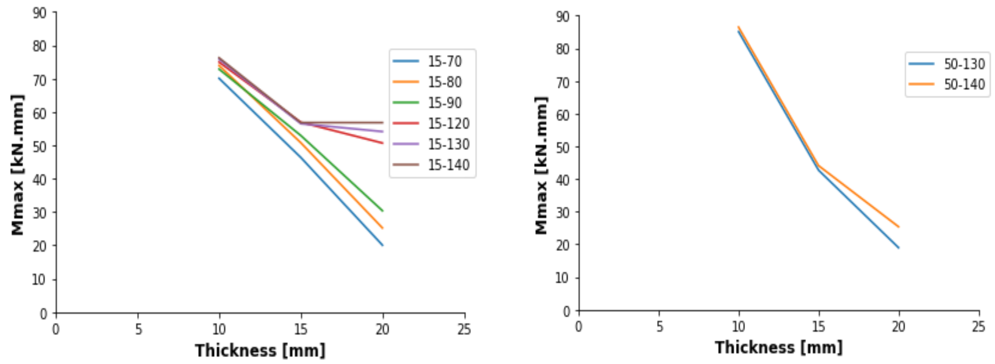

(a) n = 15 mm **(b) n = 50 mm**

Figure 3.40. *Variation of the Mmax in the function of the flange thickness for different n-w combinations*

The ultimate flexural resistance of the bolt M_{ub} computed using equations (4) was **156 kN.mm**. With flange thicknesses of 8 mm, 10 mm, 15 mm and 20 mm, the maximum bolt moment attained were respectively 65%, 55%, 41% and 38% of the M_{ub} (See **Table 3.5**). The moment in the bolts can reach proportions that are important enough for the combined tensile and flexural action to yield considerable stresses in the bolt. On that account, the bolt moment has to be considered in the design.

$$M_{ub} = W_b.f_{ub} = \frac{I}{\emptyset_b/2}.f_{ub} \tag{3.2}$$

Table 3.5. *Maximum bolt moment and their ratios to ultimate bolt flexural resistance*

Thickness	M_{max}	M_{max}/M_{ub}
8 mm	101.2 kN.mm	0.65
10 mm	86.5 kN.mm	0.55
15 mm	64.1 kN.mm	0.41
20 mm	58.5 kN.mm	0.38

M-N interactions curves

By comparing the prying force Q, the total bolt force B and the total bolt moment M for each increment to their respective maximum values, it was observed that for all the specimens, the maximum moment M_{max} was always reached before Q_{max} and B_{max} were reached. For all the T-stubs, B_{max} corresponded to the total bolt force at ultimate load. However, Q_{max} and M_{max} where different from the prying force and bolt moment values at ultimate stage. Concerning prying force, in some specimens Q_{max} and the prying force at ultimate load coincided. The specimens failed in Mode 1 or Mode 2 close to 1. For specimens with a thinner flange (t = 8 mm and t = 10 mm), the maximum values of Q and B were reached almost at the same load. However, when thicker flanges were used (t = 15 mm and t = 20 mm), for short gauge distances, Q_{max} was attained for load much lower than that of B_{max}. As the gauge distance was increased, the load of attainment of Q_{max} got closer to a load of attainment of B_{max}. **(Fig. 3.41)**

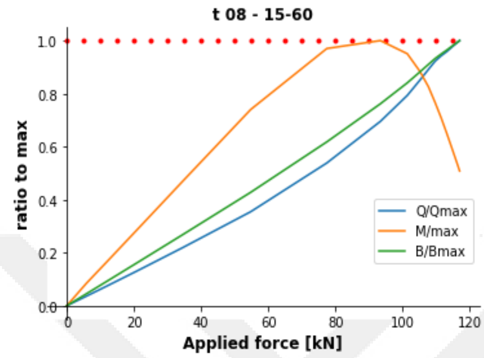

(a) t = 8 mm - n = 15 mm – w = 60 mm

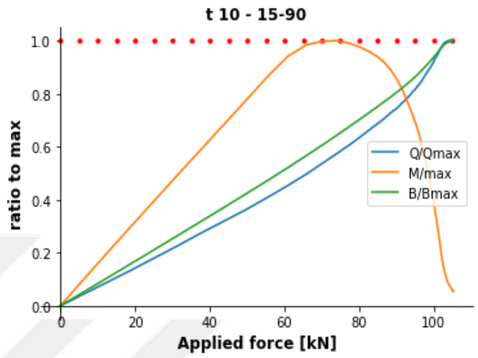

(b) t = 10 mm - n = 15 mm – w = 90 mm

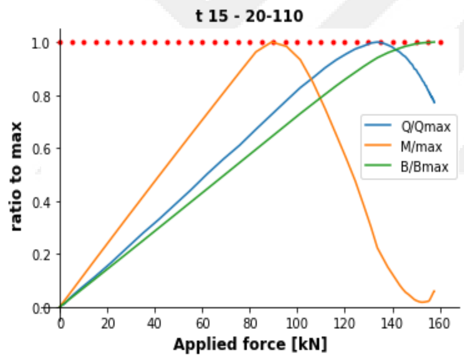

(c) t = 15 mm - n = 20 mm – w = 110 mm

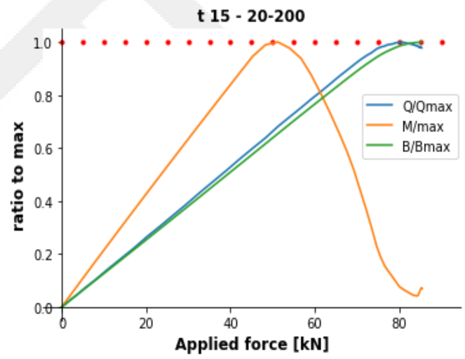

(d) t = 15 mm - n = 20 mm – w = 200 mm

Figure 3.41. *Ratio of Q, M and B to their respective maximum*

Considering that the bolts are subjected to the combined action of flexure and tension, it appeared important to analyze the M-B interaction curves of the T-stubs. As illustrated in **Fig. 3.42**, both the maximum bolt moment and the ultimate bolt moment increase as the gauge distance increases. This is compatible with the fact that deformability of flange increases in function of the gauge distance. Conversely, the maximum total force in the bolts – which is equivalent to the ultimate total bolt force - decreases as the gauge distance increases. With thicker flanges (t = 15 mm and t = 20 mm), the maximum total bolt force is practically the same in all the specimens. This is due to the fact that the failure of these specimens involves the failure of the bolts (see **Fig. 3.43**).

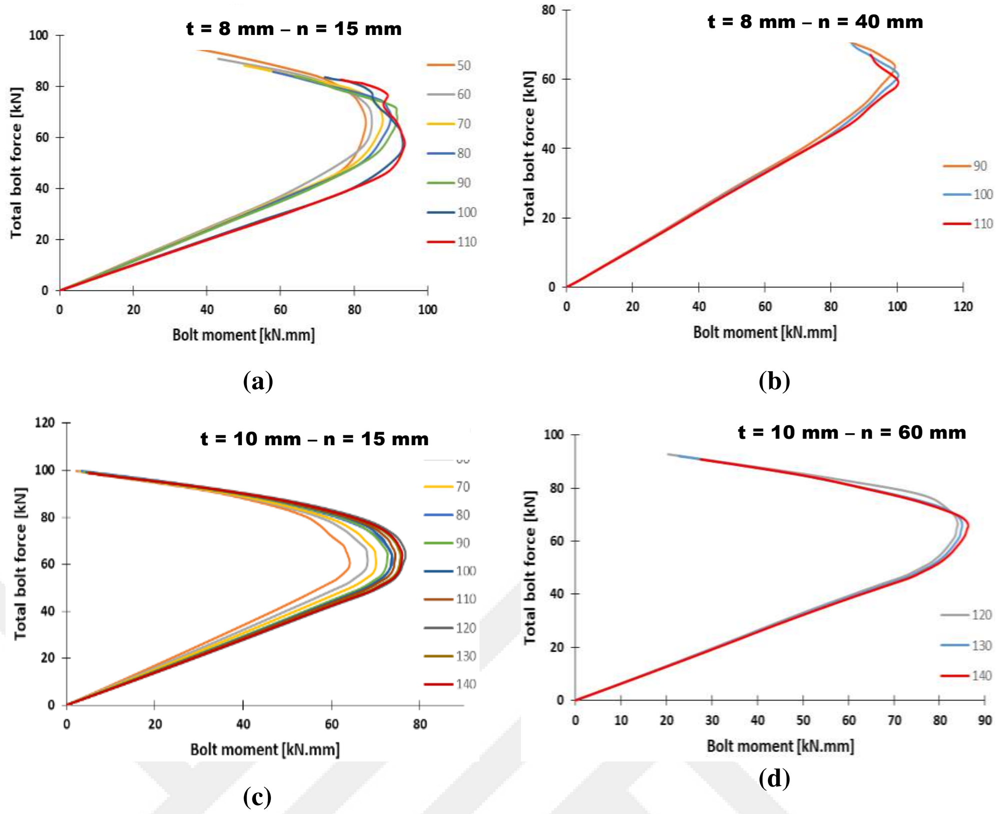

Figure 3.42. *Interaction curves for t = 8 mm and t = 10 mm*

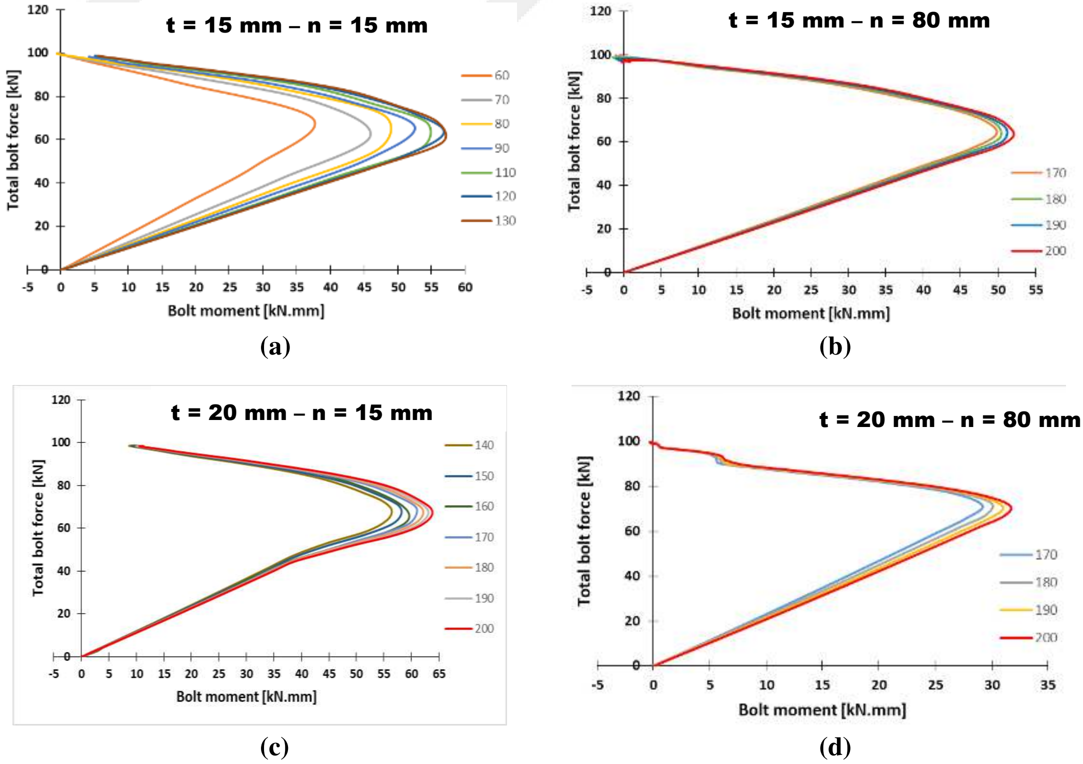

Figure 3.43. *Interaction curves for t = 15 mm and t = 20 mm*

3.5. Conclusion

An advanced FE model was constructed in ABAQUS and validated using test data available in the literature (Coelho, 2004; Bursi & Jaspart, 1997). Following the validation, over 200 models were generated and included in a parametric study aiming at investigate prying effects in bolted T-stubs. The influence of some design parameters such as flange thickness t, edge distance n, and gauge distance w was examined. The values of the edge and the gauge distances were chosen to cover all the combinations allowed by EN 1993-1-8. The formulations presented in EN 1993-1-8 were found to yield conservative estimations of the plastic resistance of T-stubs. The prying force and bolt moment increase as the gauge distance increase. As for the edge distance and flange thickness, their increase would induce a decrease in the prying force and bending moment in the bolts, with a significant decrease with the flange thickness. Conversely, the total bolt force decreases as gauge distance increases and increases as edge distance or thickness increases. Also, when non-preload bolts are used, the position of the resultant of the contact stresses is not dependent on the loading. The position depends on the flange and the bolt rigidities. The bolt moment can represent a substantial fraction (up to 65%) of the bolt flexural resistance, mainly in thin flanges where the flange deformation induces considerable bending of the bolts. Therefore, the consideration of the bending moment in the bolts is a key to a safer design of bolted steel connections. A better understanding of prying effects requires further investigations involving more key parameters such as steel grade, bolt diameter, bolt grade, the effective width of the T-stub, and considering a more comprehensive value range of flange thickness, edge distance, and gauge distance. The outcome may permit the development of an analytical model including bolt bending and a more accurate assessment of prying action (bolt moment and total bolt force).

4. EXTENSIVE PARAMETRICAL STUDY USING NOMINAL MATERIAL PROPERTIES

4.1. Introduction

The behaviour of bolted steel T-stubs depends on various geometrical and material parameters. Using the calibrated model from the previous chapter, over 3,500 additional models were generated and a parametric study was undertaken in order to investigate the influence of the geometrical and material parameters on the prying effects in the T-stubs. The main geometric parameters that were varied in the study are: the flange thickness t, the edge distance n, the gauge distance w, weld throat thickness a_w, the width of the flange b and the bold diameter $\emptyset$. The material parameters involved were the steel class and the bolt grade. Nominal material properties of three (3) steel classes, namely S235, S275, and S355; and two (2) bolt grades, namely 8.8 and 10.9 were used.

In the following sections, prying-related values such as prying force, prying ratio, bolt moment, bolt moment ratio, and the magnitude and position of the resultant of contact stresses are examined to obtain insight into the influence of the main parameters. Fluctuations were observed in the variations of the different prying-related values, particularly for the bolt moment and the bolt moment ratio, M/F. Nevertheless, a prevailing trend can be derived.

The observations made in the previous chapter were limited to a single combination of steel material, bolt material and bolt diameter. A more extensive investigation presented a two-fold advantage:

- ✓ Confirm the validity of the previous observations under analogous conditions;
- ✓ Extend the observations to other conditions in order to obtain a more general grasp

4.2. Nominal Material Properties

The mechanical properties of the material used for the flange, web and welds were chosen according to the values specified in EN 10025-2 related to hot rolled products of non-alloy structural steels. The yield strength, f_y may vary according to thickness of plate. Six different thicknesses were included in the parametric study: 5 mm, 8 mm, 10 mm, 15 mm, 20 mm, and 25 mm. The ultimate strength, f_u was taken as the minimum value specifed in the standard. The specifications in EN 14399-3 were used for the bolts. Five bolt diameters, namely M12, M16, M20, M24, and M27, were involved in the parametric study. The mechanical properties of the different steel classes and bolt grades are summarized in **Table 4.1**, along with the codification which was used for referring to each of them. For all the T-stub components, the elasticity moludu, E was taken equal to $\mathbf{210 \times 10^5}$ **MPa**

Table 4.1. *Nominal mechanical properties for plates and bolts*

	Thickness [mm]	Steel class			Bolt grade	
		S235	**S275**	**S355**	**8.8**	**10.9**
$f_y\ [MPa]$	$t \leq 16$	235	275	355	640	900
	$16 < t \leq 40$	225	265	345		
$f_u\ [MPa]$		360	410	470	800	1000
ε_u		0.259	0.229	0.218	0.117	0.086
Code		**S1**	**S2**	**S3**	**B1**	**B2**

4.3. Influence of the Design Parameters

4.3.1. Influence of the gauge distance and the edge distance

Prior to reporting the influence of the gauge distance and the edge distance, it is important to mention that some T-stubs exhibited a failure mode that was neither of the three modes mentioned in the previous chapters. The failure in these T-stubs occurred in the welds. It was the case of T-stubs with strong bolts, relatively thick flanges and short gauge distance. Due to the relative rigidity of the flanges, the yielding involved the welds. However, as the gauge distance was increased, the T-stubs could bend and the yielding moved from welds to the flanges.

The gauge distance is a geometrical parameter that governs the flexibility of the T-stub whereas the edge distance controls the potential contact area, hence the position of the resultant of the prying forces. For specimens involved in a failure mode 2 or 3, increasing the gauge distance caused an increase in the bolt moment (See **Fig. 4.1 – Fig. 4.4**). Conversely, with specimens which failed in mode 1, the bolt moment decreased as the gauge distance increased (See **Fig. 4.5** & **Fig.4.6**). In some specimens (mostly specimens with relatively large bolt diameters and relatively thin flanges), the decreasing trend is preceded by an increasing trend for low values of the edge distance (see **Fig. 4.7**).

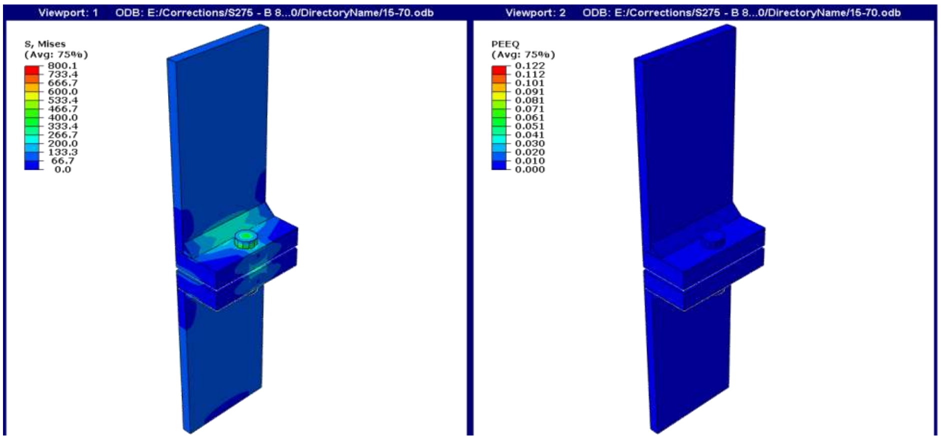

(a) *n = 15 mm – w = 50 mm*

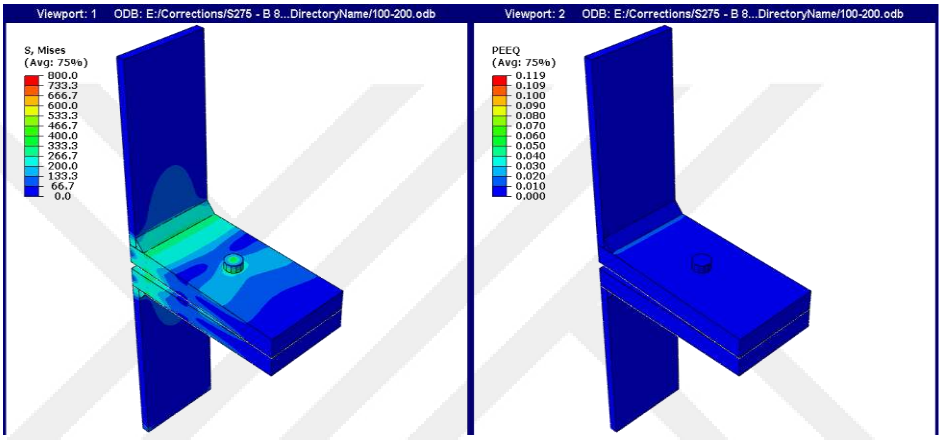

(b) *n = 100 mm – w = 200 mm*

Figure 4.1. *Ultimate stage of S2B1 – M12 – t = 20 mm*

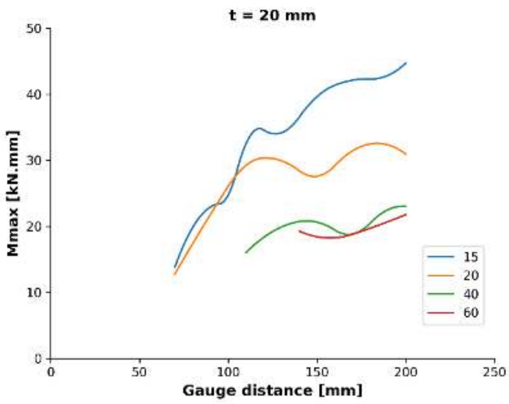

(a)

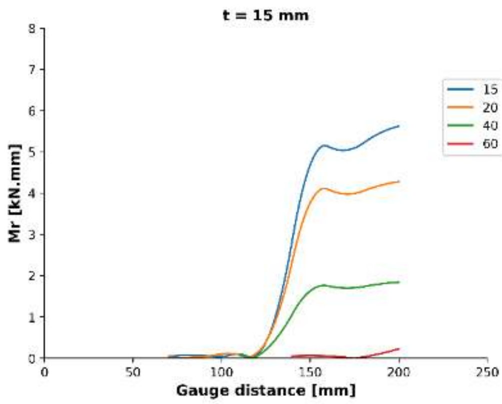

(b)

Figure 4.2. *Variations of the Mmax and Mr for S2B1 – M12 – t = 20 mm*

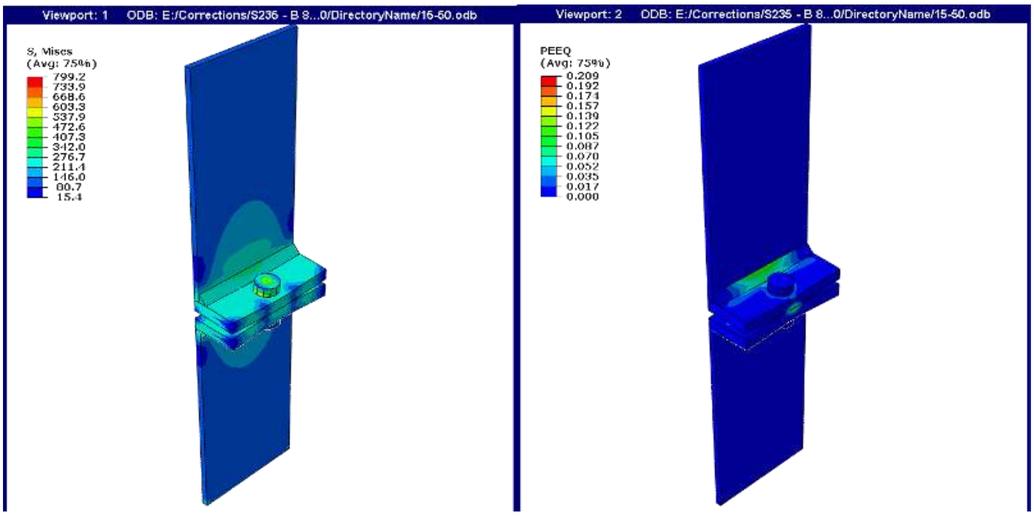

(a) ***n = 15 mm – w = 50 mm***

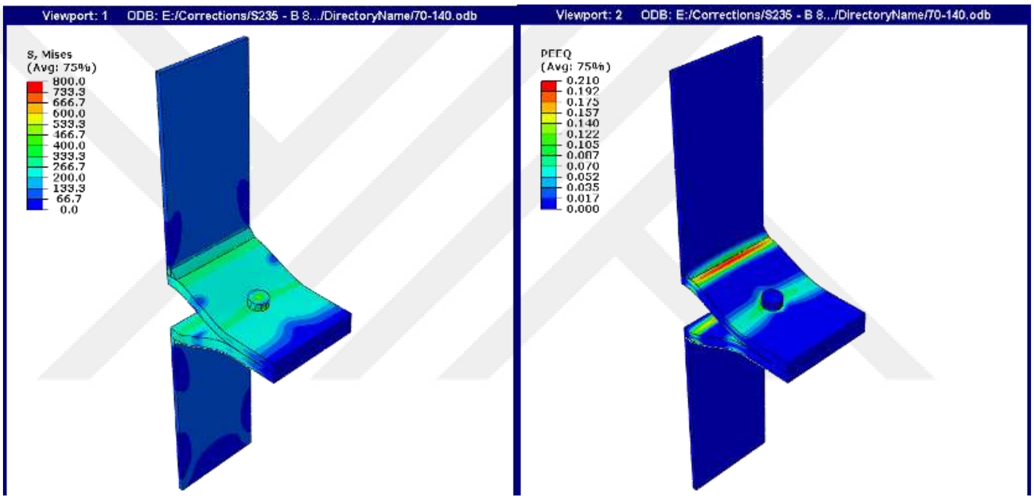

(b) ***n = 70 mm – w = 140 mm***

Figure 4.3. *Ultimate stage of S1B1 – M12 – t = 10 mm*

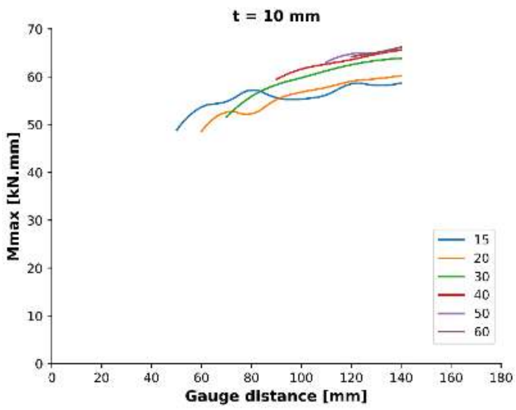

(a)

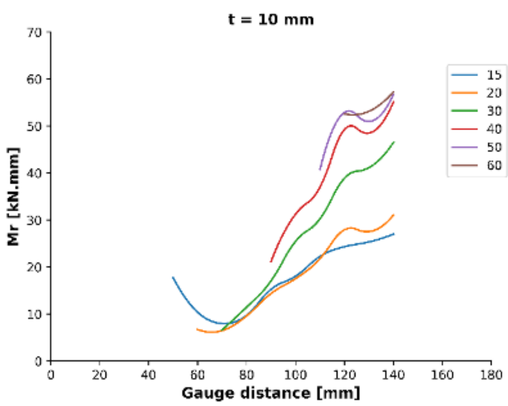

(b)

Figure 4.4. *Variations of the Mmax and Mr for S1B1 – M12 – t 10*

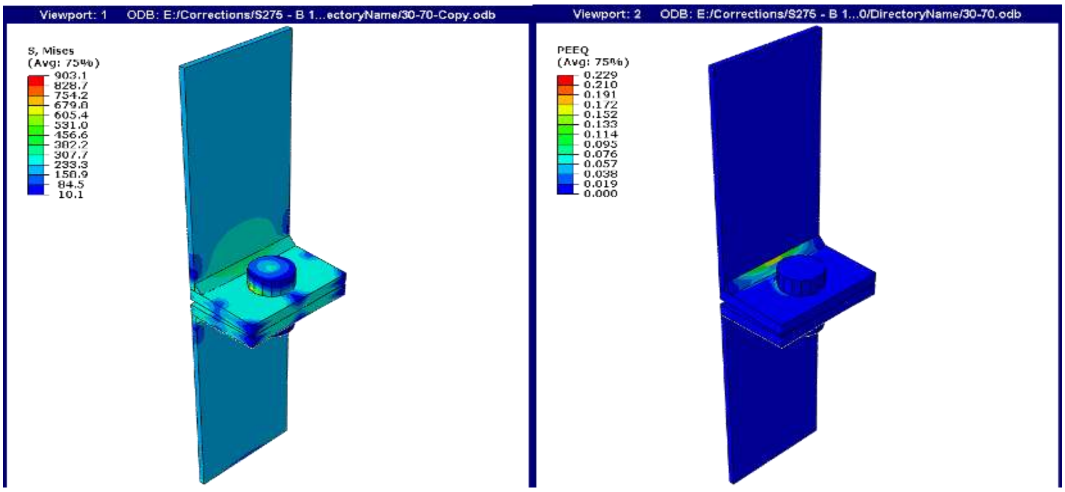

(a) n = 30 mm – w = 70 mm

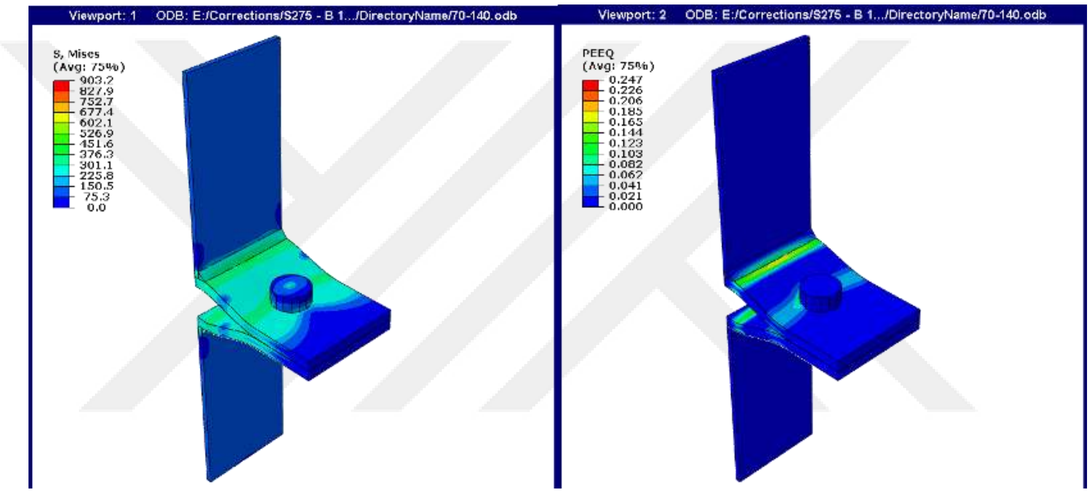

(b) n = 70 mm – w = 140 mm

Figure 4.5. *Ultimate stage of S2B2 – M24 – t = 10 mm*

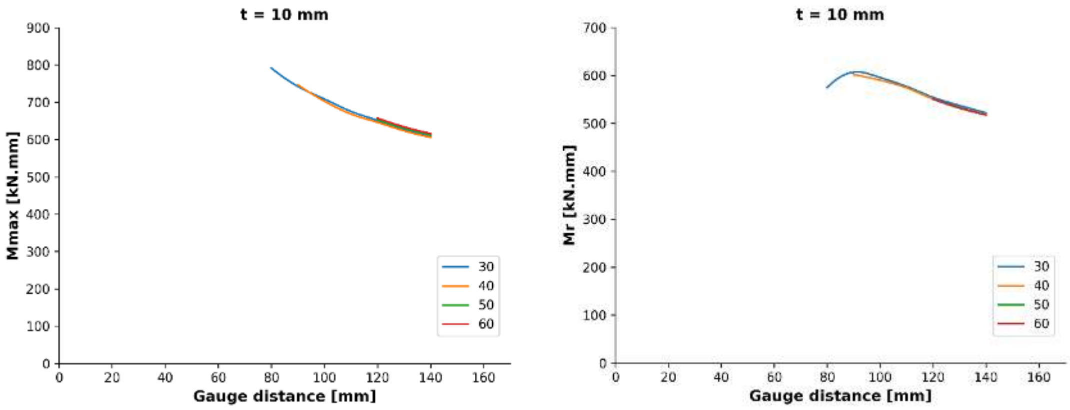

(a) *(b)*

Figure 4.6. *Variations of the Mmax and Mr for S2B2–M24 – t = 10 mm*

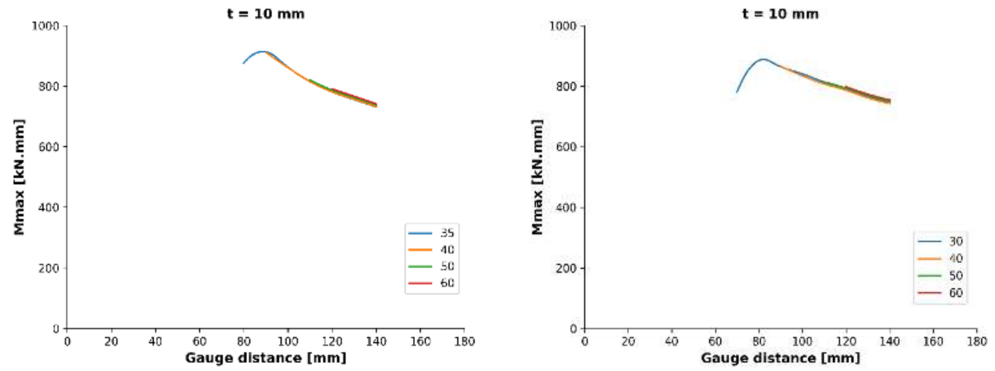

(a) S1B1–M27 *(b) S3B2–M24*

Figure 4.7. *Variations of Mmax in function of w for T-stubs with large bolts and thin flanges*

Concerning the prying forces, an increase in the gauge distance led to an increase in prying forces for specimens involved in a failure mode 2 or 3 (see **Fig. 4.8**). As the failure mode shifted to mode 1, the increasing trend is followed by an decline in the prying forces, mostly for low values of the edge distance (See **Fig. 4.9**). For higher values of the edge distance, prying forces decreased as the edge distance was increased.

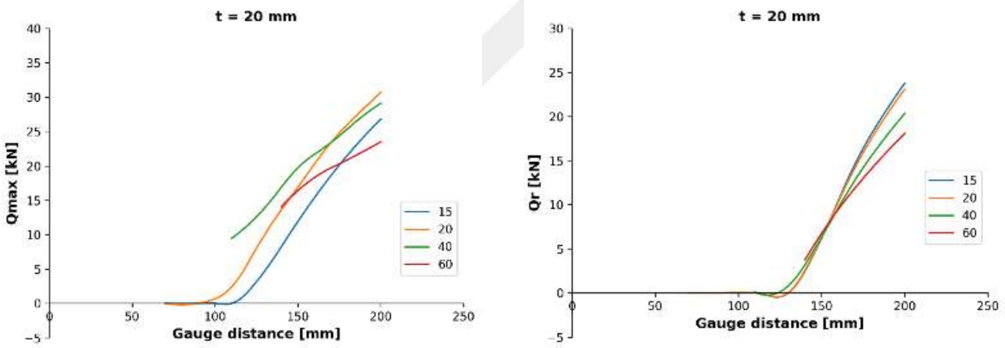

(a) S2B1-M12 - t = 20 mm

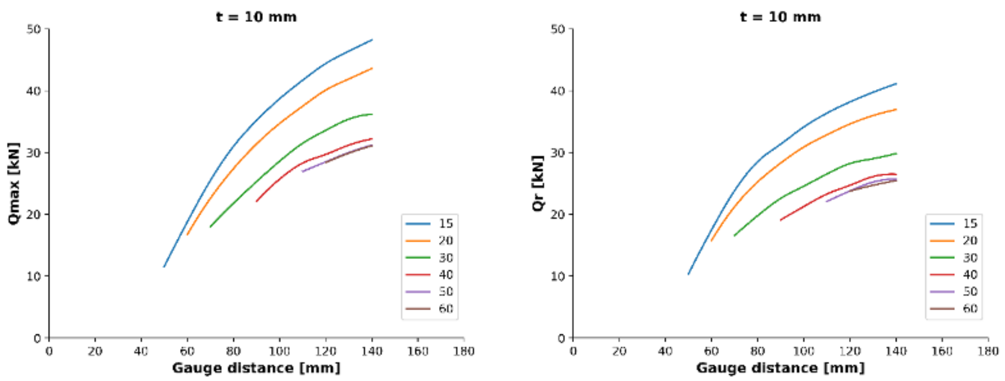

(b) S1B1-M12 – t = 10 mm

Figure 4.8. *Variations of the prying forces in function of the gauge distance for T-stubs involved in **(a)** Mode 3 and **(b)** Mode 2*

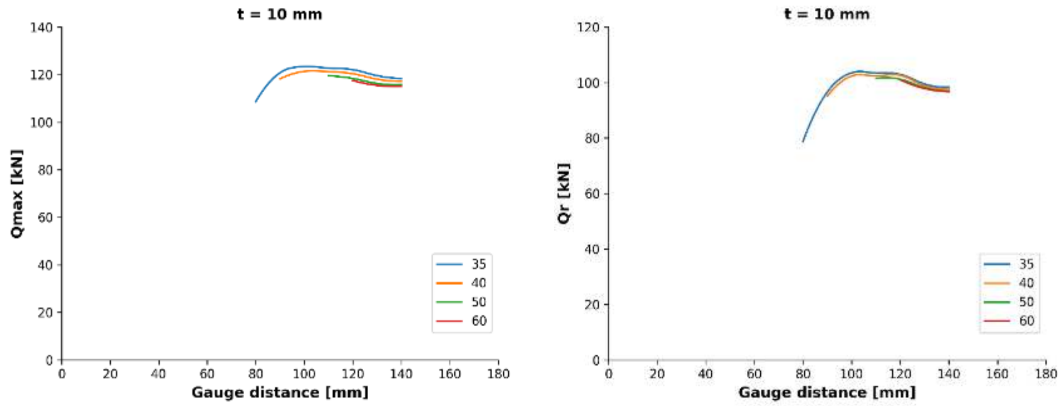

S2B2 - M24 – t = 10 mm

Figure 4.9. *Variations of the prying forces in function of the edge distance for T-stubs involved in failure Mode 1*

In accordance with the observations reported by Nair et al. (1969), there is an optimum value for the edge distance. For values of n below the optimum value, an increase in the edge distance resulted in a decrease in the bolt moment, whereas for values beyond the optimum value, the bolt moment increased for higher values of n. However, in case of a specimens involved in failure Mode 1, the observed trend was inversed: for values below the optimum value, increasing the edge distance led to an increase in the bolt moment, whereas for values beyond the optimum value, the bolt moment decreased for higher values of the edge distance (See **Fig. 4.10**).

Regarding the prying forces and for T-stubs involved in failure Mode 3, increasing the edge distance resulted to an increase in Q for values of n below an optimum value. Beyond the optimum value, prying forces decreases as the edge distance increased. When Mode 1 or 2 were involved, only a decrease in the prying forces was observed as the edge distance was increased (See **Fig. 4.11**). It seems pertinent to note that the optimum value may be different for the bolt moment and the prying force and depends on other parameters such as the gauge distance.

Additionally to the bolt moment and the prying force, their magnitude in relation to the applied load was also examined. Four categories were considered: (i) the ratio at the attainment of the plastic resistance, $(Q/F)_r$ or $(M/F)_r$, (ii) the ratio when the Qmax or Mmax are reached, (Q_{max}/F) or (M_{max}/F), (iii) the ratio at ultimate stage, $(Q/F)_u$ or $(M/F)_u$, and (iv) the maximum ratio QR_{max} or MR_{max}. As illustrated in **Fig. 4.12**, the ratio corresponding to Q_{max} or M_{max} doesn't always correspond to the maximum ratio.

This is particularly noticeable for the ratio related to the bolt moment. The maximum ratio can be reached at the beginning of the loading and correspond to very low values of the moment. Therefore, little attention will be given to the the maximum ratios.

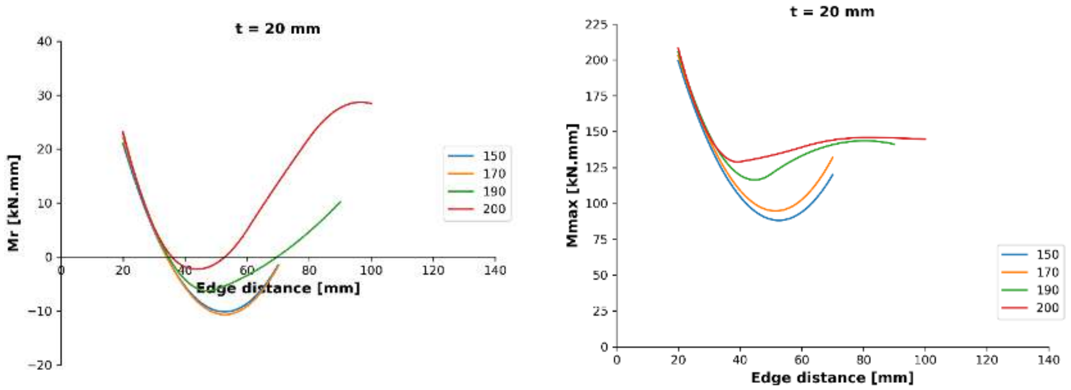

(a) S3B2 - M16

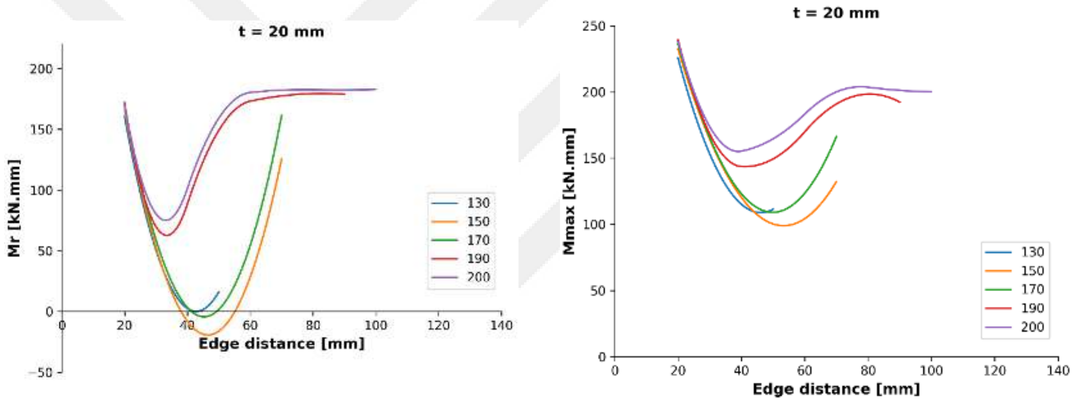

(b) S1B2 - M16

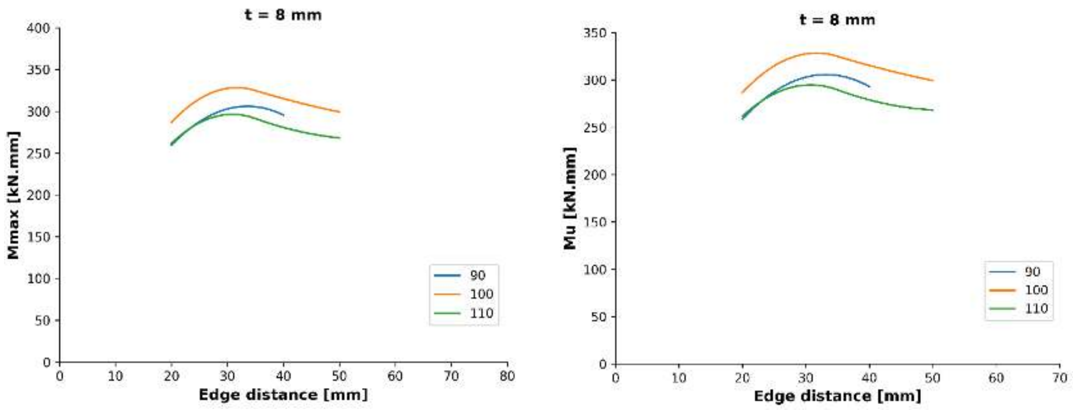

(c) S2B2 - M16

Figure 4.10. *Variations of the bolt moment in function of the edge distance*

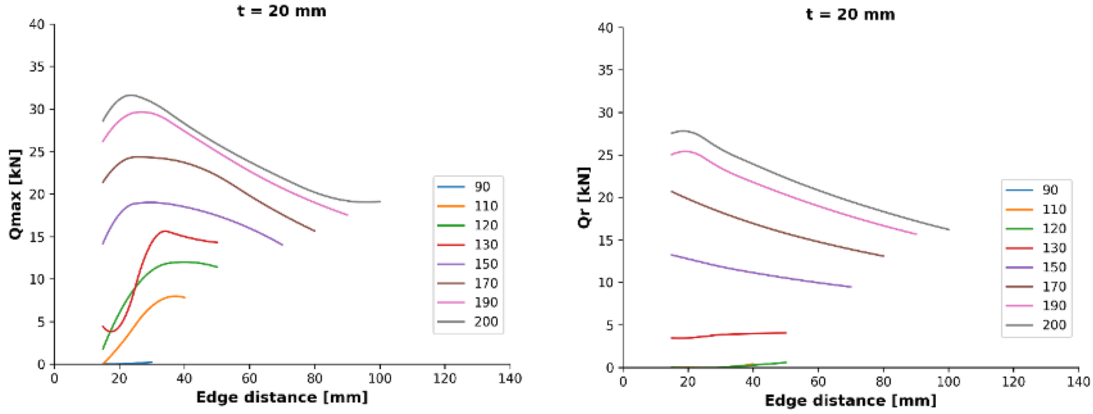

(a) S1B1 - M12

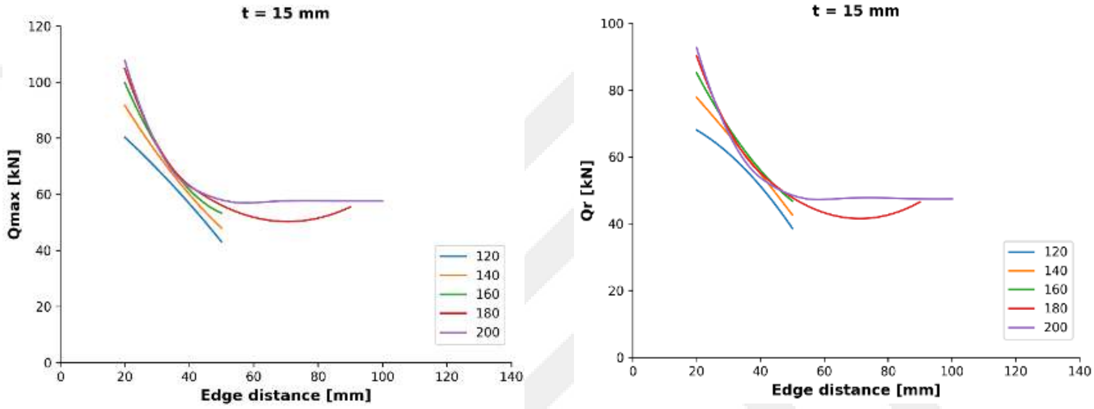

(b) S2B1 - M16

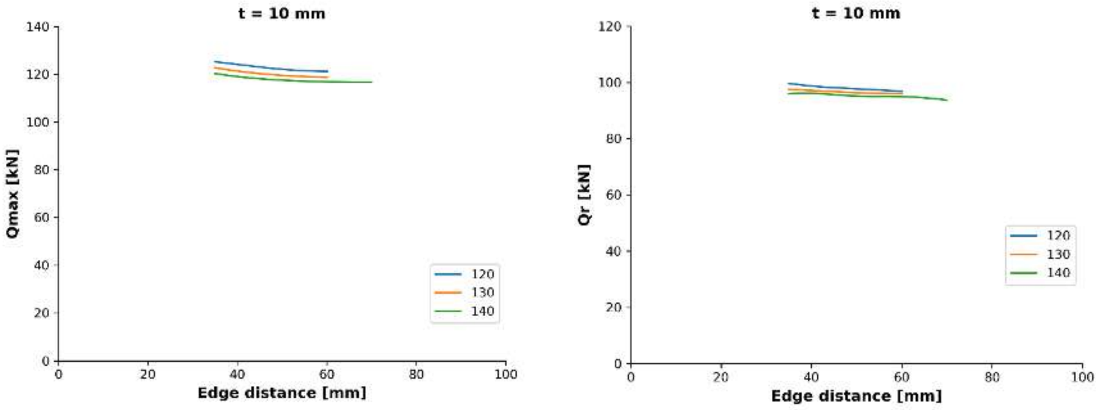

(c) S3B1 - M27

Figure 4.11. *Variations of the pring forces in function of the edge distance*

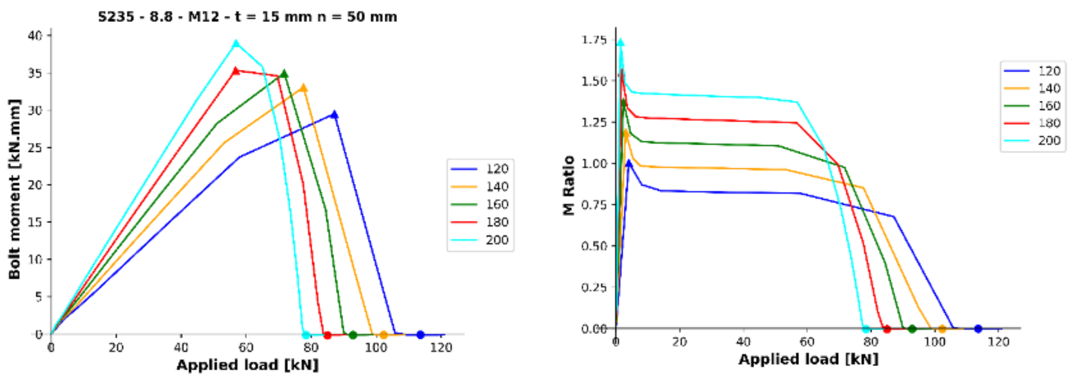

(a) S1B1 - M12

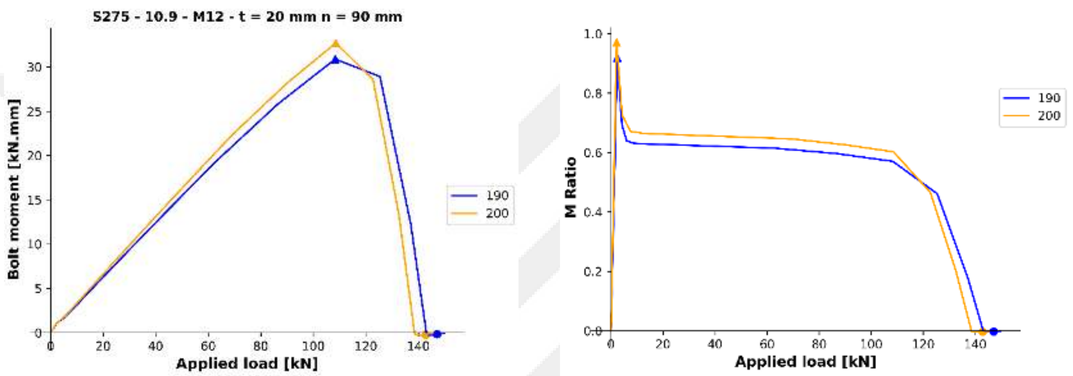

(b) S2B2 - M12

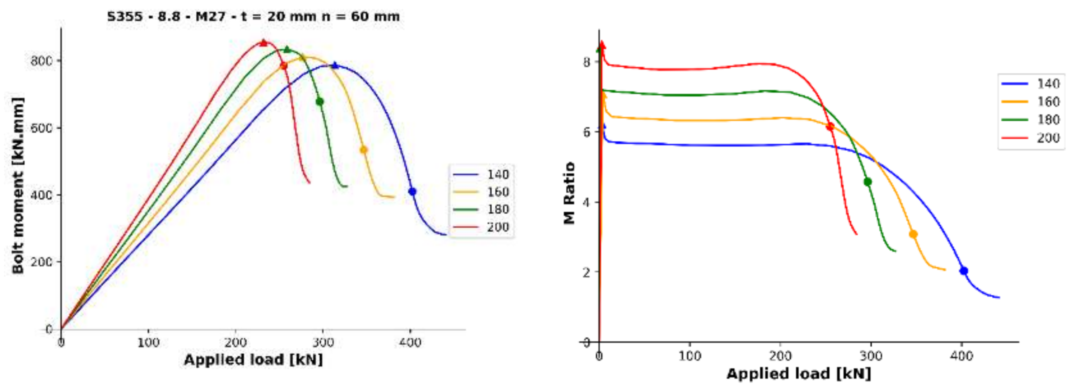

(c) S3B1 - M27

Figure 4.12. *Specimens with the maximum bolt moment ratio at the beginning of the loading*

As reflected in Fig.**4.13** and **Fig. 4.14**, the prying ratio, Q/F and the bolt moment ratio, M/F exhibited variations similar to those of their respective component, Q and M. However, the decline in prying forces observed in specimens with mode 1 failure for higher gauge distance was not exhibited for prying ratios (see **Fig. 4.13 – Fig. 4.16**)

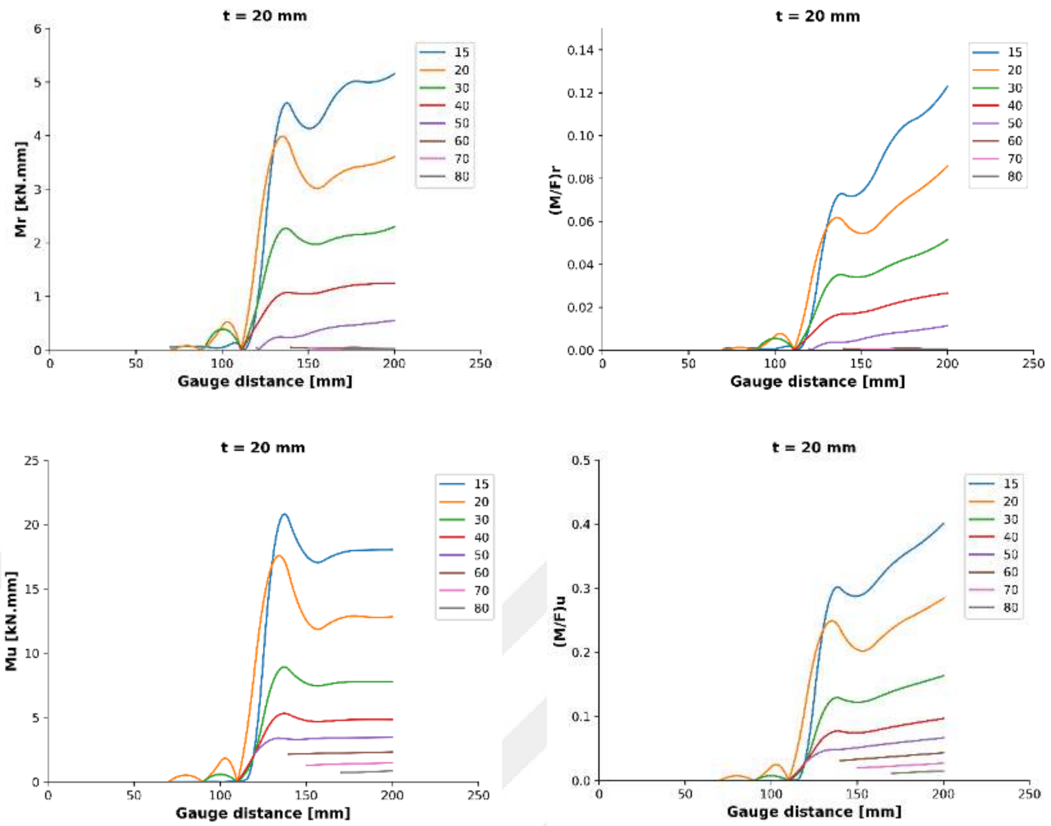

Figure 4.13. *Variations of M and M/F in function of the gauge distance for S1B1-M12*

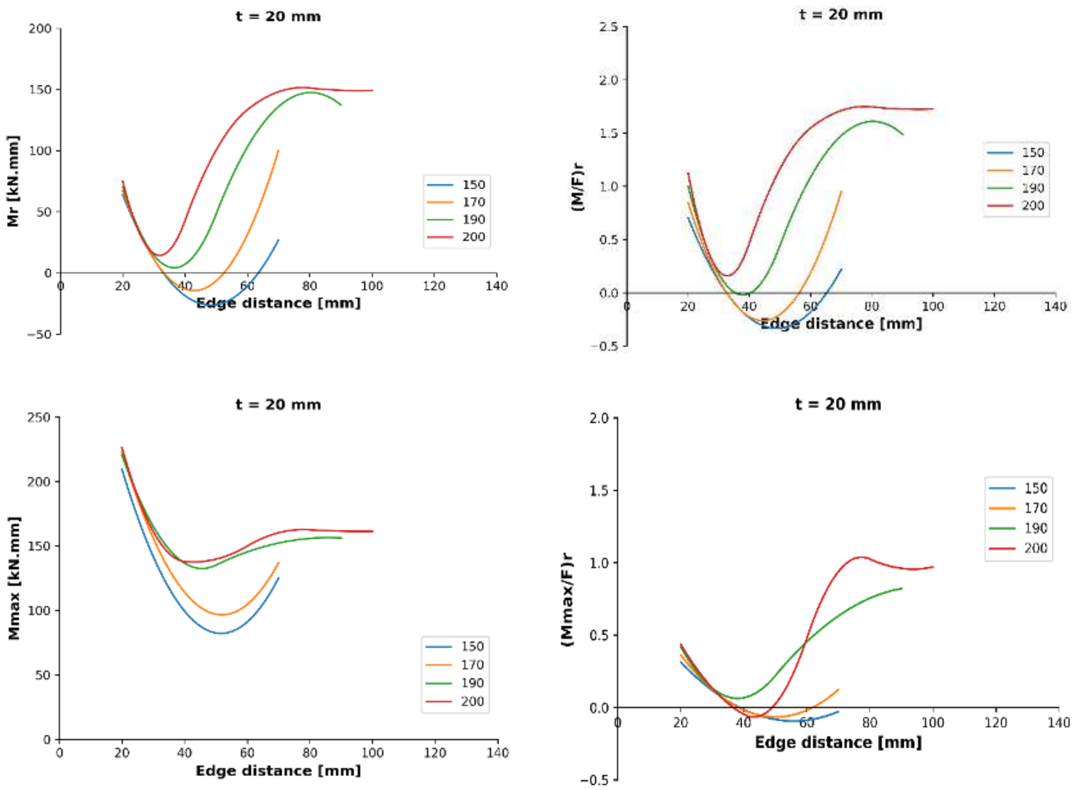

Figure 4.14. *Variations of M and M/F in function of the edge distance for S2B2-M16*

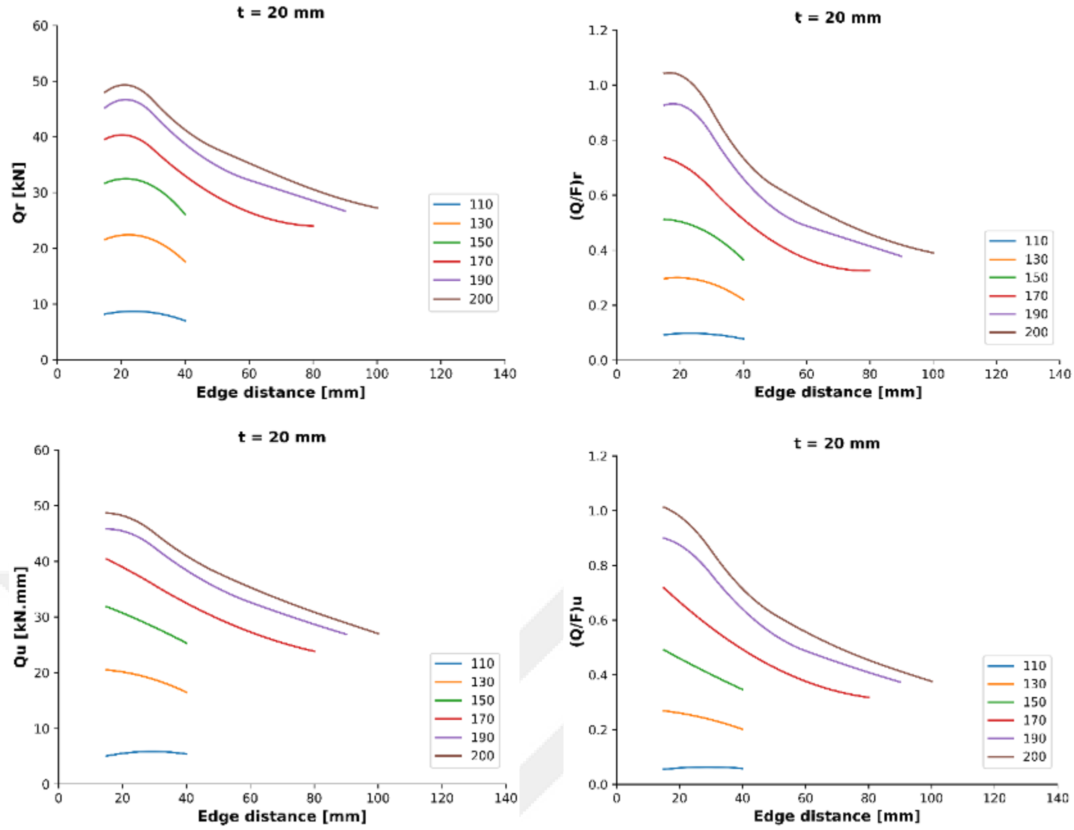

Figure 4.15. *Variations of Q and Q/F in function of the edge distance for S1B2 - M12*

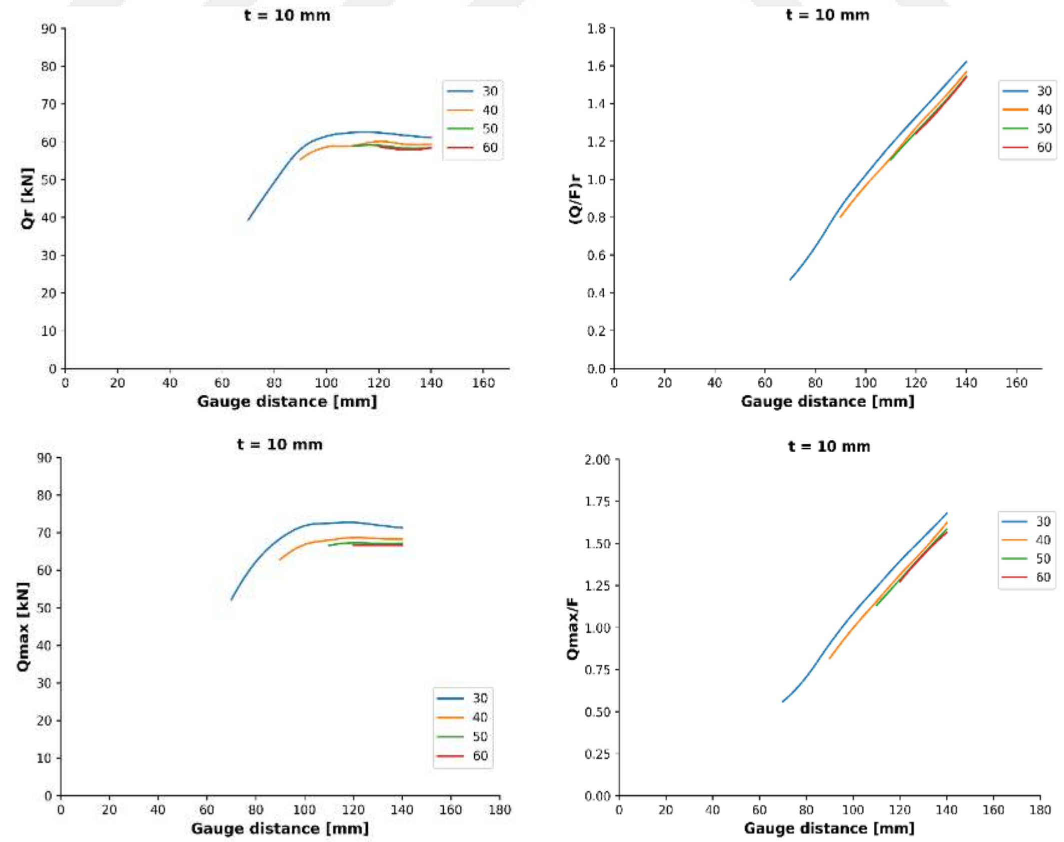

Figure 4.16. *Variations of Q and Q/F in function of the gauge distance for S2B1-M24-t 10 (Mode 1)*

Regarding the position of the prying forces resultant, the conclusions made in the previous chapter are still valid. It is, however worth mentioning that, for very flexible flanges (relatively to the bolt), the difference between the positions at the attainment of the T-stubs plastic resistance and at the ultimate stage is more noticeable (See **Fig. 4.17**).

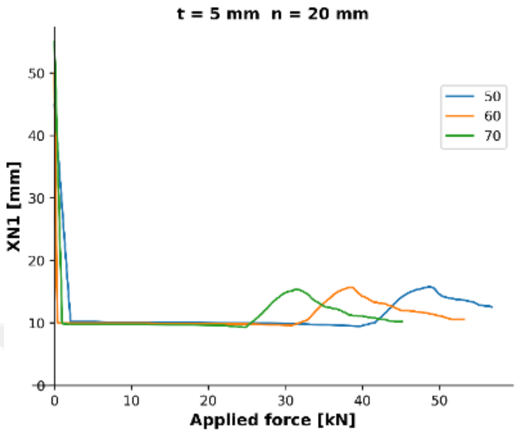

(a) S1B2 - M12 - t = 5 mm

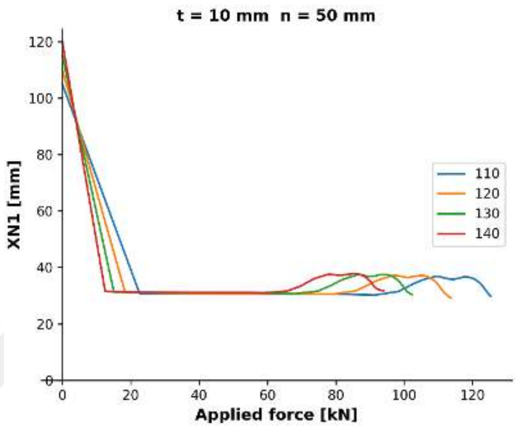

(b) S2B1 - M24 - t = 10 mm

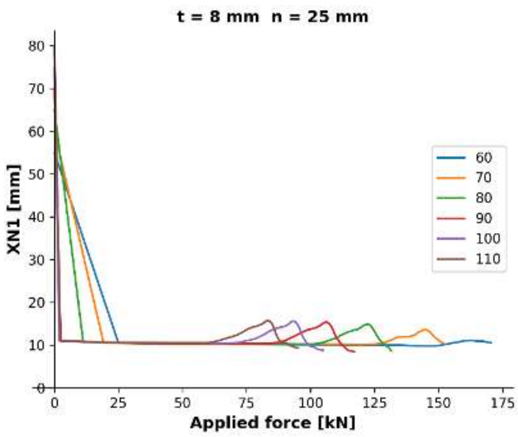

(c) S3B1 - M20 - t = 8 mm

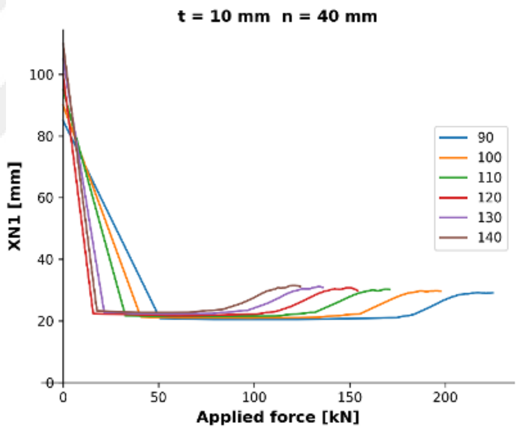

(d) S3B2 - M27 - t = 10 mm

Figure 4.17. *Variations of XN1 in function of the applied force for T-stubs with flexible flanges*

4.3.2. Influence of flange thickness

The flange thickness is one the parameters with a significant influence on the behaviour of bolted steel T-stubs. In most cases, an increase in the thickness led to a sharp decrease in the prying forces, as well as in the bolt moment, as reported by Nair et al. (1969) and observed in the previous chapter. In some cases, a thicker flange could actually increase the bolt moment or the prying forces. However, for all the specimens, thicker flanges resulted in lower bolt moment ratio and prying ratio (see **Fig. 4.18 – Fig. 4.21**). It also caused the resultant of the prying forces to shift closer to the edge. In some cases, the increase in the thickness could lead to a complete lift-off of the flanges (See **Fig. 4.22** and **Fig. 4.23**).

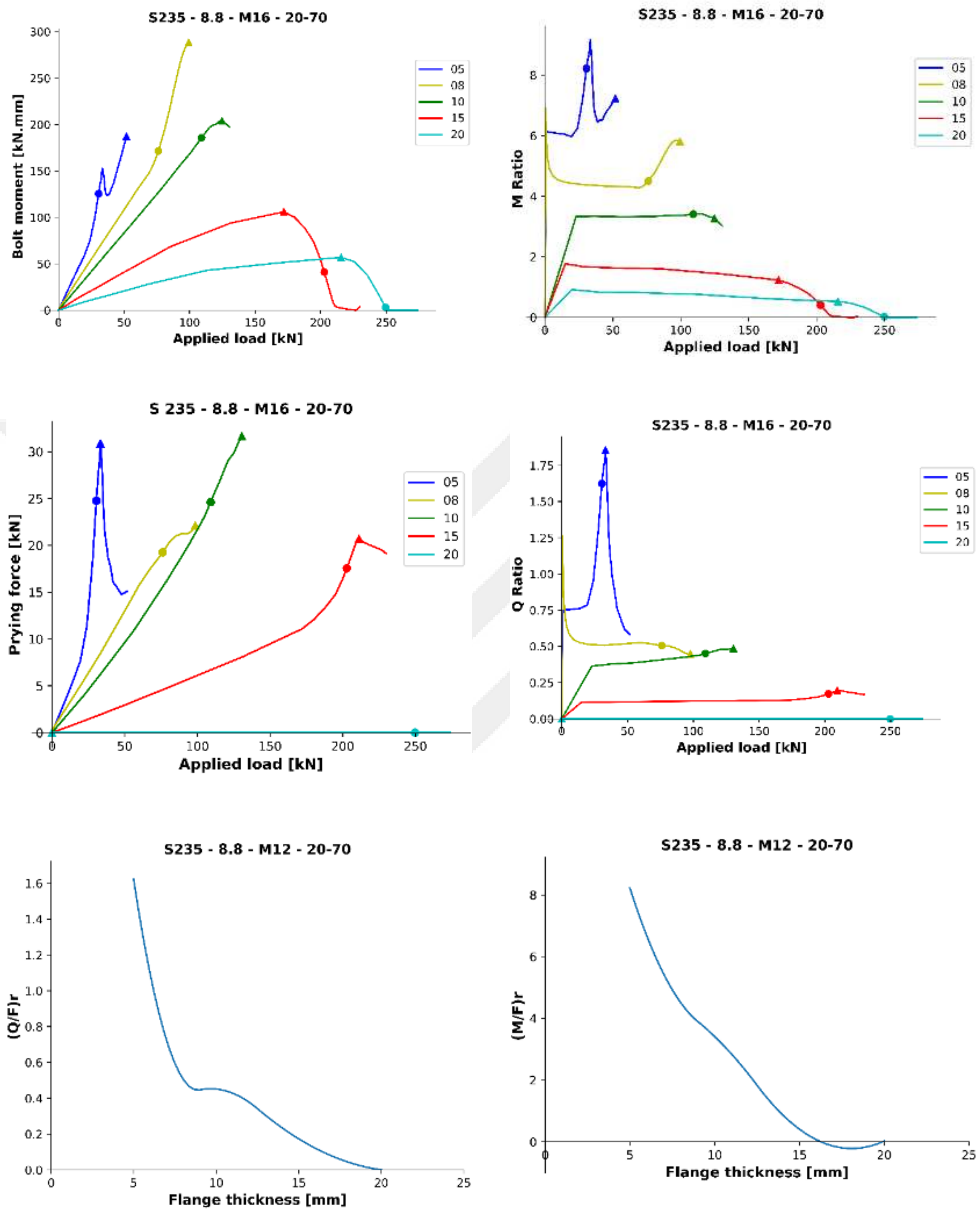

Figure 4.18. *Influence of the flange thickness on Q, Q/F, M and M/F*

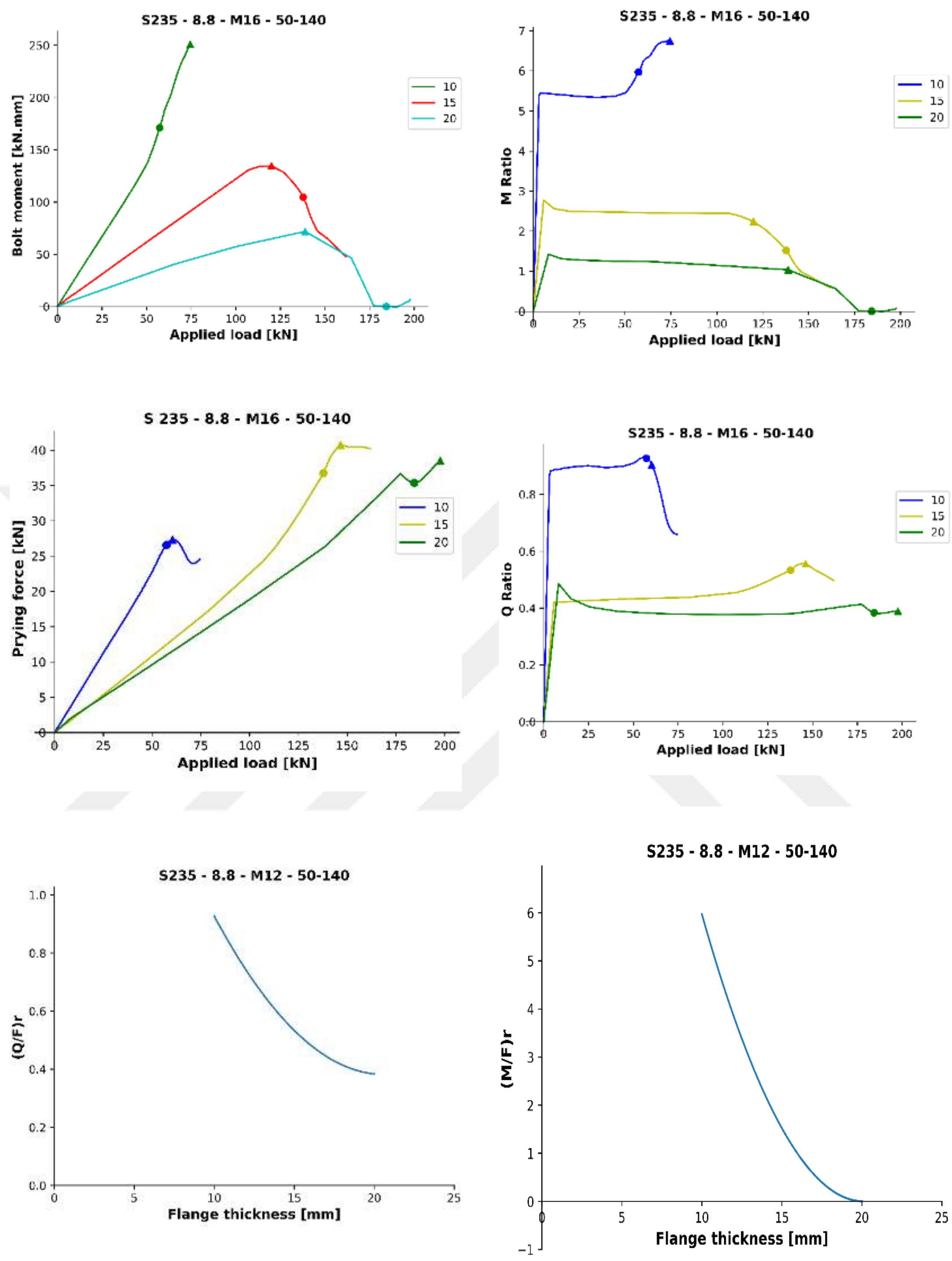

Figure 4.19. *Influence of the flange thickness on Q, Q/F, M and M/F*

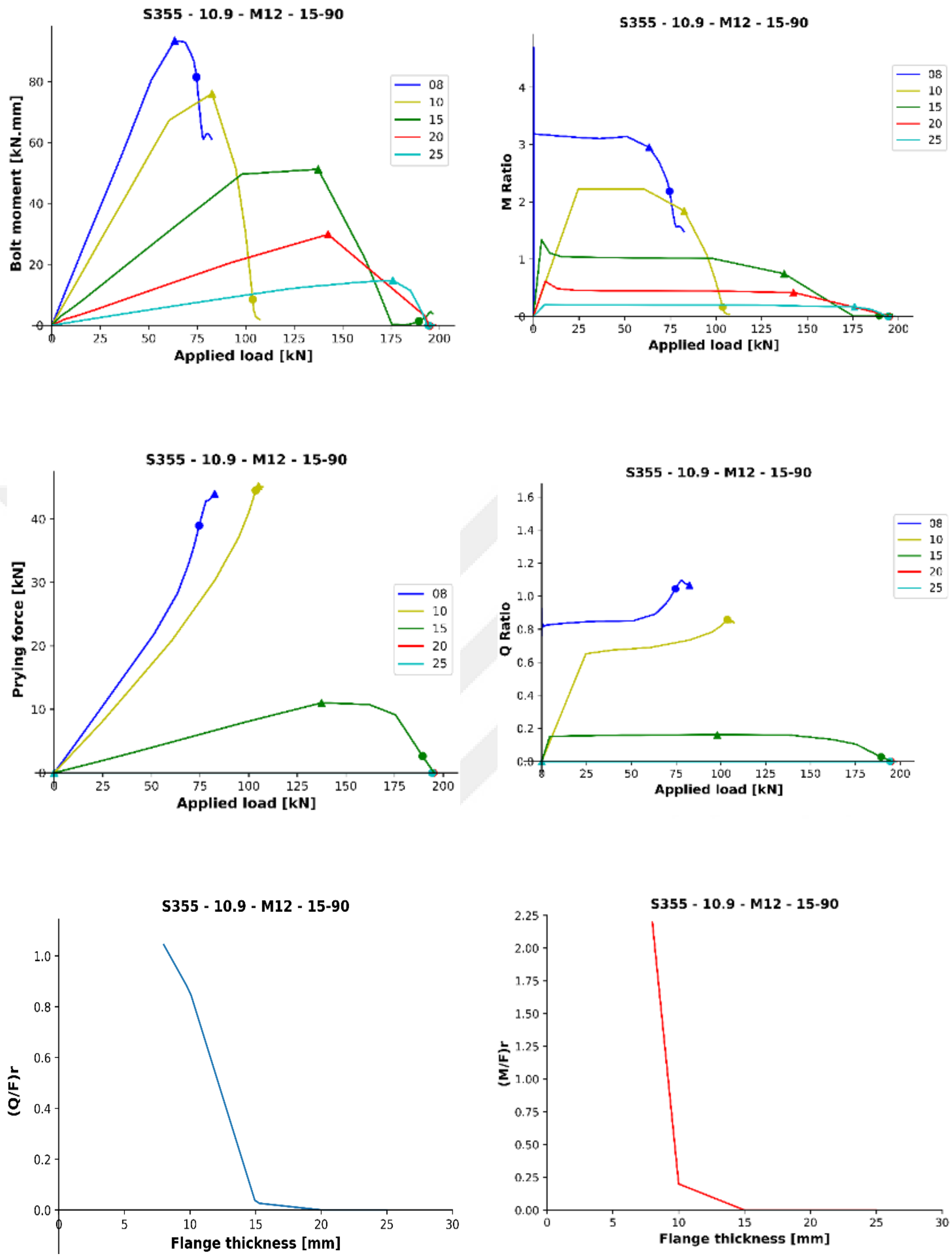

Figure 4.20. *Influence of the flange thickness on Q, Q/F, M and M/F*

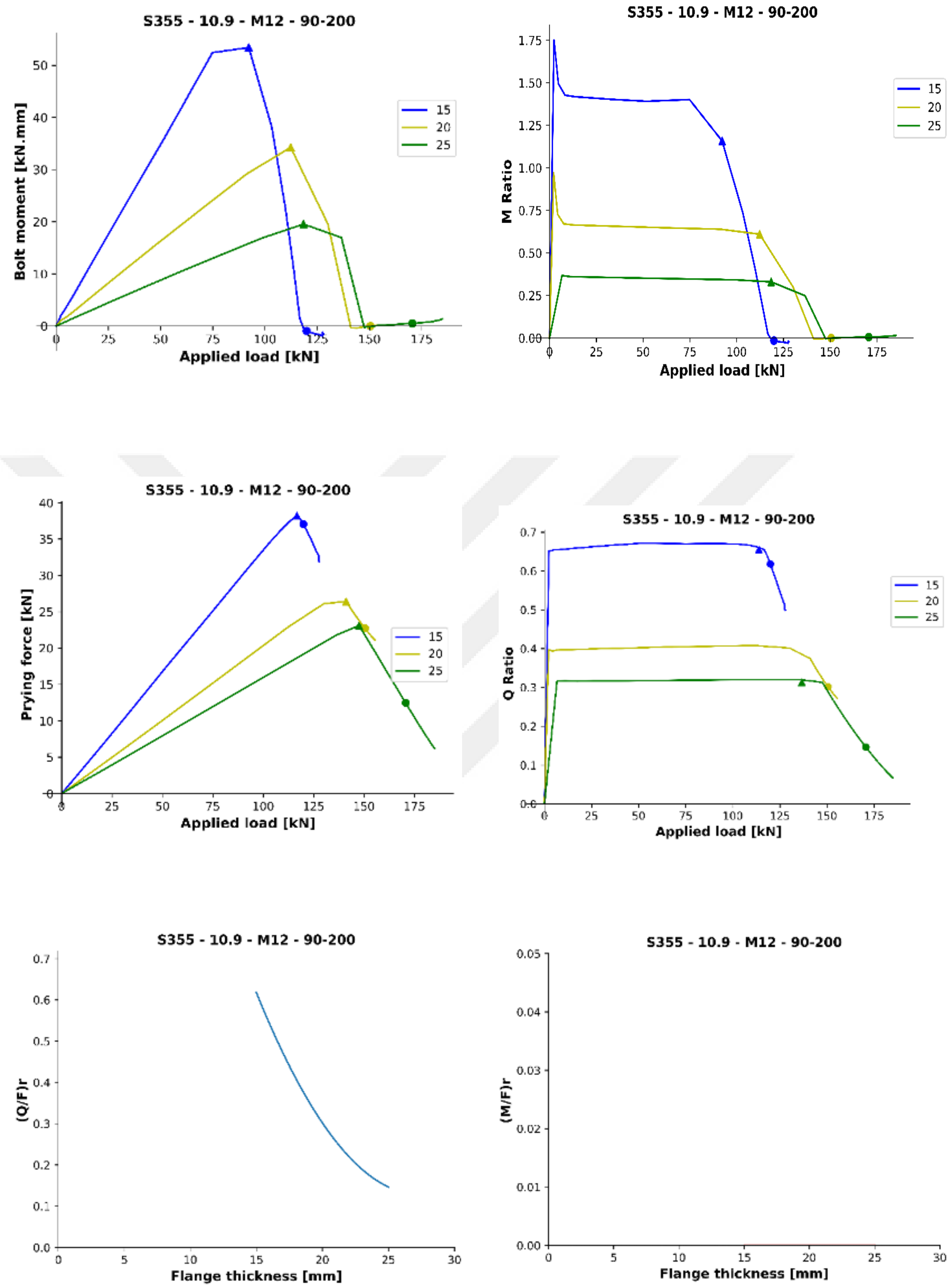

Figure 4.21. *Influence of the flange thickness on Q, Q/F, M and M/F*

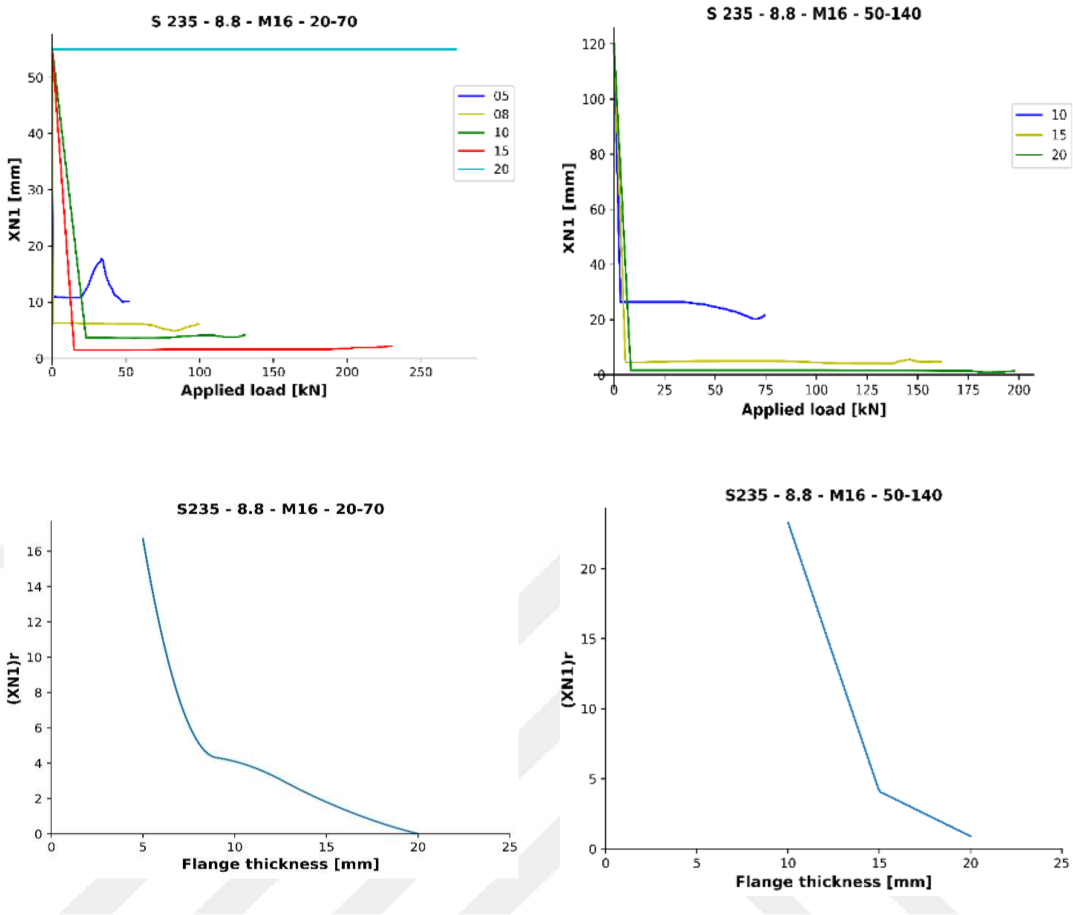

(a) *n = 20 mm w = 70 mm* **(b)** *n = 50 mm – w = 140 mm*

Figure 4.22. *Influence of the flange thickness on XN1 for S1B1 - M16*

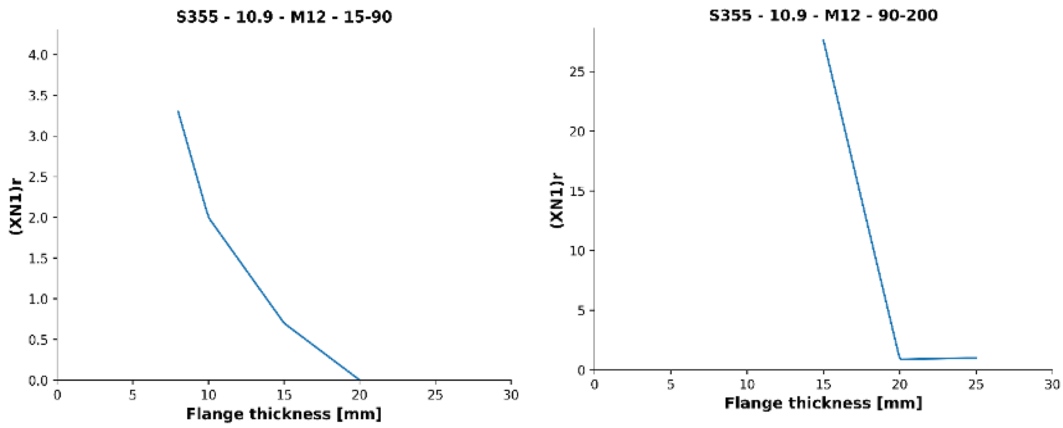

(a) *n = 15 mm w = 90 mm* **(b)** *n = 90 mm – w = 200 mm*

Figure 4.23. *Influence of the flange thickness on XN1 for S3B2 - M12*

4.3.3. Influence of flange width

In order to investigate the influence of the flange width on prying action, T-stubs with a width $b = 70\ mm$ have been analyzed. The influence of the flange width depended on the failure mechanism of the T-stub. When the flange is the weakest component of the T-stub, decreasing the flange width may reduce the ability of the flange to exert bending on the bolt. As a consequence, the bolt moment would be lower in the T-stub with a reduced flange width. When other failure mechanisms were involved, the bolt moment in the T-stub with a reduced flange width was higher due the decreased rigidity. Despite all the changes observed for M depending on the failure mechanism, the variations of the bolt moment ratios were the same regardless of the failure mechanism: a reduced flange width led to an increase in the bolt moment ratio (See Fig. 4.24). For all the T-stubs, the reduced flange width resulted in higher prying forces for low values of the gauge distance and in lower prying forces for high values of the gauge distance (see Fig. 4.25). Similarly to M/F, the prying ratio increased when the flange width was reduced.

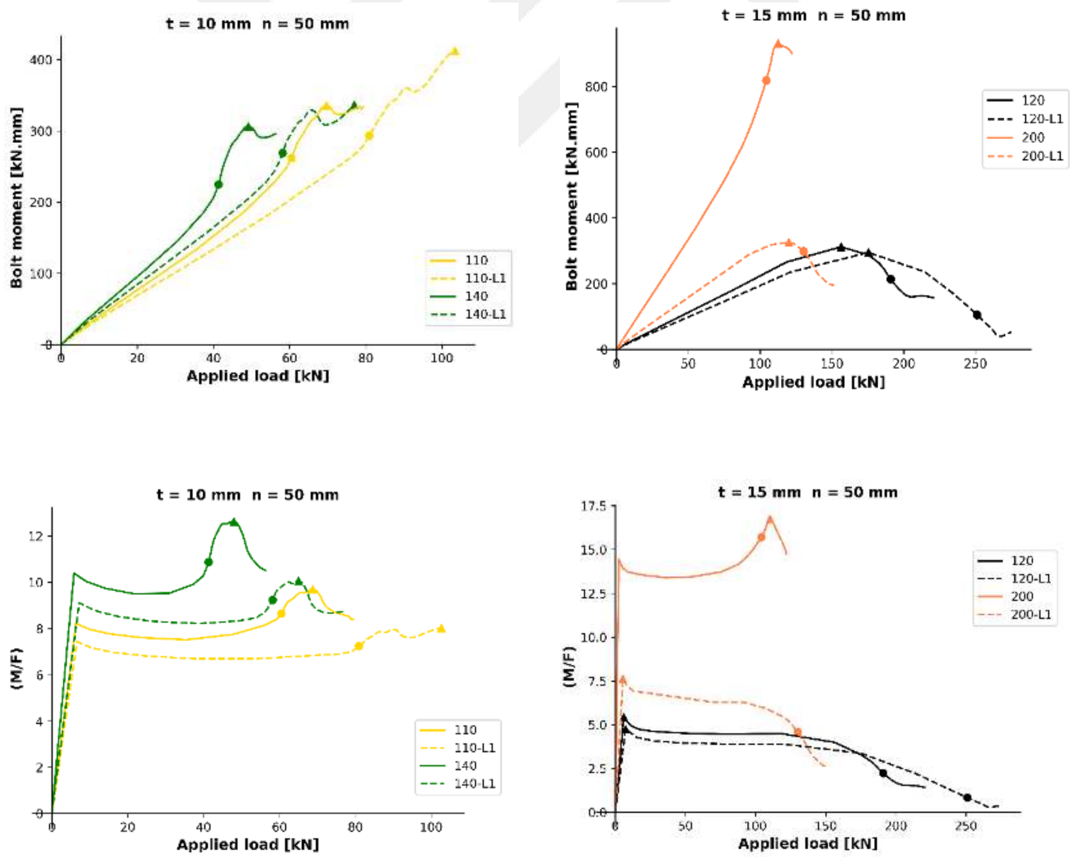

(a) S1B1 - M20 *(b) S3B1 - M20*

***Figure 4.24**. Influence of the flange width on M and M/F*

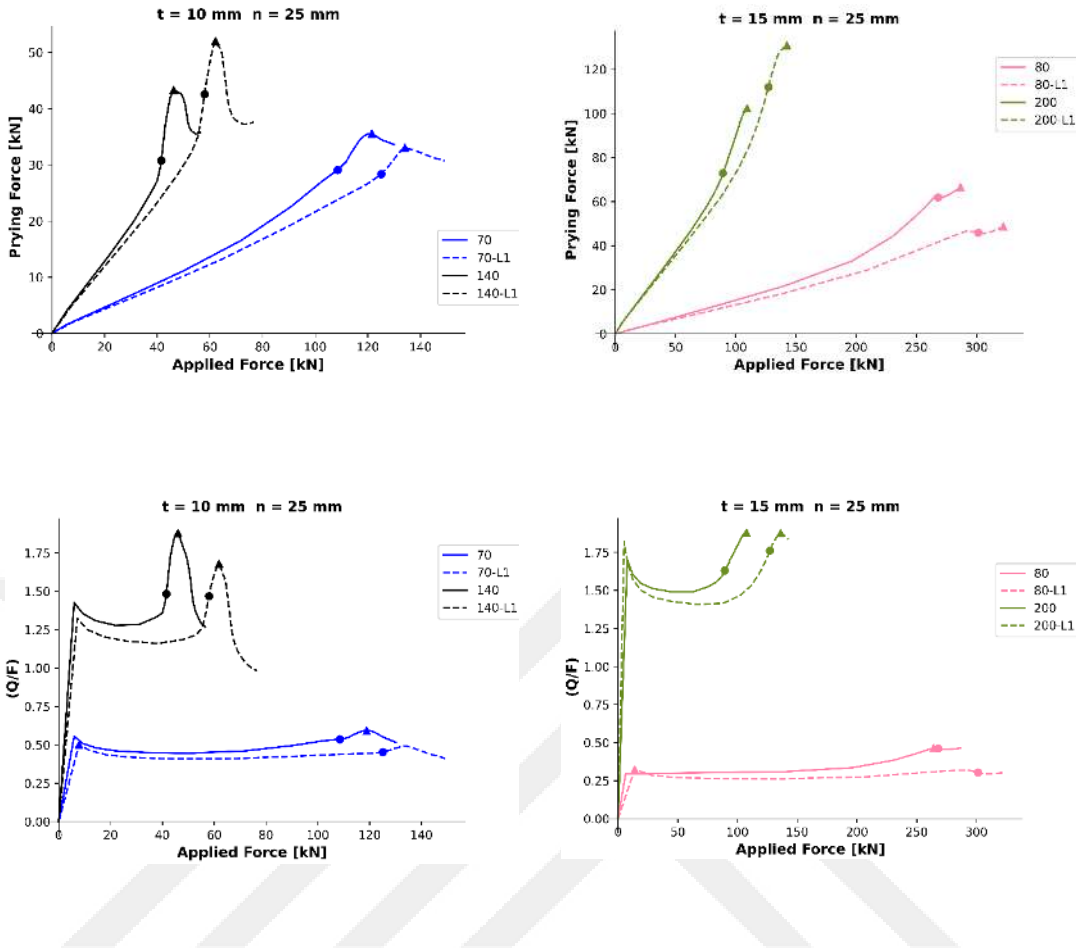

(a) *S1B1 - M20* ***(b)*** *S3B1 - M20*

Figure 4.25. *Influence of the flange width on Q and Q/F*

Regarding the location of the prying force, it moved farther from the edge when the flange width decreased. However, for very low values of the edge distance, the flange width had little effect of the position of the resultant (See **Fig. 4.26**). In some cases, the decrease of the flange width would could cause the T-stub to shift from a complete lift-off instance to an instance with contact.

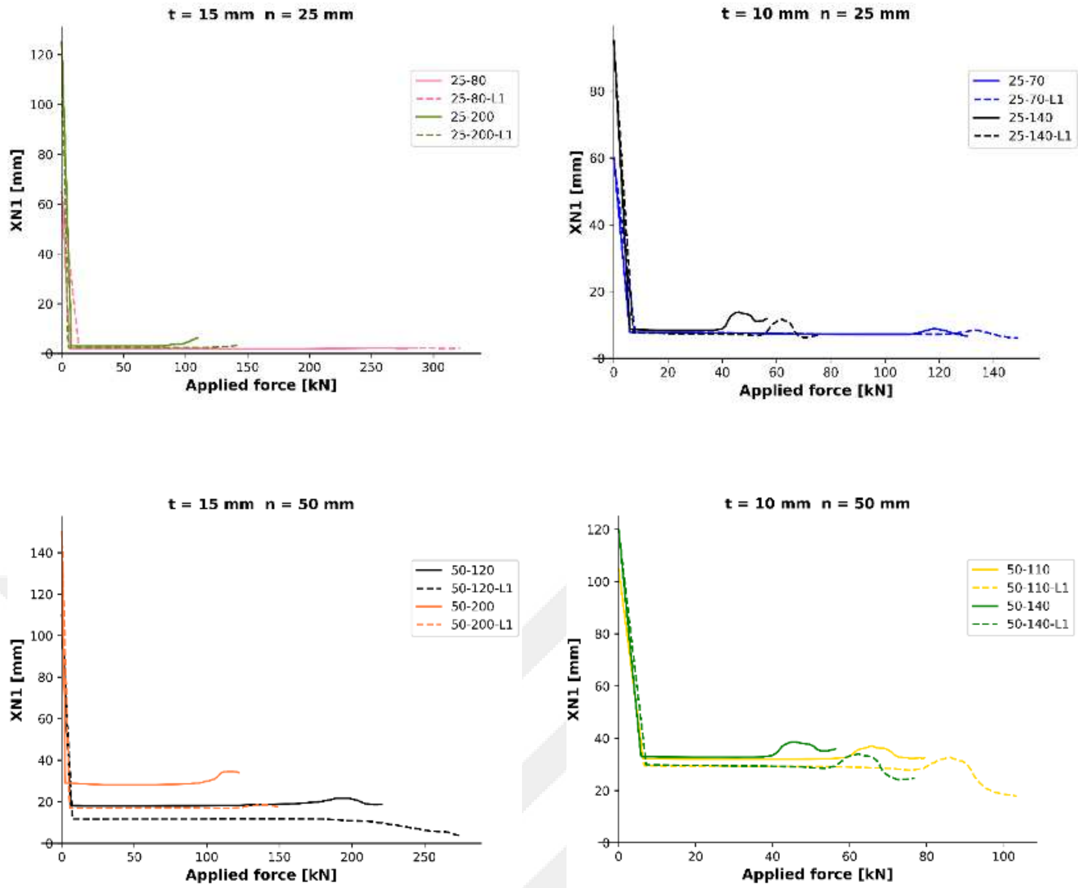

***(a)**) S1B1 - M20* *(**b**) S3B1 - M20*

***Figure 4.26**. Influence of the flange width on XN1*

4.3.4. Influence of steel class

The steel class may affect the relative flexibility of the flanges. If the flange is the weakest component of the T-stub (failure mode 1), the relative strength of the bolts will play an important role in the way the steel class influences the behaviour of the T-stubs.When, the bolt is strong enough for the steel class, hence the flange flexibility, not to have any influence on the behaviour of T-stub, the values of bolt moment ratio and the prying ratio at the attainment of the plastic resistance and at the attainment of Q_{max} and M_{max} were similar or exhibited very little variations for almost all the steel classes although the bolt moment and the prying forces were higher when a higher steel class was used (See **Fig. 4.27** and **Fig. 4.28**). It is worth mentioning that the complete M/F and Q/F graphs for each steel class were different due to their corresponding resistance.

On the contrary, if the bolt is the weakest component, using higher steel class wouldn't have any influence of the failure mode of the T-stub. However, higher steel class resulted relatively higher bolt moment but had little influence on the bolt moment ratio. The bolt moment, and therefore the bolt moment ratio, beyond the point of plastic resistance is rather low (close to zero). Regarding the prying forces and the prying ratios, the plots against the applied load appeared coincident or showed very little differences for the different steel classes. Nevertheless, their values at the attainment of the plastic resistance, Q_r and $(Q/F)_r$ were higher with a lower steel class. In overall, the prying forces and the prying ratios can be considered higher when a lower steel class is used due to the fact higher steel class could result in less flexible flanges and lead to limited deformation in the flanges prior to their separation (see **Fig. 4.29**).

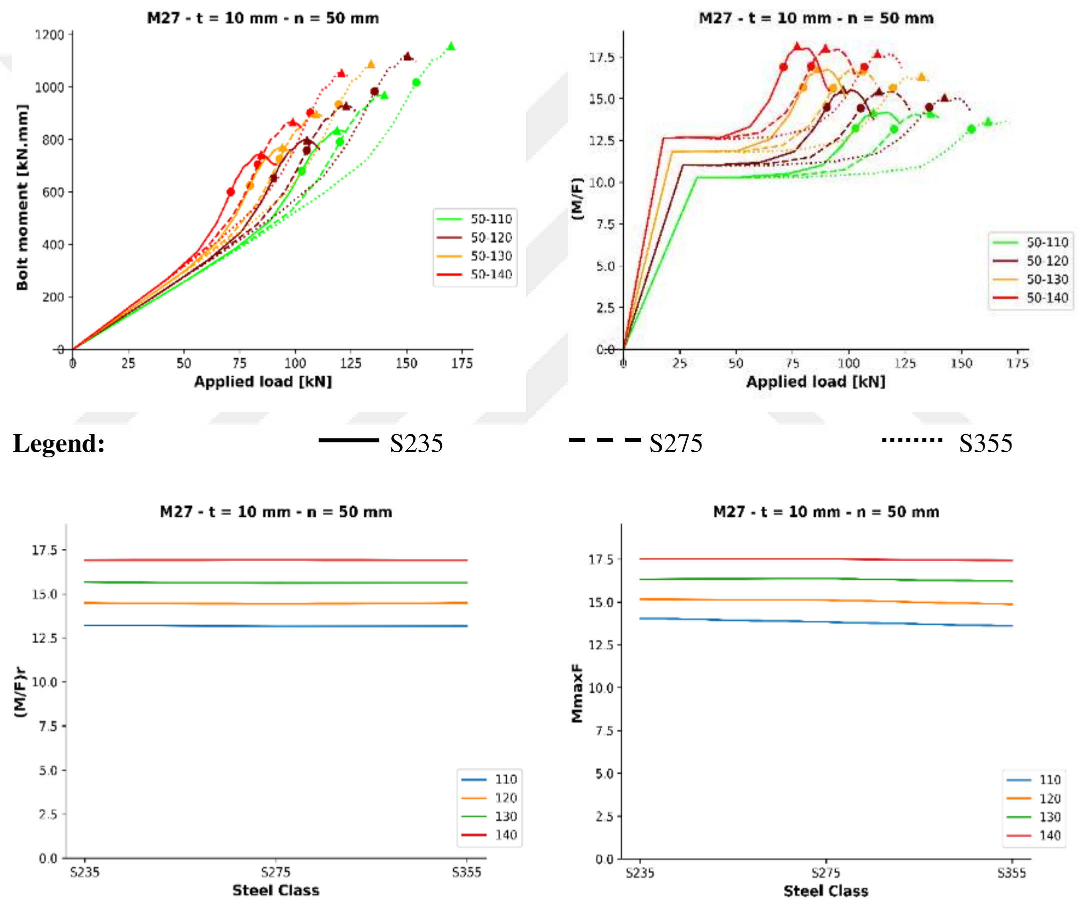

Figure 4.27. *Influence of the steel class on M and on M/F for M27 – t 10 – n = 50 mm (Mode 1)*

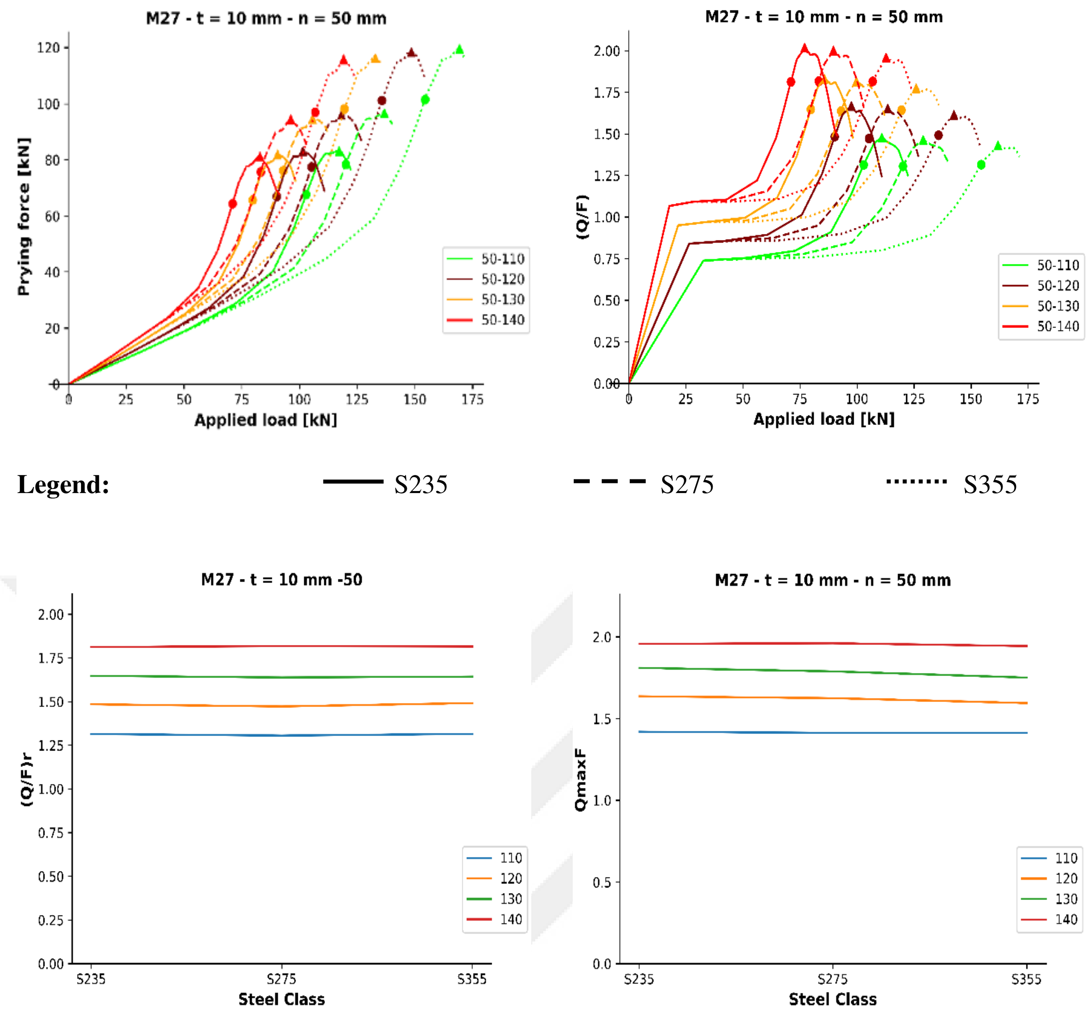

Figure 4.28. *Influence of the steel class on Q and on Q/F for M27 – t 10 – n = 50 mm (Mode 1)*

The use of higher steel classes can cause a shift in the failure mechanism, from mode 1 to mode 2 or from mode 2 to mode 3, and therefore result in lower values of Q/F and M/F. Although the resultant of the contact stresses moved closer to the edge when a higher steel class was used, the variations were negligible (See **Fig. 4.30**).

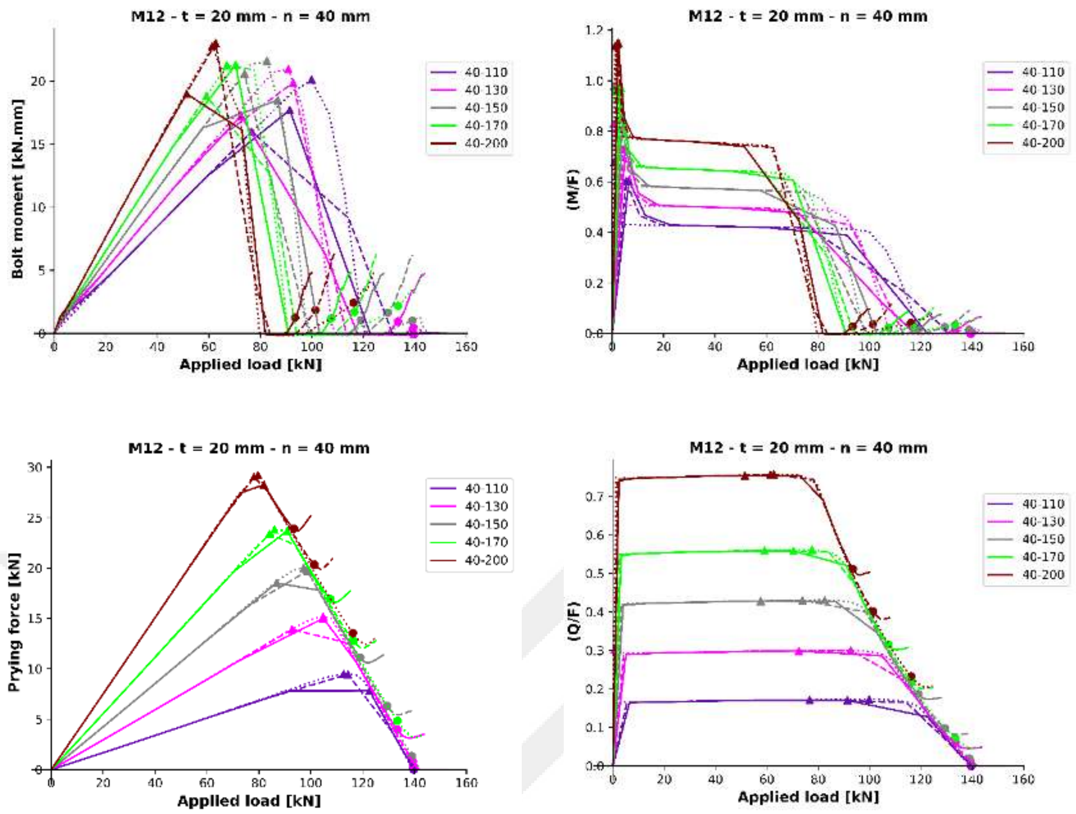

Legend: S235 S275 S355

Figure 4.29. *Influence of the steel class on the M, M/F, Q and Q/F for M12 – t 20 – n = 40 mm (Mode 3)*

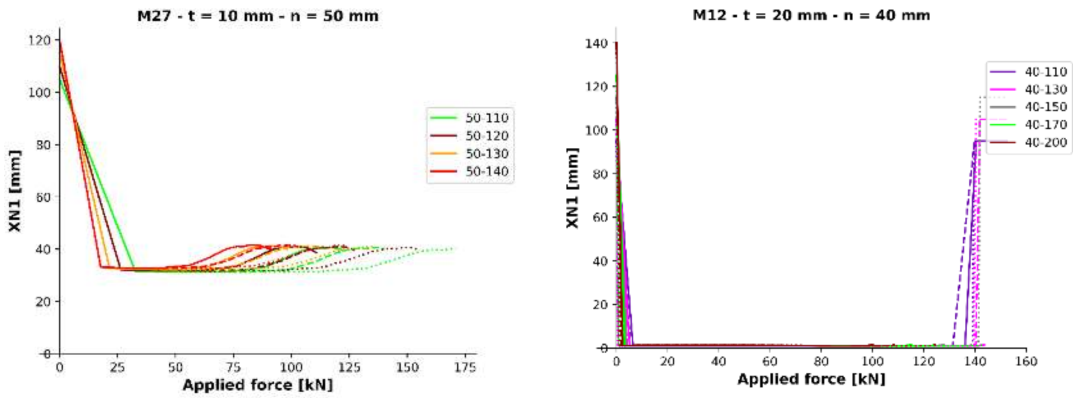

Legend: S235 S275 S355

(a) *M27 – t 10 – n = 50 mm (Mode 1)* **(b)** *M12 – t 20 – n = 40 mm (Mode 3)*

Figure 4.30. *Influence of the steel class on XN1 considering different failure mechanisms*

4.3.5. Influence of weld throat thickness

Welds can be a limiting component for the T-stub and in order to investigate their influence, the size of the welds throats was varied and summarized in Table. Three thicknesses (10 mm, 15 mm, and 25 mm) and three bolt diameters (M12, M20, and M27) were considered.

Table 4.2. *Weld throat thickness*

Flange thickness	Initial weld throat W_1	Increased weld throat
10 mm	5 mm	8 mm
15 mm	8 mm	10 mm
25 mm	8 mm	10 mm

The change in the weld throat size appeared to have little influence on the position of the prying forces resultant. Neverthless, the resultant was closer a little bit closer to the edge for smaller weld throat. As illustrated in **Fig. 3.23**, the larger size of the weld throat correspond to smaller value of m and would result in smaller lever arm for the flexural deformation of the flange. Consequently, M/F and Q/F decreased as the weld throat thickness was increased. The influence of the weld throat thickness is depicted in **Fig. 4.31** and **Fig. 4.32.**

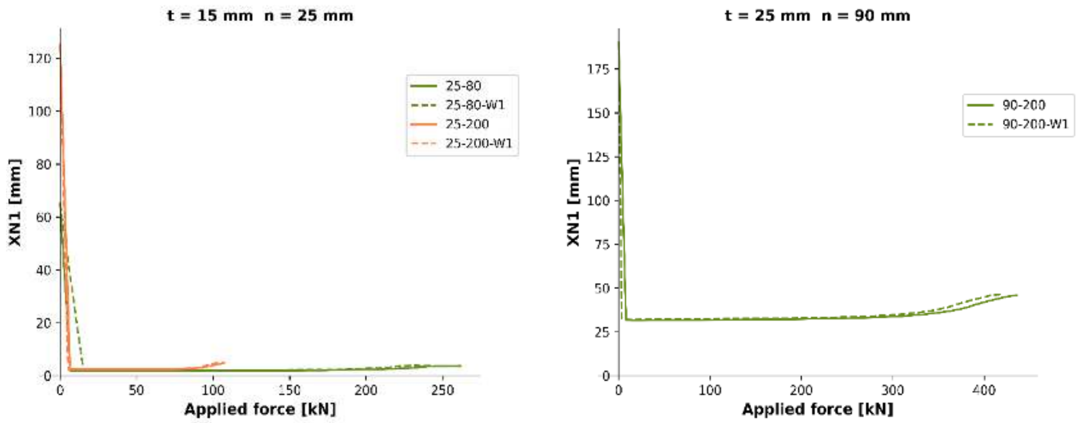

(a) *S1B1 - M20* **(b)** *S3B2 - M27*

Figure 4.31. *Influence of the weld throat thickness on the location of the prying force*

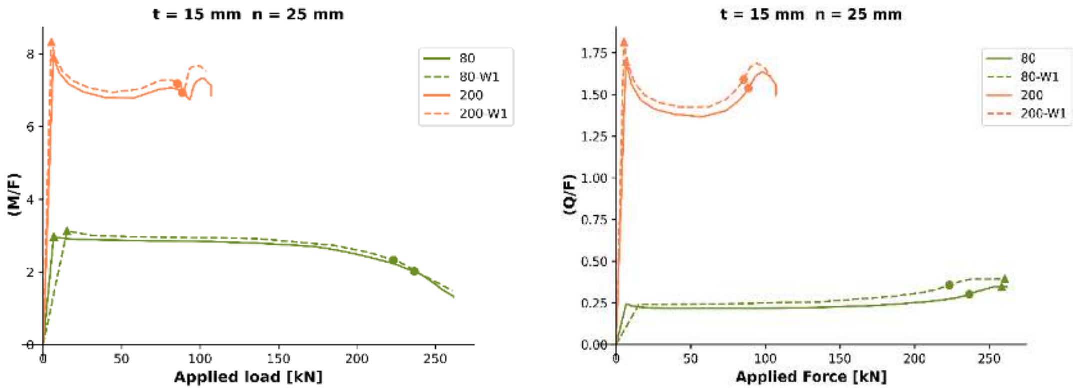

(a) S1B1 - M20

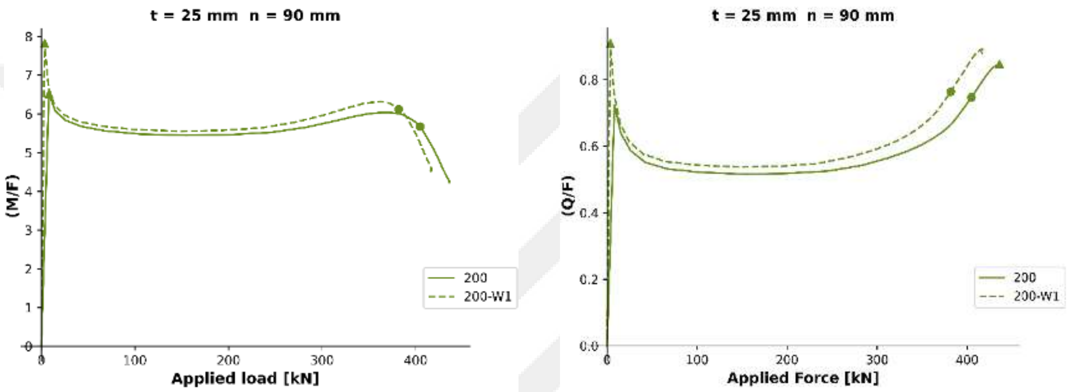

(b) S3B2 -M27

Figure 4.32. *Influence of the weld throat thickness for on M/F and Q/F*

4.3.6. Influence of bolt diameter

For a certain configuration, as the bolt diameter increased, the bolt would become relatively stronger as to the flange; allowing the flange to deform more and inducing increased moment in the bolts. Additionally, stronger bolts would maintain the flanges connected more firmly and would undergo less deformation as to the flanges. As a result, increased prying forces were observed. Similarly, the prying ratios and bolt moment ratios increased as the bolt diameter increased. Increasing the bolt diameter, resulted in a shift in the failure mechanism of the T-stub: from mode 3 to 2 or even 1 or from mode 2 to 1. As a consequence, the resultant of prying forces moved farther from the edge.

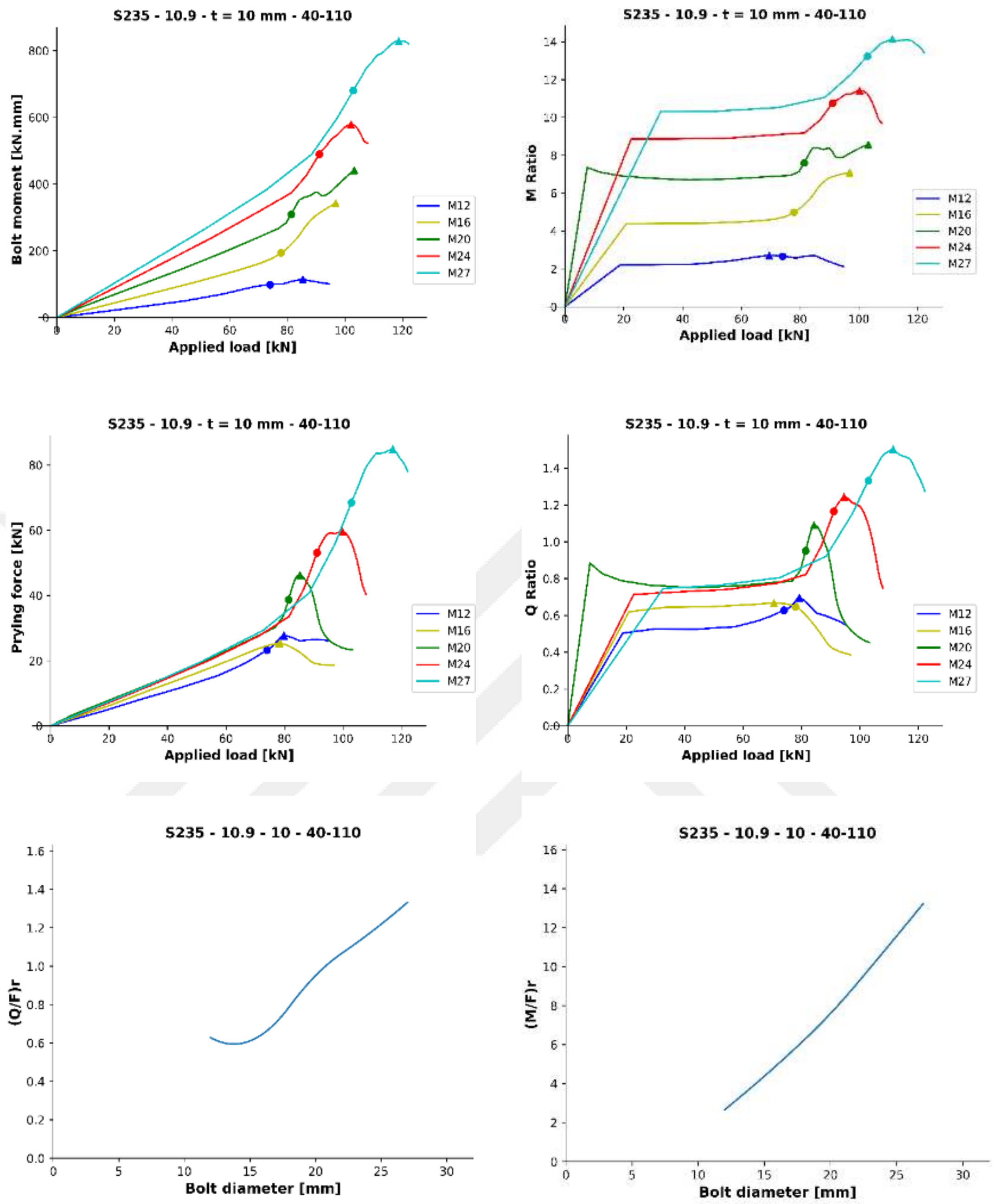

Figure 4.33. *Influence of the bolt diameter on M, M/F, Q and Q/F for S1B2 – t = 10 mm*

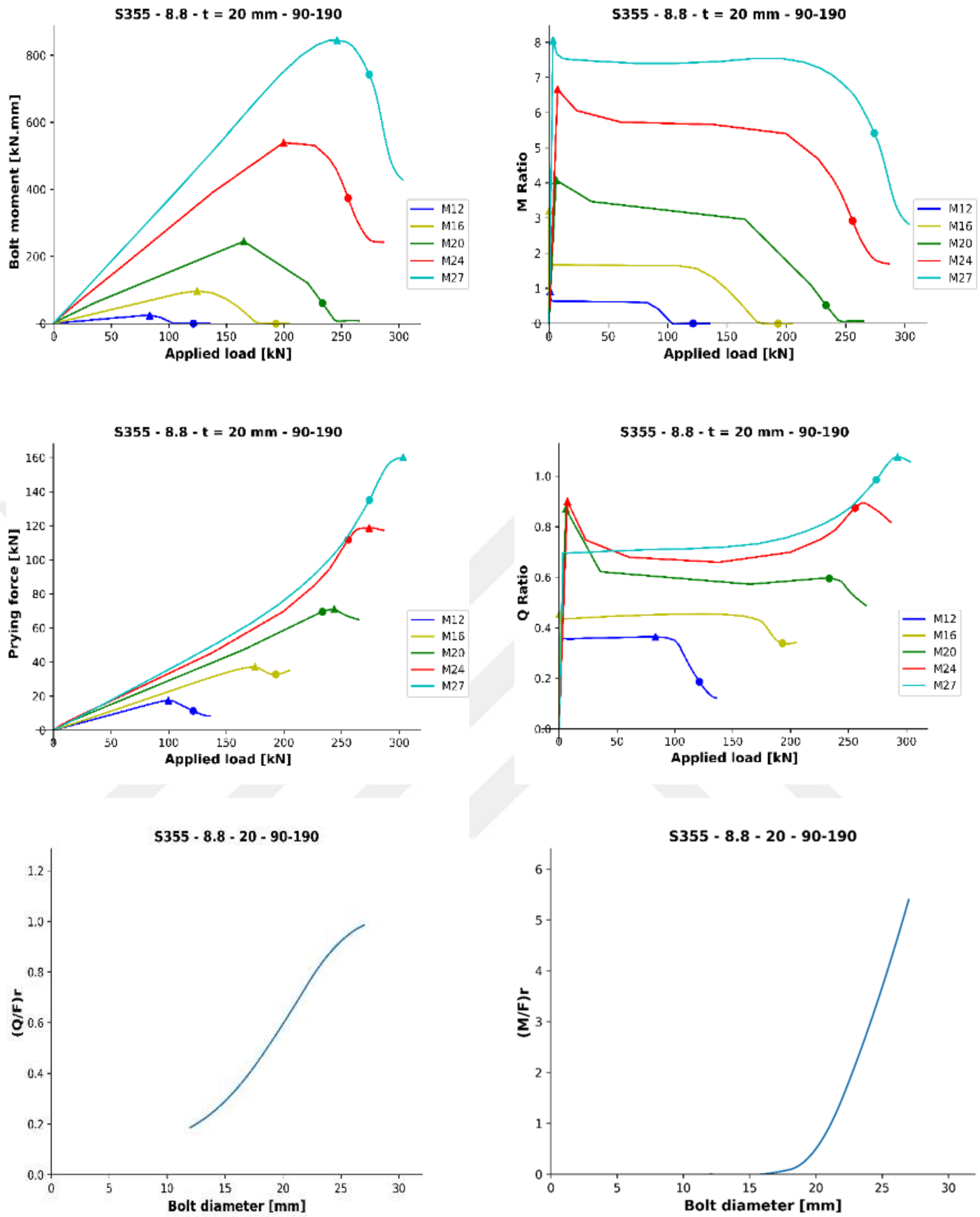

Figure 4.34. *Influence of the bolt diameter on M, M/F, Q and Q/F for S3B1 – t = 20 mm*

4.3.7. Conclusion

This additional investigagtion allowed to explore the influence of more design parameters including the flange thickness t, the edge distance n, the gauge distance w, weld throat thickness a_w, the width of the flange b and the bold diameter $\emptyset$. The investigation provide more insight into the prying effects in bolted steel T-stubs. Overall, the flange thickness, the bolt diameter and the gauge distance were the parameters which had significant influence on prying effects. An increase in the bolt diameter, just like an increase in the gauge distance results in higher prying forces and bolt moment. The steel class, the bolt grade and the flange width had less influence, although in some situations they could result in a shift in the failure mechanism of the T-stub. It has been observed that the variations of the prying force and the bolt moments were dependent on the failure mechanism of the T-stub, mostly for the gauge distance, the edge distance, the flange width and the steel class. Their ratios, namely M/F and Q/F exhibited more consistency in their variations. With the large number of data obtained from the parametric study, a regression can be undertaken to provide a estimation of the prying force and the bending moment in the bolts.

5. DEVELOPMENT OF AN ASSESSMENT PROCEDURE FOR THE PRYING FORCE AND THE BENDING MOMENT IN THE BOLT

5.1. Considerations for the Prying Effects

M-N interaction curves provide the combinations of the acceptable bolt moment and total bolt force to consider for the bolts. Constructing the complete interaction curves for the bolts requires to consider the maximum bolt moment, M_{max} and the corresponding total bolt force, as well as the total bolt force at ultimate stage and the corresponding bolt moment. For T-stubs involved in a failure mode 3 or 2, the total bolt force at ultimate stage corresponds to the axial resistance of the bolt. Taking into account the ultimate stage presents a difficulty because it would involve the consideration of the ultimate strength, f_u and the ultimate strain, ε_u, and the ultimate moment of the flange would need to be defined. Moreover, some specimens may exhibit different failure mechanisms at the plastic resistance stage and at the ultimate stage and would require more complex models that are able to encompass their behavior at the different stages. As a simplification and considering that, for design purposes the yielding of the plate is an acceptable stage for the flange, in the following sections, only the prying force and the bolt moment at plastic resistance stage will be considered.

The limit state and the behavior of each T-stub depend on the failure mechanism involved. The total bolt force at the attainment of the plastic resistance, B_r was considered and compared to the axial resistance of the bolt, B_{rd}. For T-stubs involved in a failure mechanism 3 or 2, the ratio B_r/B_{rd}, was equal to 1 due to the fact that they involved bolt failure. In some of the T-stubs involved in a failure mechanism 1, the ratio B_r/B_{rd} was as low as 0.2 (see **Fig. 5.1**). From a design standpoint, these configurations are not reasonable considering that a large reserve of the bolts' capacity is still available. Prying force and bolt moment were equal to zero in the T-stubs that failed in Mode 3. Subsequently, these specimens were not considered for the estimation of Q_r and M_r.

5.2. Mechanical Models Considering Prying Effects

Various models have been suggested to represent the behavior of bolted T-stubs. In some models, the bending of the bolts is disregarded whereas in other models it is taken into account (See **Fig. 5.2).** For specimens involved in a failure mode 3, the bending of the bolts can be disregarded. However, when other failure modes are involved, the bending induced in the bolts can be considerable and needs to be taken into account. The equations of equilibrium for each model are summarized in **Table 5.1**.

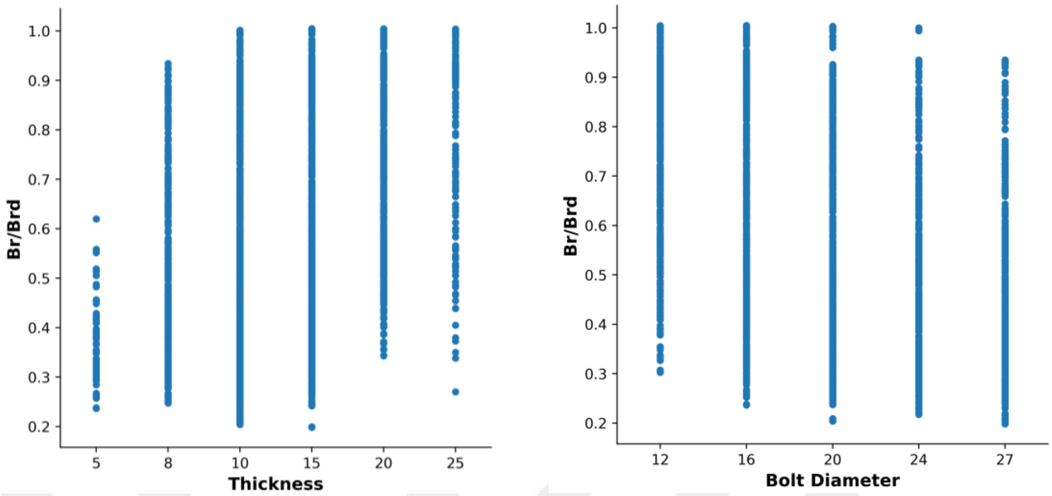

(a) *(b)*

Figure 5.1. *Ratio Br/Brd for different* ***(a)*** *flange thicknesses and* ***(b)*** *bolt diameters*

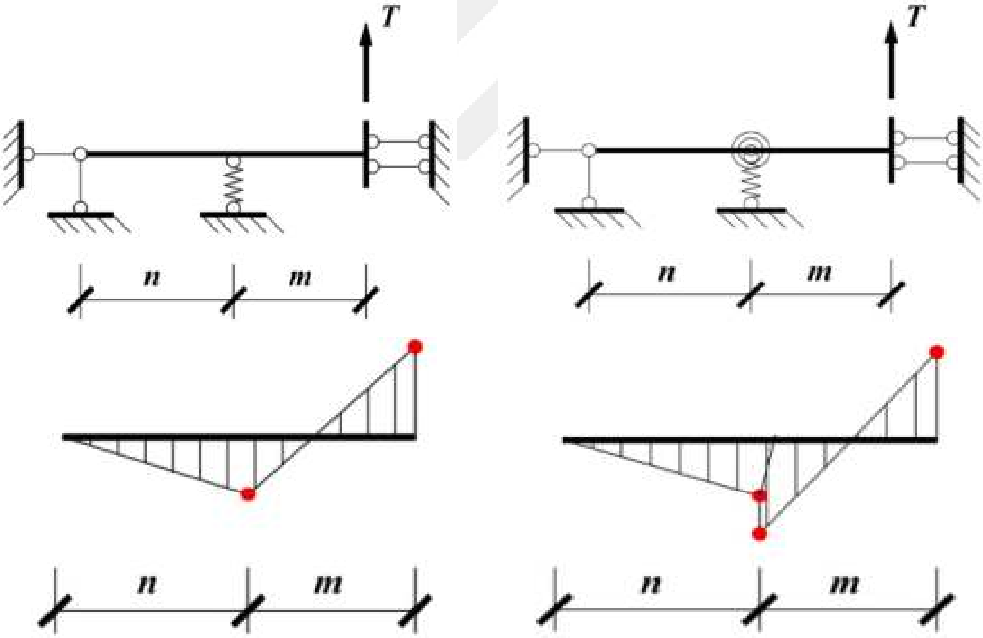

(a) (b)

Figure 5.2. *Mechanical model of T-stub* ***(a)*** *disregarding the bolt bending* ***(b)*** *considering the bolt bending*

Table 5.1. *The equations of equilibrium for the different models*

Model disregarding bolt bending		Model considering bolt bending	
$M_1 + M_2 - T.m = 0$	$(\mathbf{5.1})$	$M_1 + M_2 - T.m = 0$	$(\mathbf{5.5})$
$M_2 = \alpha M_1 = Q.n$	$(\mathbf{5.2})$	$M_2 = \alpha' M_1 = Q.n + M_b$	$(\mathbf{5.6})$
$B = T + Q$	$(\mathbf{5.3})$	$B = T + Q$	$(\mathbf{5.7})$
$Q = \frac{\alpha}{1+\alpha}.T.\frac{m}{n}$	$(\mathbf{5.4})$	$Q = \frac{\alpha'}{1+\alpha'}.T.\frac{m}{n}$	$(\mathbf{5.8})$

Considering a limit state without prying in the T-stub and at most with yielding at the web-to-flange connection, the required thickness can be given by Eq.:

$$t_{zp} = \sqrt{\frac{4 \times B_{rd} \times m}{L_{eff} \times f_y}} \tag{5.9}$$

For any given thickness, t, the coefficient α can be assessed using Eq.:

$$\alpha = \left(\frac{t_{zp}}{t}\right)^2 \times \frac{T}{B_{rd}} - 1 \tag{5.10}$$

α is often recommended to be taken between 0 and 1 ($0 \leq \alpha \leq 1$). Values of α greater than 1 are considered inadequate because the configuration has insufficient strength to develop the available tensile strength of the bolts. However, in our study this restriction was not applied

A simplification in the previous models is the consideration that the prying force is a concentrated force located at the edge of the flange. Prying force is actually the resultant of contact stresses distributed over a portion of the edge distance. Taking into consideration the location of the resultant of the contact resultant, the prying force equations in the models above can be revised as presented in **Table 5.2**.

Table 5.2. *Modified prying formulas for the prying force*

Model disregarding bolt bending		Model considering bolt bending	
$Q = \frac{\alpha}{1+\alpha}.T.\frac{m}{x}$	$(\mathbf{5.11})$	$Q = \frac{\alpha'}{1+\alpha'}.T.\frac{m}{x}$	$(\mathbf{5.12})$

5.3. Location of the Prying Force

The contact stresses distribution, hence the location of the resultant depends on the flange stiffness and the bolt stiffness. Several authors (Chasten et al., 1992; Huang et al., 2017) suggested a conservative value $x = 0.6n$. However, as illustrated in **Fig. 5.3**, this value may be acceptable for some specimens but totally inaccurate for other specimens. For specimens involved in a mechanism 1, the ratio x/n ranged from 0.12 (farthest from the edge) to 0.9 (closest to the edge). As for specimens involved in a mechanism 2, the ratio ranged from 0.6 to 1 (case of point-wise contact). It is, therefore, essential to obtain a better estimation of the prying force position.

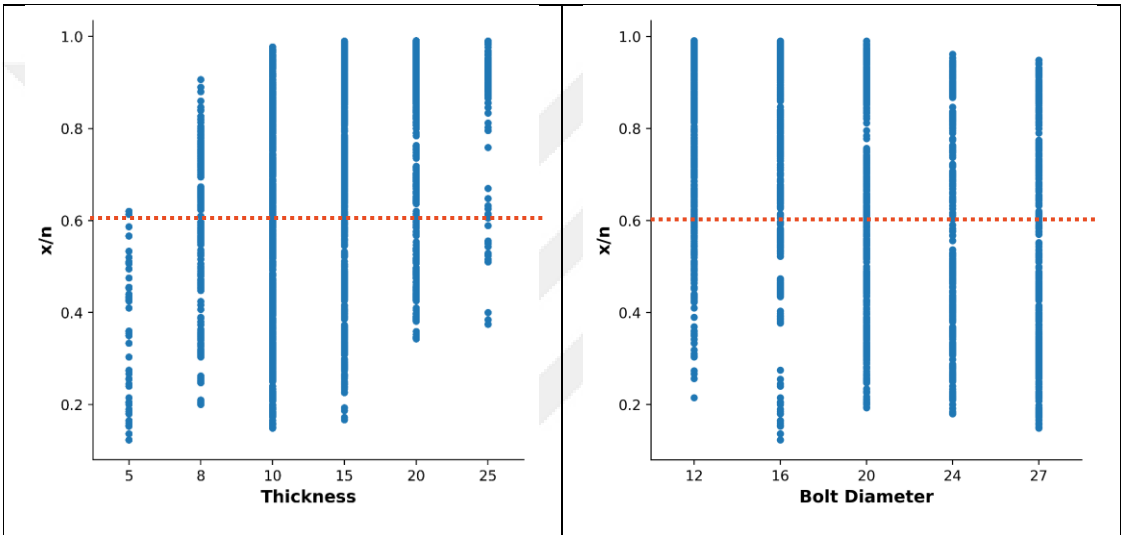

(a)	*(b)*

Figure 5.3. *Ratio x/n for for different* ***(a)*** *flange thicknesses and* ***(b)*** *bolt diameters*

The model suggested by Couchaux et al. (2017), was able to predict with satisfactory accuracy the location of the prying force. The distance between the location of the prying force and the bolt axis can be expressed as:

$$x = \xi + l(\xi) \quad (5.13)$$

The separation length ξ is the solution to a third degree equation:

$$\left(\frac{k_b \times m^3}{6 \times E \times I_f}\right) \cdot \left(\frac{\xi}{m}\right)^3 - \left(\frac{\xi}{m}\right) - 1 = 0 \quad (5.14)$$

Where $k_b = \frac{E \times A_b}{(L_b/2)}$ and L_b is the elongation length of the bolt as provided in EN 1993-1-8.

As for $l(\xi)$, it can be obtained from the expression below:

$$l(\xi) = \frac{2(n-\xi)}{3} . \frac{1}{[1 + (n-\xi)/1.11 \times t)^6]^{\frac{1}{6}}} \tag{5.15}$$

An overestimation of the location of the location of the resultant was observed in very thin flanges, probably due to membrane effects that occurred. As a simplification, it could be recommended to avoid using very thin plates: $D/t > 2.4$

5.4. Estimation of prying force

Using the prying model without considering the flexural engagement of the bolts, curve fitting procedure was undertaken in order to deduce a coefficient, C that would allow to integrate the effects of the bolt bending.

$$Q = C.\left(\frac{\alpha}{1+\alpha}\right).T.\frac{m}{x} \tag{5.16}$$

The influence of the bolt head dimension, hence of the bolt diameter on the position of the yielding line has been reported by several others (). This influence is more noticeable when large bolt diameters are used. The variable m was modified according to the expressions below:

$$m' = m - 0.3D \tag{5.17}$$

Through the curve-fitting procedure, a convergent solution was obtained with ***C* = *0.829***. The equation was able to provide satisfactory prediction of the prying forces in the bolts.

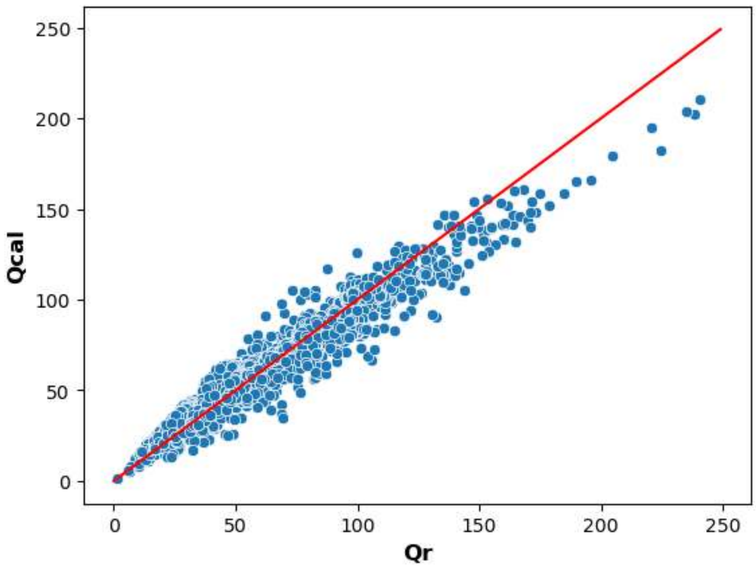

Figure 5.4. *Prediction of the prying force*

5.5. Estimation of the Bending Moment in the Bolts

Following the evaluation of the prying force location and magnitude, the bolt moment can be deduced from the equilibrium equations provided in the previous sections. The bolt moment, M_b can be calculated as:

$$M_b = (T \times m) - (Q \times x) - M_{pl} \tag{5.18}$$

The value of M_b should be positive. M_b can be taken as zero when a negative value is obtained from Eq 5.18. In fact, the bolt moment was relatively low (less than 10% of M_{ub}) in T-stubs that yielded negative values with Eq. 5.18. Additionally, in the analyzed T-stubs, the maximum value for M_r/M_{ub} was 0.65.

Although the formula was able to provide a satisfactory estimation for high bolt moment, an overestimation was observed for very low values of M_r. The real value of the moment in the flanges, M_1 was compared to the plastic moment of the flange, M_{pl} through a coefficient γ.

$$M_1 = (T \times m) - (Q \times x) - M_r \tag{5.19}$$

$$\gamma = M_1/M_{pl} \tag{5.20}$$

The values of γ were as low as 0.65 for the cases where the bolts and the flanges were relatively strong and the gauge distance was short. In these cases, the yielding and the failure occurred in the welds in lieu of the flanges. The flanges did not develop the full plastic resistance M_{pl} before the failure. However, in T-stubs where the flanges were very flexible, the values of were greater than 1.4. In fact, the first yielding occurring in the flange-to-web region, the deformation of the flanges continued until the yielding occurred in the bolt line region. At that stage, the moment in the flange-to-web region was greater than the plastic moment M_{pl}.

5.6. Conclusion

Constructing the complete M-B interaction curves for the bolts of a steel T-stub presents a certain difficulty because it requires to take into consideration the ultimate behaviour of the T-stubs and some T-stubs exhibit a different behaviour at ultimate stage and at the plastic resistance stage. For design purposes, considering only the plastic resistance stage can be sufficient. Models have been proposed, some neglecting the bending moment in the bolts and some other models taking it into account. In these models, the position of the prying force is usually assumed fixed, either at the edge of the flange or at a distance $x = 0.6n$. This assumption is reasonable for only certain configurations. A more general approach requires to evaluate the position of the prying force for each configuration. The procedure was reported in the chapter used the model suggested by Couchaux et al. (2017). Using the data obtained from the extensive parametric studies that were conducted in this dissertation and implementing a curve fitting process, a formula which integrates bolt bending was suggested for the estimation of the prying force. The suggested formula yielded satisfactory results. With the prying force location and magnitude evaluated, it is possible to calculate the bending moment in the bolts using the equations of equilibrium. The formula was able to provide an estimation of the bolt moment with sufficient accuracy when high bending moment were involved. It was also found that the moment in the flange at the flange-to-web connection could be different from the plastic moment M_{pl}.

6. CONCLUDING REMARKS

6.1. Summary of Research

The objective of this dissertation was to investigate prying effects in bolted steel T-stubs, with a focus on the bending moment that may develop in the bolts. Although prying action is considered in some design codes, the bolt bending is usually disregarded. The mechanical behavior of bolted steel T-stubs and subsequently prying effects in the bolts are influenced by various geometrical and material parameters such as the flange thickness, the gauge distance, the edge distance, the bolt diameter, the steel class, and the bolt grade. Prying-related variables such as prying force magnitude, prying force location, bolt moment, prying ratio, and bolt moment ratio were investigated. Afterwards, a procedure taking into account the flexural engagement of the bolts was proposed for evaluation of the prying force and the bending moment in the bolts.

The equivalent T-stub model is powerful tool for simulating the mechanical behavior connection components subjected to tensile loads. A T-stub consist of two T-shaped elements connected through the flanges by means of one or more bolt rows. Under the applied load, the deformation of the flanges can induce additional forces and bending moment in the bolts. This phenomenon is known as prying action. Although the prying forces and bolt bending are negligible with thick flanges, they can be considerable with more flexible flanges and cause a premature failure of the bolts. Considering the prying effects is essential for a safer design of bolted steel connections. The prying effects and their influence on the behavior of bolted connections have been investigated in many studies. As simplification, in most analytical models, the prying forces are modelled as a concentrated force applied at the edge of the flange and the flexural flexibility of the bolts is disregarded. As a result, the prying effects are usually underestimated. Taking into consideration the location of the prying force and the bending of the bolt would allow for a more accurate evaluation of the prying effects.

An advanced FE model of both hot-rolled T-stub and welded plate T-stub was developed in ABAQUS and validated against test data from the work of Coelho (2004) and that of Bursi and Jaspart (1997). The model, which integrated geometrical, material and contact nonlinearities, performed satisfactorily. Afterwards, 226 models were generated and a parametrical study was conducted to examine the influence of some geometrical parameters such the flange thickness, the edge distance and the gauge distance on the prying action. The study was further extended with over 3000 models in order to include the bolt diameter, weld throat thickness, the T-stub width, the bolt grade and the steel class. In this extended study, nominal material properties were used. The formulations provided in EN 1993-1-8 yield conservative estimations of the plastic resistance of T-stubs. Additionally to the three failure mechanisms usually considered, a mechanism involving failure of the welds can occur. This kind of failure, which should normally be avoided, may happen in T-stubs with strong bolts, relatively thick flanges and short gauge distance. The parameters that significantly influence the prying effects are the flange thickness, the bolt diameter and the gauge distance. The influence of design parameters such as gauge distance, the edge distance, the flange width and the steel class depended on the failure mechanism of the T-stub. With the data acquired from the parametric studies, a curve fitting process carried out and an improved formula taking into account the bolt bending was suggested for the prying force and the bolt moment.

6.2. Recommendations for Future Work

This research relied on the FE modelling of bolted steel T-stubs. Although the models were calibrated using test data from literature and yielded satisfactory simulation of the behaviour of bolted steel T-stubs, it would be recommended to conduct an experimental campaign that would allow a validation of the observations made from the parametric studies. Also, with the increasing use of high-strength steels, it would be useful to extend the study and include high-strength steels.

In order to improve the formula for the estimation of the bolt moment, it would be recommended to develop a model which takes into account the deformed shape of the flange and the bolt, as well as the interaction between the flange and the bolt head.

In many studies, the T-stub is treated as a deformable body in contact with a rigid foundation. This consideration is acceptable for column bases and for symmetrical specimens where the flange and the bolts on each side undergo similar deformations, allowing the plane of symmetry to be considered as a rigid foundation. However, in some practical situations, such as in endplate connections with a column and an endplate of different thicknesses, the rigid foundation condition may not be fulfilled. An investigation into the prying effects and their influence on the behaviour of non-symmetrical T-stubs (different flange thickness on each side) would be recommended.

REFERENCES

ABAQUS. (2014). *Analysis User's Manual 6.14-2.* Providence, RI, USA: Dassault Systèmes Simulia Corp.

Abidelah, A., Bouchaïr, A., & Kerdal, D. (2014, 12). Influence of the flexural rigidity of the bolt on the behavior of the T-stub steel connection. *Engineering Structures, 81*, 181-194.

Aggerskov, H. (1977). Analysis of bolted connections subjected to prying. *Journal of the Structural Division, 103*(11), 2145-2163.

Ahmed, A., & Hasan, R. (2015, 6). Effect and evaluation of prying action for top- and seat-angle connections. *International Journal of Advanced Structural Engineering, 7*(2), 159-169.

Al-Khatab, Z., & Bouchaïr, A. (2007, 12). Analysis of a bolted T-stub strengthened by backing-plates with regard to Eurocode 3. *Journal of Constructional Steel Research, 63*(12), 1603-1615.

Anwar, G., Dinu, F., & Ahmed, M. (2019, 6). Numerical Study on Ultimate Deformation and Resistance Capacity of Bolted T-Stub Connection. *International Journal of Steel Structures, 19*(3), 970-977.

Aquino, G., Amador, A., Miranda, J., & de Cisneros Fonfría, J. (2021, 11). A review of the t-stub components for the analysis of bolted moment joints. *Applied Sciences, 11*(22).

Atasoy, M. (2012). *Determinatıon of Prying Load on Bolted Connections.* Master's Thesis, Middle East Technical University, Ankara, Turkey.

Bahaari, M., & Sherbourne, A. (1996). *3D Simulation of Bolted Connections to Unstiffened Columns II. Extended Endplate Connections.*

Bai, R., Chan, S. L., & Hao, J. P. (2015). Improved design of extended end-plate connection allowing for prying effects. *J. Constr. Steel Res., 113*, 13-27.

Bai, R., Chan, S., & Hao, J. (2015, 6). Improved design of extended end-plate connection allowing for prying effects. *Journal of Constructional Steel Research, 113*, 13-27.

Baldassino, N., Bernardi, M., & Zandonini, R. (n.d.). Experimental AND Numerical Analyses of the Loading Rate Influence on the T-stub Response.

Bao, W., Jiang, J., Yu, Z., & Zhou, X. (2019, 10). Mechanical behavior of high-strength bolts in T-stubs based on moment distribution. *Engineering Structures, 196*.

Berrospi Aquino, G., Gómez Amador, A., Alencastre Miranda, J., & Jiménez de Cisneros Fonfría, J. (2021). A Review of the T-Stub Components for the Analysis of Bolted . *Applied Sciences, 11*(10731).

Bezerra, L., Bonilla, J., Freitas, C., & Massicotte, B. (2022, 5). Behavior of T-stub steel connections bolted to rigid bases. *Journal of Constructional Steel Research, 192*.

Bezerra, L., Bonilla, J., Silva, W., & Matias, W. (2020, 9). Experimental and numerical studies of bolted T-stub steel connection with different flange thicknesses connected to a rigid base. *Engineering Structures, 218*.

Bouchaïr, A., Averseng, J., & Abidelah, A. (2008, 11). Analysis of the behaviour of stainless steel bolted connections. *Journal of Constructional Steel Research, 64*(11), 1264-1274.

Bursi, O., & Jaspart, J. (1997). Benchmarks for Finite Element Modelling of Bolted Steel Connections. *J. Construct. Steel Res, 43*(1), 17-42.

Bursi, O., & Jaspart, J. (1997). Calibration of a Finite Element Model for Isolated Bolted End-Plate Steel Connections. *J. Construct. Steel Res, 44*(3), 225-262.

Bursi, O., & Jaspart, J. (1998). Basic issues in the Finite element simulation of extended end plate connections. *Journal of Constructional Steel Research, 69*, 361-382.

Chasten, C. P., Lu, L.-W., & Driscoll, G. C. (1992). Prying and Shear in End-plate Connection Design. *Journal of Structural Engineering, 118*(5), 1295-1311.

Chen, C., Zhang, X., Zhao, M., Lee, C., Fung, T., & Chiew, S. (2017, 2). Effects of Welding on the Tensile Performance of High Strength Steel T-stub Joints. *Structures, 9*, 70-78.

Chen, Z., Gao, F., Wang, Z., Lin, Q., Huang, S., & Ma, L. (2023, 2). Performance of Q690 high-strength steel T-stub under monotonic and cyclic loading. *Engineering Structures, 277*.

Couchaux, M., Hjiaj, M., & Ryan, I. (2015). Enriched beam model for slender prismatic solids in contact with a rigid foundation. *International Journal of Mechanical Sciences, 93*, 181-190.

Couchaux, M., Hjiaj, M., Ryan, I., & Bureau, A. (2017, 6). Effect of contact on the elastic behaviour of tensile bolted connections. *Journal of Constructional Steel Research, 133*, 459-474.

De Matteis, G., Brescia, M., Formisano, A., & Mazzolani, F. (2009, 8). Behaviour of welded aluminium T-stub joints under monotonic loading. *Computers and Structures, 87*(15-16), 990-1002.

De Matteis, G., Mandara, A., & Mazzolani, F. (2000). T-stub aluminium joints: influence of behavioural parameters. *Computers and Structures, 78*, 311-327.

Douty, R., & McGuire, W. (1964). *High strength bolted connections with.* IABSE congress report. doi:https://doi.org/10.5169/seals-7868

El Kalash, S., & Hantouche, E. (2018, 6). Secondary prying of column flange in Tee-connections: Experimental investigation and mechanical modeling. *Journal of Constructional Steel Research, 145*, 518-528.

El Kalash, S., & Hantouche, E. (2019, 9). Prying effect in unstiffened extended endplate connection with circular bolts configuration. *Journal of Constructional Steel Research, 160*, 402-410.

EN-1993-1-1. (2005, 7 7). *Eurocode-3.* Retrieved from Eurocode-3: https://eurocodeapplied.com/design/en1993/steel-design-properties

EN-1993-1-8. (2005). *Design of Steel Structures—Part 1-8: Design of Joints.* Brussels, Belgium: Eurocode 3.

EN-1993-3. (2005). *Design of Structures for Earthquake Resistance. Assessment and Retrofitting of Buildings.* Eurocode 8.

Farajpour, M. R. (2017). Effect of prying action forces on design method of rigid bolted connections with circular end plate. *2017 World Congress on Advances in Structural Engineering.* Seoul, Korea.

Faralli, A., Latour, M., Tan, P., Rizzano, G., & Wrobel, P. (2021, 5). Experimental investigation and modelling of T-stubs undergoing large displacements. *Journal of Constructional Steel Research, 180.*

Fernández-Ceniceros, J. (2014). *Numerical-Informational methodology for characterising steel bolted components coupling finite element simulations and soft computing techniques.* PhD Thesis, University of La Rioja, Department of Mechanical Engineering, La Rioja.

Fernandez-Ceniceros, J., Sanz-Garcia, A., Antoñanzas-Torres, F., & Martinez-de-Pison, F. (2015, 1). A numerical-informational approach for characterising the ductile behaviour of the T-stub component. Part 1: Refined finite element model and test validation. *Engineering Structures, 82*, 236-248.

Fernandez-Ceniceros, J., Sanz-Garcia, A., Antoñanzas-Torres, F., & Martinez-de-Pison, F. (2015). A numerical-informational approach for characterising the ductile behaviour of the T-stub component. Part 2: Parsimonious soft-computing-based metamodel. *Engineering Structures, 82*, 249-260.

Francavilla, A., Latour, M., Piluso, V., & Rizzano, G. (2015, 10). Simplified finite element analysis of bolted T-stub connection components. *Engineering Structures, 100*, 656-664.

Gantes, C., & Lemonis, M. (2003, 5). Influence of equivalent bolt length in finite element modeling of T-stub steel connections. *Computers and Structures, 81*(8-11), 595-604.

Girão Coelho, A. M. (2004). *Characterization of the ductility of bolted end plate beam-to-column steel connections.* PhD Thesis, University of Coimbra, Civil Engineering, Coimbra.

Girão Coelho, A. M., Bijlaard, F. S., Gresnigt, N., & da Silva, L. S. (2004). Experimental assessment of the behaviour of bolted T-stub connections made up of welded plates. *Journal of Constructional Steel Research, 60*(2), 269-311.

Girão Coelho, A. M., Bijlaard, F., & Simões da Silva, L. (2006). Finite-Element Modeling of the Nonlinear Behavior of Bolted T-Stub Connections. *Journal of Structural Engineering, 132*, 918-928.

Girão Coelho, A. M., Simões da Silva, L., & Bijlaard, F. S. (2006). Finite-Element Modeling of the Nonlinear Behavior of Bolted T-Stub Connections. *Journal of Structural Engineering, 192*, 918-928.

Gödrich, L., Wald, F., Kabeláč, J., & Kuříková, M. (2019, 6). Design finite element model of a bolted T-stub connection component. *Journal of Constructional Steel Research, 157*, 198-206.

Guo, H., Liang, G., Li, Y., & Liu, Y. (2017, 12). Q690 high strength steel T-stub tensile behavior: Experimental research and theoretical analysis. *Journal of Constructional Steel Research, 139*, 473-483.

Hantouche, E., & Abboud, N. (2014, 4). Stiffness modeling of bolted thick built-up T-stub connections including secondary prying effect. *Journal of Constructional Steel Research, 95*, 279-289.

Hantouche, E., Kukreti, A., & Rassati, G. (2012, 3). Investigation of secondary prying in thick built-up T-stub connections using nonlinear finite element modeling. *Engineering Structures, 36*, 113-122.

Hantouche, E., Kukreti, A., Rassati, G., & Swanson, J. (2013). Modified stiffness model for thick flange in built-up T-stub connections. *Journal of Constructional Steel Research, 81*, 76-85.

Hantouche, E., Kukreti, A., Rassati, G., & Swanson, J. (2015, 2). Prying Models for Strength in Thick-Flange Built-Up T-Stubs with Complete Joint Penetration and Fillet Welds. *Journal of Structural Engineering, 141*(2).

Herrera, R., Desjouis, G., Gomez, G., & Sarrazin, M. (2008). *Behavior of welded t-stubs subjected to tensile loads.* The 14th World Conference on Earthquake Engineering, Beijing, China.

Hu, D., Papadopoulos, J., & Adams, G. (2020, 6). Prying action in an elastic T-stub tensile connection. *Journal of Constructional Steel Research, 169*.

Hu, J., Chun, S., & Noh, M. (2013, 2). Mechanical prying and slip model for bolted clip-angle components. *Journal of Mechanical Science and Technology, 27*(2), 477-482.

Hu, J., Leon, R., & Park, T. (2011, 11). Mechanical modeling of bolted T-stub connections under cyclic loads Part I: Stiffness modeling. *Journal of Constructional Steel Research, 67*(11), 1710-1718.

Hu, J., Leon, R., & Park, T. (2012, 11). Mechanical models for the analysis of bolted T-stub connections under cyclic loads. *Journal of Constructional Steel Research, 78*, 45-57.

Huang, F., Zhang, D., Hong, W., & Li, B. (2017, 5). Mechanism and calculation theory of prying force for flexible flange connection. *Journal of Constructional Steel Research, 132*, 97-107.

Katula, L., & Márai, P. (2013). Study the prying effect on bolted base-plate connections. *Periodica Polytechnica Civil Engineering, 57*(2), 157-172.

Katzeff, S. (2019, 12). An investigation into prying models in tension clips. *Thin-Walled Structures, 145*.

Khani, R., Hosseinzadeh, Y., & Hoseinzadeh Asl, M. (2023). Investigating the prying force magnitude and location in the T-stub connection based on the energy method. *Engineering Structures, 280*(115655).

Komuro, M., Kishi, N., & Ahmed, A. (2006). Elasto-plastic finite element analysis of prying of top-and seat-angle connections. *Solid Mechanics and its Applications, 140*, 289-301.

Krishnamurthy, N., & Thambiratnam, D. (1990). Finite element analysis of column base plates. *Computers & S/rucrures, 34*(2), 215-223.

Kukreti, A. R., Murray, T. M., & Ghassemieh, M. (1989). Finite element modeling of large capacity stiffened steel tee-hanger connections. *Computers & Strcutures, 32*(2), 409-422.

Kulak, G. L., Fisher, J. W., & Struik, J. H. (2001). *Guide to design criteria for bolted and riveted joints* (2nd Edition ed.). Chicago: American Institute of Steel Construction, Inc.

Latour, M., Rizzano, G., Santiago, A., & Simoes, D. (2014). Experimental analysis and mechanical modeling of T-stubs with four bolts per row. *Journal of Constructional Steel Research, 101*, 158-174.

Lemonis, M., & Gantes, C. (2003). Numerical analysis of simple and preloaded T-stub steel connections. *Second MIT Conference on Compurational Fluid and Solid Mechanics.* Cambridge: Elsevier.

Lemonis, M., Gantes, C., & Gantes, C. (2002). *Finite Element Modeling of T-Stub Steel Connections Buckling strength of multi-story frames View project structural control View project Finite Element Modeling of T-Stub Steel Connections.* Retrieved from https://www.researchgate.net/publication/257876080

Liang, G., Guo, H., Liu, Y., & Li, Y. (2018, 1). Q690 high strength steel T-stub tensile behavior: Experimental and numerical analysis. *Thin-Walled Structures, 122*, 554-571.

Liang, G., Guo, H., Liu, Y., Yang, D., & Li, S. (2019, 4). A comparative study on tensile behavior of welded T-stub joints using Q345 normal steel and Q690 high strength steel under bolt preloading cases. *Thin-Walled Structures, 137*, 271-283.

Liu, M., Zhu, X., Wang, P., Tuoya, W., & Hu, S. (2017, 11). Tension strength and design method for thread-fixed one-side bolted T-stub. *Engineering Structures, 150*, 918-933.

Loureiro, A., Gutiérrez, R., Reinosa, J., & Moreno, A. (2010, 12). Axial stiffness prediction of non-preloaded T-stubs: An analytical frame approach. *Journal of Constructional Steel Research, 66*(12), 1516-1522.

Lyu, J., Yan, S., He, S., Zhao, X., & Rasmussen, K. (2023, 1). Mechanical model for the full range behaviour of bolted T-stubs. *Journal of Constructional Steel Research, 200*.

Maggi, Y., Gonçalves, R., Leon, R., & Ribeiro, L. (2005). Parametric analysis of steel bolted end plate connections using finite element modeling. *Journal of Constructional Steel Research, 61*(5), 689-708.

Mistakidis, E., Baniotopoulos, C., Bisbos, C., & Panagiotopoulos, P. (1997). *Steel T-Stub Connections Under Static Loading: an Effective 2-D Numerical Model.*

Muresan, I., & Balc, R. (2015, 3). Finite element analysis of an extended end-plate connection using the T-stub approach. *AIP Conference Proceedings, 1648*.

Mureşan, I., & Bâlc, R. (2017, 7). Parametric study of extended end-plate connection using finite element modeling. *AIP Conference Proceedings, 1863*.

Nair, R., Birkemoe, P., & Munse, W. (1969). *Behavior of Bolts in Tee-Connections Subject to Prying Action.* University of Illinois, Department of Civil Engineering, Urbana.

Nemati, N., Le Houedec, D., & Zandonini, R. (n.d.). *Numerical modelling of the cyclic behaviour of the basic components of steel end plate connections.* Retrieved from www.elsevier.com/locate/advengsoft

Numerical evaluation of the flange thickness effect on the contact stress and prying action in T-Stub steel connection. (n.d.).

Piluso, V., Faella, C., & Rizzano, G. (2001, 6). Ultimate Behavior of Bolted T-Stubs. I: Theoretical Model. *Journal of Structural Engineering, 127*(6), 686-693.

Piluso, V., Faella, C., & Rizzano, G. (2001). Ultimate behavior of bolted T-stubs. II: Model validation. *Journal of Structural Engineering, 127*(6), 694-704.

Plastic capicity of end-plate and flange cleated connections-predictions and design rules. (n.d.).

Qiang, X., Shen, Y., Jiang, X., & Bijlaard, F. (2020, 10). Theoretical study on initial stiffness of thin-walled steel T-stubs taking account of prying force. *Thin-Walled Structures, 155*.

Raebel, C., Desimone, R., & Meier, A. (2013). Effects of Bolt Spacing On Prying Forces in WT Connections. *2013 Architectural Engineering Conference* (pp. 745-754). State College, Pennsylvania: American Society of Civil Engineers (ASCE).

Reinosa, J., Loureiro, A., Gutierrez, R., & Lopez, M. (2013). Analytical frame approach for the axial stiffness prediction of preloaded T-stubs. *Journal of Constructional Steel Research, 90*, 156-163.

Santiago, A., Simões da Silva, L., Latour, M., Rizzano, G., & Trezza, S. (2013). Theoretical and experimental analysis of T-stubs with four bolts. *High Strength Steel in Seismic Resistant Structures (HSS-SERF).* Naples, Italy.

Sebbagh, H., Kerdal, D., Abidelah, A., & Bouchaïr, A. (2021, 3). T-stubs with two and four bolts under monotonic and cyclic loading. *Journal of Constructional Steel Research, 178.*

Sherbourne, A., & Bahaari, M. (1996). *3D Simulation of Bolted Connections to Unstiffened Columns-I. T-stub Connections.*

Shi, G., Shi, Y., Wang, Y., & Bradford, M. (2008, 10). Numerical simulation of steel pretensioned bolted end-plate connections of different types and details. *Engineering Structures, 30*(10), 2677-2686.

Simon, M., & Hengehold, J. (1978). *Finite Element Analysis of Prying Action in Bolted Joints.*

Soltani, R., & Kerdal, D. (2011). Behaviour of elementary bolted steel T-stub connections: An evaluation of EC3 design procedure. *Turkish Journal of Engineering and Environmental Sciences, 35*(1), 1-20.

Soltani, R., & Kerdal, D. (2012, 12). Elastoplastic analysis of elementary bolted steel tee-stub connections. *Journal of Constructional Steel Research, 79*, 71-82.

Sun, F., Xue, X., Xiao, Y., Le, Y., & Li, G. (2018, 11). Effect of welding and complex loads on the high-strength steel T-stub connection. *Journal of Constructional Steel Research, 150*, 76-86.

Swanson, J. A., & Leon, R. T. (2000). *Bolted steel connections: Tests on T-stub components.* Journal of Structural Engineering.

Swanson, J. A., & Leon, R. T. (2001). Stiffness Modeling of Bolted T-Stub Connection Components. *Journal of Structural Engineering, 127*(5). doi:https://doi.org/10.1061/(ASCE)0733-9445(2001)127:5(498)

Swanson, J., Kokan, D., & Leon, R. (2002). Advanced finite element modeling of bolted T-stub connection components. *Journal of Constructional Steel Research, 58*, 1015-1031. Retrieved from www.elsevier.com/locate/jcsr

Tartaglia, R., D'Aniello, M., & Zimbru, M. (2020, 10). Experimental and numerical study on the T-Stub behaviour with preloaded bolts under large deformations. *Structures, 27*, 2137-2155.

Thornton, W. (1985). Prying Action - A General Treatment. *Engineering Journal*, 67-75.

Van Rossum, G., & Drake, F. L. (2009). *Python 3 Reference Manual.* Scotts Valley, CA: CreateSpace.

Vilela, P., Carvalho, H., & Filho, O. (2018). Numerical simulation of bolted connections. *Latin American Journal of Solids and Structures, 15*(10MecSol2017Joinville).

Wang, Z., Tizani, W., & Wang, Q. (2010, 9). Strength and initial stiffness of a blind-bolt connection based on the T-stub model. *Engineering Structures, 32*(9), 2505-2517.

Wang, Z., Zhang, J., & Jiang, J. (2016, 6). A multi-spring component modelling approach for T-stub connections. *Advances in Structural Engineering, 19*(6), 883-896.

Wulan, T., Ma, Q., Liu, Z., Liu, M., Song, J., Cai, J., & Wang, P. (2020, 6). Experimental study on T-stubs connected by thread-fixed one-side bolts under cyclic load. *Journal of Constructional Steel Research, 169*.

Wulan, T., Wang, P., Li, Y., You, Y., & Tang, F. (2018, 8). Numerical investigation on strength and failure modes of thread-fixed one-side bolted T-stubs under tension. *Engineering Structures, 169*, 15-36.

Yang, J., Kim, H., Park, J., & Back, M. (2013, 6). Analytical models for the initial axial tensile stiffness and ultimate tensile load of a T-stub, including the effects of prying action. *International Journal of Steel Structures, 13*(2), 341-352.

Yang, J., Park, J., Kim, H., & Back, M. (2013). A prying action force and contact force estimation model for a T-stub connection with high-strength bolts. *Journal of Asian Architecture and Building Engineering, 12*(2), 309-316.

Yuan, H., Gao, J., Theofanous, M., Yang, L., & Schafer, B. (2020, 10). Initial stiffness and plastic resistance of bolted stainless steel T-stubs in tension. *Journal of Constructional Steel Research, 173*.

Yuan, H., Hu, S., Du, X., Yang, L., Cheng, X., & Theofanous, M. (2019, 1). Experimental behaviour of stainless steel bolted T-stub connections under monotonic loading. *Journal of Constructional Steel Research, 152*, 213-224.

Yun, X., & Gardner, L. (2017, 6). Stress-strain curves for hot-rolled steels. *Journal of Constructional Steel Research, 133*, 36-46.

Zhao, M., Lee, C., & Chiew, S. (2016, 7). Tensile behavior of high performance structural steel T-stub joints. *Journal of Constructional Steel Research, 122*, 316-325.

Zhao, M., Lee, C., Fung, T., & Chiew, S. (2017, 4). Impact of welding on the strength of high performance steel T-stub joints. *Journal of Constructional Steel Research, 131*, 110-121.

Zhu, X., Wang, P., Liu, M., Tuoya, W., & Hu, S. (2017, 7). Behaviors of one-side bolted T-stub through thread holes under tension strengthened with backing plate. *Journal of Constructional Steel Research, 134*, 53-65.

CURRICULUM VITAE

ORCID ID : https://orcid.org/0000-0002-5366-0315

Name Surname : Tchabremane Jean de la Croix KOMBATE

Educational Background And Working Experience

- 2012, University of Sciences and Technology of Oran, Algeria, Department of Civil Engineering
- 2015, University of Sciences and Technology of Oran, Algeria, Department of Civil Engineering, Conception and Calculation of Structures

Publications

- Kombate, T.J.C., Taşkın, K. (2022). State-of-the-art review on the behaviour of T-stubs and prying action. Journal of Constructional Steel Research, 191, 107203